ABSTRACT

Title of dissertation: COLLECTIVE DYNAMICS OF ASTROCYTE AND CYTOSKELETAL SYSTEMS

Nicholas John Mennona
Doctor of Philosophy, 2024

Dissertation directed by: Professor Wolfgang Losert
Physics

Advances in imaging and biological sample preparations now allow researchers to study collective behavior in cellular networks with unprecedented detail. Imaging the electrical signaling of neuronal networks at the cellular level has generated exciting insights into the multiscale interactions within the brain. This thesis aims at a complementary view of the general information processing of the brain, focusing on other modes of non-electrical information. The modes discussed are the collective, dynamical characteristics of non-electrically active, non-neuronal brain cells, and mechanical systems. Astrocytes are the studied non-neuronal brain cells, and the cytoskeleton is the studied dynamic, mechanical system consisting of various filamentous networks. The two filamentous networks studied herein are the actin cytoskeleton and the microtubule network. Techniques from calcium imaging and cell mechanics are adapted to measure these often overlooked information channels, which operate at length scales and timescales distinct from electrical information transmission.

Structural, astrocyte actin images, microtubule structural image sequences, and the calcium signals of collections of astrocytes are analyzed using computer vision and information theory. Filamentous alignment of actin with nearby boundaries reveals that stellate astrocytes have more perpendicularly oriented actin than undifferentiated astrocytes. Harnessing the larger length scale and slower dynamical time scale of microtubule filaments relative to actin filaments led to the creation of a computer vision tool to measure lateral filamentous fluctuations. Finally, we adapt information theory to the analog calcium (Ca^{2+}) signals within astrocyte networks classified according to subtype. We find that, despite multiple physiological differences between immature and injured astrocytes, stellate (healthy) astrocytes have the same speed of information transport as these other astrocyte subtypes. This uniformity in speed persists when either the cytoskeleton (Latrunculin B) or energy state (ATP) is perturbed. Astrocytes, regardless of physiological subtype, tend to behave similarly when active under normal conditions. However, these healthy astrocytes respond most significantly to energy perturbation, relative to immature and injured astrocytes, as viewed through cross-correlation, mutual information, and partitioned entropy.

These results indicate the value of drawing information from structure and dynamics. We developed and adapted tools across scales from nanometer scale alignment of actin filaments to hundreds of microns scale information dynamics in astrocyte networks. Including all potential modalities of information within complex biological systems, such as the collective dynamics of astrocytes and the cytoskeleton in brain networks is a step toward a fuller characterization of brain functioning and cognition.

Collective Dynamics of Astrocyte and Cytoskeletal Systems

by

Nicholas John Mennona

Dissertation submitted to the Faculty of the Graduate School of the
University of Maryland, College Park in partial fulfillment
of the requirements for the degree of
Doctor of Philosophy
2024

Advisory Committee:
Professor Wolfgang Losert: *Advisor, Chair*
Professor Pratyush Tiwary: *Dean's Representative*
Professor Arpita Upadhyaya
Professor Ronald Walsworth
Dr Ibtissam Echchgadda: *Special Member*

Dedication

I dedicate this thesis (and much more) to my family. I love my family. Their existence and the love we share is a miracle for which I am frequently overwhelmed and eternally grateful.

Acknowledgments

This effort over the six years at graduate school in Maryland was amazing. I have so many people to thank—almost too many. My family and friends know who they are and how important they are to me! Life is wonderful and amazing.

Specifically, regarding the thesis as a work document, I must thank Professor Wolfgang Losert. From the day I walked in, eager to do physics of the brain (thinking I knew a lot about the brain already), I never could have expected the immense personal benefits extracted from this opportunity. The experiences and people I met...it's extraordinary to know (not just think) that graduate school was both an amazing research experience and, more importantly, a personal journey that allowed me to become a better man. Thank you for this opportunity, Wolfgang. The support and freedom provided to me to develop personally is something for which I remain grateful.

In this day and this information age, we have an explosion of information, much of which is personal (which is often perceived as providing genuine knowledge). I have retained an internal debate throughout the years (even before graduate school) regarding how much I should share. The reason these internal debates are essential is that while I think it is too easy (especially now) to be misguided by information that is out there (e.g., exercise 'literature' is mired in a cataclysm of misinformation, and, really, private lives should be a bit more private than there are becoming), a lack of information may equally 'damage' an individual standing to benefit immensely by the correct information. An acknowledgments section may not be where one finds

wisdom (indeed, you're—the reader—about to read audaciously awesome advances in astrocyte appreciation!). Still, the acknowledgments sections were sections I read in depth when I was developing and trying to figure out what I was doing at Vassar. I would frequently read some of these acknowledgments sections and be completely demotivated and bewildered by their coldness. Perhaps the brevity of many acknowledgments is to preserve the intimacy and privacy of loved and cherished ones. Perhaps, it's just professional behavior. I don't know. It remains baffling to me. But, I want the 'future me' reading this to realize that you can forge your path within a (seemingly) rigid academic environment while injecting your volcanic energy and extroversion into it. John Steinbeck has a fantastic novella, 'The Pearl.' One of the devices used in the novella is to use music (conveying such music to the reader, which heightens the book as a quasi-cinematic experience). I don't have the literary skill set to convey my emotions (or the emotions of the scene) through text. But, in essence, every word that follows should be read dramatically. Why? In frankness, this document is about my "individual effort" in research, which couldn't be further from the truth. Behind the scenes, any fraction of exciting research embedded in this document was bolstered by hangouts with a close group of friends that I lived with, with a family who was there for me to enjoy life, old friends who made travel plans, strangers who welcomed me to faraway lands with welcoming arms such that they were no longer strangers, new friends with whom I could wrestle (grapple), lift, go-karting, and release my energy, supervisors with whom I developed strong friendships, coworkers who were brutally honest with me to help me understand what I missed in my reasoning (and let me tell you the brutal honesty was brutal... but

hilarious). To all my friends who have been with me through everything...thank you. I hope I have provided as much companionship, compassion, loyalty, love, reliability, and good entertainment as has been humbly blessed to me.

Hopefully, this chronological retelling is sufficient. I aim to do this 'quickly,' so I hope no feelings are injured. Everybody mentioned knows my retellings can be much longer! The dedications section is to my family: Grandpa John, Grandpa Pat, Grammy Phyllis, Grammy Jan, Aunt Phyllis, Carl, Aunt Christine, Anne-Marie, Aunt Laurie, Uncle Tommy, my dad, my mom, and my wonderful sister. I hope I have made you as proud as I am to be a part of this family. Aram, care take on all our future adventures together except Rapture; Stinny, for all the future Guinness and uneated steak at the top of the Pole (or a turtle bowl?); Will, who has been with me through the lowest of the lows and highest of the highs, let me see Finny; Sean, who can cure any sadness with a 30-second monologue; Craig, 890¡910; Jake, who was there for me when I needed a wake-up call, so I hope I have been there equally for you; Romeo, Deep, Ivan, all luv; Peter, as my first mentor and who is always there for me; Swarnav, who needs to get out of California (but without whom I would never have joined the Losert Lab); Sarthak, who is always down to see any movie no matter what with Nicky!; Lenny, whose word I now worship as the word of God; Zack, I need to come to TN and find the next Town Hall; Martin, who is truly a big brother and whom I am now in extreme 'lift' debt to and I don't know how I can ever repay it; Dhruvit, who knows the struggles never cease because it always gets heavier, but at least we have 3 hrs each way to talk about it; Stefano, who knows that we never daje, we daje forte because we luv life; Xach, who I probably

shouldn't have been so Halo 1v1 with because he's a fantastic electrician and we luv Spotify playlists; Jake, who knows that there is more knowledge in a hamburger than in all the world's ideas; Selu, who will always be together strong; Giova, I'm coming in hot with Dostoy!; Masoud, you know how much we luved going out and experiencing all that DC has to offer; Kate, who is both a mentor and a role model; I cannot express my gratitude for your patience in dealing with me and for our time together as an army of two. Maybe it works because we're both from NJ, but I think it's the effort we both put in, always together; Barbara, allora please let me know when I can be useful again; Hoony, superficial LA (cue leg kick); Corey, whose opinions are not even incorrect they're so wrong; Grazia, for whom our taste in movies is our little secret; Shaalini, who matches my energy perfectly; Rosetti, who is like McDonald's in that I know exactly what I'm getting every time—untamed energy!; Melanie, danke; Cara, I'm shocked you came to the defense, but now this has granted you extra random texts!; Chris, we need to watch more David Lynch together; Alex, for all the amazing fantasy and sci-fi movies we watched together; Dawid, for all the challenging but exciting go-karting we did together; Sylvester, for our shared luv of cinema; Evan, who needs to stop blocking me... both in basketball and in spending time with sweet Queen B; Adam, like a ray of sunlight, who is a great person and hope he knows that; Big Al, for always being generous with his time and insights; Kellen, whose laugh at movies makes me laugh more; Zhiyin, for having great energy; Anna, Jeneh, and Cathy for being incredible lab-mates.

Table of Contents

List of Figures

List of Abbreviations

AQP4	Aquaporin-4
BOLD	Blood oxygenation level detection
Cx43	Connexin 43
DF/F	Fluorescent normalization
GFAP	Glial fibrillary acidic protein
HTlc	Hydrotalcite-like compounds (nanotopographic films)
LATB	Latrunculin B
LoG	Anisotropic Laplacian of Gaussian filtering
MRI	Magnetic Resonance Imaging
MT	Microtuble
OF	Optical Flow
PDL	Poly-d-lysine (coated glass)

Chapter 1: Overlooked information in neuronal networks and complex biological systems: An introduction to astrocytes and cytoskeletal dynamics

1.1 Introduction

The brain is not just neurons, and biological structures are not static.

The brain is a complex container of vast, dynamic, interacting subsystems communicating and signaling in known and unknown ways. Brain cognition is the epiphenomenon aggregating from these subsystems. Bolstered by technological advances in imaging and information technology, the sheer amount of data on the brain is extraordinary. The number of datasets, data size, and types of biological data collected continually increases. However, data acquisition related to the brain is typically conducted with a focus on understanding neuron-based interactions and activity. The methods used to capture neuronal activity are extensive.

Methods used to capture the electrical activity of neurons at a large-scale and cell-group scale include EEGs [1], and MEAs [2, 3], respectively. Advances in fluorescence microscopy and biomarker technology now also provide individual cell-level images. Two-photon optical imaging allows researchers to follow calcium

fluctuations within neuronal networks [4]. Other light microscopy modalities offering higher-spatial resolution (e.g., confocal) are used to identify functional (e.g., monosynaptic retrograde neuronal tracers and neuropeptides) and structural markers (e.g., neuronal nuclei and cytoplasms) [5]. The complexity of this data is explored using sophisticated computer vision and machine learning algorithms. Such algorithms have highlighted heterogeneity in neuron morphology [6] and enabled 3D dendritic reconstructions [7].

A powerful mesoscale imaging modality is magnetic resonance imaging (MRI). One such technique is diffusion tensor imaging (DTI) [8,9]. This method focuses solely on the white-matter connections in the brain. A more popular method, functional MRI (fMRI), is adapted to measure dynamic blood oxygenation (BOLD-blood oxygenation level detection) in the brain [10, 11]. BOLD signals follow localized changes (fluctuations) in brain blood flow. A network is formed by the mesoscale functional links inferred from tracking these local flows across regions. Detailing the dynamics embedded across nodes (brain regions) in these networks (set of all links) are represented by topology models of the brain [12]. On a behavior study scale, fMRI has been used to study reward processing [13] and stroke [14, 15]. It is now proposed that fMRI, rather than indirectly measuring neuron activity, could directly measure the magnetic fields produced by action potentials [16]. With a rapid expansion in data, the scientific community and the general public are gaining increased awareness of how neuronal activity integrates into macroscopic behavior patterns. Indeed, emotions [17], sleep states [18], executive functioning, and memory [19–21] are all now envisioned via neural circuits and the complex network

topology of neurons [12, 22, 23]

However, information at the resolution of individual cells and their synapses is proving drastically more daunting to collect and interpret. In organisms with a smaller number of neurons, exciting data visualization of neural connectomes [24] of *C. Elegans* [25] and *C. Intestinalis* [26] capture imaginations. These visualizations frequently populate the internet, generating interest in exploring the wonders of neuroscience. Notably, however, *C. Elegans* only has 302 neurons (50 glial cells) [27]. These studies on the connectomes of the brain use a wide range of techniques for mapping connections [28, 29]. Some of these techniques include but are not limited to axon staining [24], molecular composition [30], and the synapse proteome [31]. These technologies are difficult to scale to higher organisms with more complex brain structures. Additional 3D reconstructions of neuronal components are generated using FIB/SEM [32] for such dense networks. A recent paper found $57e3$ cells with $150e6$ synapses within a petabyte (1.4) of data in the human cortex using FIB/SEM. This imaging was, however, confined only to $1mm^3$ of the cerebral cortex, showing the challenge of mapping large-scale brain structure in exquisite detail [33]. Much less is known about astrocytes at the macro and cell levels. It is only very recently that astrocytic (i.e., non-neuronal) component reconstructions have been investigated with this technology [34], see Fig. 1.1. As a focus of such a wide breadth of active research, the neuronal cellular system is the brain's most studied and highlighted subsystem.

Studying the brain became possible with the advent of pioneering neuroscientific technologies. The neuron-centered focus is partly historical, as these

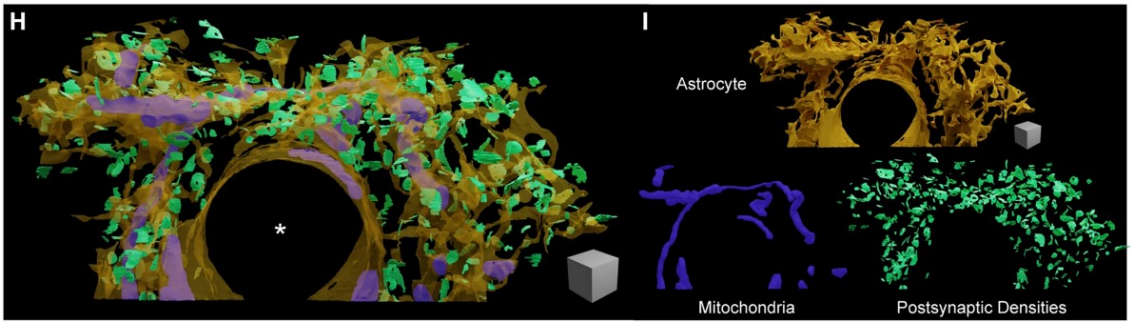

Figure 1.1: Micron scale FIB/SEM architecture of astrocytes. Representative cube is $1\mu m^3$. Reproduced with permission from Elsevier. Adapted from [34].

pioneering technologies captured electrical excitability [35]. New technologies can measure a broader range of dynamics. But, largely, the dynamic signals measured from these new technologies are not analyzed in their own right but as proxies for electrical signals. Indeed, even when calcium markers are used for optical imaging of neuronal networks, these markers serve as a proxy for occurrences of action potentials on the order of 50 milliseconds [4]. In other words, the focus is still on the electrical signaling of neurons. The range of achievements in neuroscience only via examining the neuronal axis of information processing is remarkable.

Similarly, the multi-scale tools used to establish links in the brain are only (1) electrical and (2) energy-based (fMRI). In this thesis, I study the dynamical patterns of other spontaneously active informational modalities that are non-neuronal. But, both astrocytes and the cytoskeleton possess functional roles that are energy-expensive. Both of these systems possess dynamical patterns, albeit not electrically active ones. How do these two systems fit into the pre-existing neuronal framework? How could the inclusion of the dynamics of these systems improve our understanding of brain functionality? What is it about these additional information channels

that will enhance our knowledge? Are these modalities of information more crucial to understanding health or disease in the brain? As a specific example, while researchers may assume that fMRI measures neuronal activity, the active involvement of astrocytes-enriched genes in cellular metabolism and astrocytes' high oxidative metabolism can significantly impact BOLD signals [27, 36]. Since BOLD signals correlate with actual information processing in the brain, these discoveries provide more evidence of the active contribution of astrocytes to cognition. Future research will tap into these burgeoning developments outside of pure neuroscience; the brain's non-neuronal and mechanical states will provide platforms for enhanced understanding. This dissertation aims to contribute to the burgeoning developments happening in this area.

Information had previously been an ambiguous term before it was assigned meaning by Claude Shannon [37]. While information as a physical concept has only been recently defined, the dynamics of physical quantities in the universe, whether electrical circuits or cells have always undergone information processing. In other words, just because astrocytes and cytoskeletal dynamics have not been incorporated into past models of the brain does not indicate that these dynamics did not affect the brain. In an interesting parallel, the views of both the brain and general cell biology have been inadequately defined; in essence, a complete investigation of all modalities capable of producing some form of information has yet to be considered. Indeed, the study of information science is used herein to tease out some of these modalities. The brain is not just neurons, and cells do not only follow biochemical or bioelectrical law; astrocytes are non-neuronal brain cells (glial cells) that have

signaling properties, and cells have internal mechanical dynamics that are intrinsic properties of their states. In this regard, the conventional readouts of both the brain and cells have yet to analyze the entirety of the informational dynamics as measurable and dynamical quantities.

Glial cells are the traditionally acknowledged supportive, non-neuronal brain cells. Astrocytes are an essential sub-type of glial cells. Astrocytes operate on slower time scales in the brain relative to neurons and via non-electrical activity. Moreover, the cytoskeleton has distinct dynamical modalities separate from biochemical and bioelectrical dynamics [38,39]. All cells (including neurons) possess cellular states (or characteristics) definable by the mechanical dynamics of the cytoskeleton. Within the complexity of biological systems, foundational neural research has overlooked the importance of the excitable nature of astrocytes, and foundational cell biology has similarly overlooked the excitable mechanical dynamics of the cell. This neglect is not a scientific problem but, as previously mentioned, a result of the sheer success of focusing on neurons. Why include more elements in an already overburdened dataset? However, there is a growing field linking these glial cells, linking the spatiotemporal patterns of cells to pressing scientific problems, such as neurological disorders. To better grasp the physical information embedded within astrocytes and the cytoskeleton, this collection of works focuses on *in vitro* techniques. *in vitro* data provides a degree of control and cellular detail, enabling robust physics-based and statistical analysis. In this dissertation, I demonstrate unique approaches to characterize cytoskeletal filaments in their angle organization and spatiotemporal dynamics. Additionally, I study the slow signals arising from astrocyte networks.

Different physiologies of astrocytes, as well as different components within astrocyte networks, are examined. More precisely, I quantify cytoskeletal organization and dynamics using STED microscopy, anisotropic Laplacian of Gaussian filtering, and Optical Flow. Additionally, I apply symbolization to astrocyte Ca^{2+} dynamics; symbol dynamics is a powerful tool for adequately addressing the information processing of astrocytes. I analyze the prominent physiological classes of astrocytes: immature (polygonal), healthy (stellate), and injured (reactive). A follow-up investigation on the information dynamics of stellate bodies versus processes is included. This research and its impacts are enabled by the power of interdisciplinary research, motivated by physics, at the intersection of biology, computer vision, and information theory.

The cytoskeleton is analyzed from both a structural and dynamical perspective. First, structural, static STED images of astrocyte actin are analyzed using computer vision techniques. It is found that preferential angle alignment exists for differentiated astrocytes relative to undifferentiated astrocytes. Building upon the work done in astrocyte actin organization, I next studied another cytoskeletal system: the microtubule network. One way to probe changes in cytoskeletal information is by using optical flow. Dynamics arising from this information channel have shown wave-like patterns demonstrating excitable systems phenomena. The microtubule network has only been analyzed in specific circumstances. Primarily, dynamical processes and characteristics attributed to the microtubule network signaling are from particle-tracking analysis on the end-tip proteins of microtubules. This analysis provides important insights into the depolymerization processes of this network, known as dynamic instability. However, filamentous microtubule work has been done on

single or isolated filaments. Due to the advances in imaging and biological markers, we can now harness the physical information gained from microtubule filament dynamics from high frame-rate image sequences. Utilizing the insights gained on static astrocyte angle organization, we combine Optical Flow and LoG filtering to generate a robust methodology for assessing lateral dynamics in microtubule filaments. This ability to analyze the dynamical forcing properties *in vitro* enables robust studies in evaluating the native forcing environment, provided as a readout by assessing lateral dynamics, and, importantly, enables robust quantification for assessing external forces on the microtubule network such as via electric field forcing. This framework is discussed in Chapter 3.

Not much is known about astrocyte signaling. It has come a long way within the past 30 years that astrocytes have been recognized as active, rather than passive, components of information processing in the brain. Much less has been discussed about the signaling differences within different physiologies of astrocytes. Using in vitro biological protocols, I assess the signals generated from polygonal, stellate, and reactive astrocytes. *In vitro* image sequences provide proper resolution for individual astrocyte segmentation, enabling reliable time series extraction from astrocytes. Given that these astrocyte networks retain unique morphological complexity and that the physical interactions between brain cells have been underexplored, this study opens up the possibilities of linking cytoskeletal differences more causally within brain signals and information processing. In this work, I apply amplitude ordering symbolization, derived from information theory, and partitioned entropy to analyze astrocyte time series individually and in pairs. This application of information theory

to astrocyte signaling is demonstrated in Chapter 4

Neuronal literature frequently discusses synapses and synaptic connections due to their ability to link nodes (neuronal cell bodies). Typically, the dynamics of neuronal cell bodies are analyzed. If any dynamics are prescribed to synapses, it is via weight regulations in simulated neuronal networks. Calcium signaling in dendrites has been studied briefly, but the impact and attention given pales in comparison. While astrocytes have neither synapses (the counterpart to synapses is gap junctions in astrocytes) nor dendrites, they have filamentous processes. We use in vitro astrocyte protocols to induce stellation (the most robust method for analyzing astrocyte processes) to explore the information processing contained within the stellate processes. Increasing the magnification of image sequences relative to the work described in Chapter 5, we can demonstrate embedded differences between rising and falling state distributions between stellate bodies and processes. This work has implications for the underlying processes arising in the unique behavior of stellate astrocytes, as evidenced in Chapter 4.

Astrocytes and the cytoskeletal both have adaptative roles. Astrocytes have homeostatic functions and respond to injury. The cytoskeletal reorganizes in response to environmental cues. These roles promote the maintenance of water balance in the brain and cell migration, respectively. These adaptative mechanisms persist in defining the nature of these systems. This persistence prevents a complete adoption of these two systems as modes of information. Neurons perform other tasks other than electrical signaling. Additionally, neurons adapt and respond to stimuli. However, the primary way neurons are thought of is as constantly active cells, contributing to brain

functionality and cognition. Indeed, this natural (spontaneous) activity is a hallmark of the neuron as a cell. In this regard, it is unsurprising that information-theoretic and physics-based methodologies are applied to neuronal activity; the information embedded in these cells provides rich dynamics. Astrocytes and the cytoskeleton are spontaneously active and rich in information. Both astrocytes and the cytoskeleton must be thought of as modes of information with naturally active dynamics that may provide a readout for brain functionality. Notably, the issue in elucidating these active modes is technological. A foundation of Chapters 4 and 5, *in vitro* stellate astrocyte cultures only recently were made readily accessible [40, 41]. Past culture models of astrocytes only respond under exogenous influence. Dicty cells needed to be fused to provide spatial resolution large enough to analyze actin waves [39], which may account for the limited understanding of natural cytoskeletal activity.

When actin dynamics are discussed [42], it is similar to the difference between how astrocyte signaling was traditionally conceptualized versus how this dissertation treats this signaling (consult Figures 1.5 and 1.6, respectively)–without any consideration to the complex spatiotemporal patterning and waves. Even when astrocytes were found to signal in waves, it took several decades to develop models to study these waves spontaneously. Moreover, only recently has the mechanical system been regarded as having its own waves and oscillations. The spontaneous rhythms in both channels could actively contribute to the brain's information processing. This dissertation aims to show results that demonstrate the insights to be gained from taking this physics-based perspective. Additionally, it is hoped that this work will push the interdisciplinary field of biophysics more toward this direction.

In this dissertation, I present my cytoskeleton organization and dynamics work in Chapters 2 and 3. An in-depth analysis of astrocyte signaling will follow in Chapters 4 and 5. The methods and techniques I have applied to characterize overlooked dynamics in astrocyte and cytoskeleton systems open up pathways for further analysis. In the final summary chapter, Chapter 6, I hint at projects established to causally connect signaling and cytoskeletal dynamics using the previously described techniques. Researchers can use these techniques to elucidate the same physical information in systems previously analyzed. For an overview of more theoretical considerations of optical flow and previous uses of computer vision techniques on the spatiotemporal dynamics within biological systems, consult [43]. I conclude with a final remark on the motivation behind this dissertation. Active oscillations exist across different scales in the spatiotemporal organization of cells, not just in the brain [44]. While the information exchanges between astrocytes and neurons is an active area of research, the existence of active oscillations in astrocytes is increasingly acknowledged. Such acknowledgment of active oscillations extends to the cytoskeletal subsystem as well. As the brain architecture is composed of various structural interactions, as showcased in Fig 1.1, it is increasingly necessary to understand how the active nature of these mechanical interactions [45] is contributing. We seek to understand both astrocyte signaling dynamics and cytoskeletal dynamics not as players that adapt dynamically but as naturally dynamic systems. Moreover, regarding astrocyte signaling, we advance the notion of astrocyte signaling as an analog signal. The slope and heights of the calcium events in astrocyte time series are relevant. Thus, we need more complex information-theoretic tools suited to handle these data. Unlike for neurons,

the information does not reside only in the peaks (for which neuronal signals are frequently digitized). Astrocyte time series are not just on a slower time scale than neuronal firing; astrocyte dynamics have more complex shapes, carrying different dynamical properties. This argument is extendable to cytoskeletal dynamics as well. Acceptance and acknowledgment of this dynamism may provide additional readouts of brain activity and functionality akin to the BOLD signals found in MRI. A breakdown of the different scales and the proximity of interactions to a known active contributor (neuron) is found in Fig 1.2. The following sections provide the reader with adequate background to understand this work's contributions to neuroscience and biological physics.

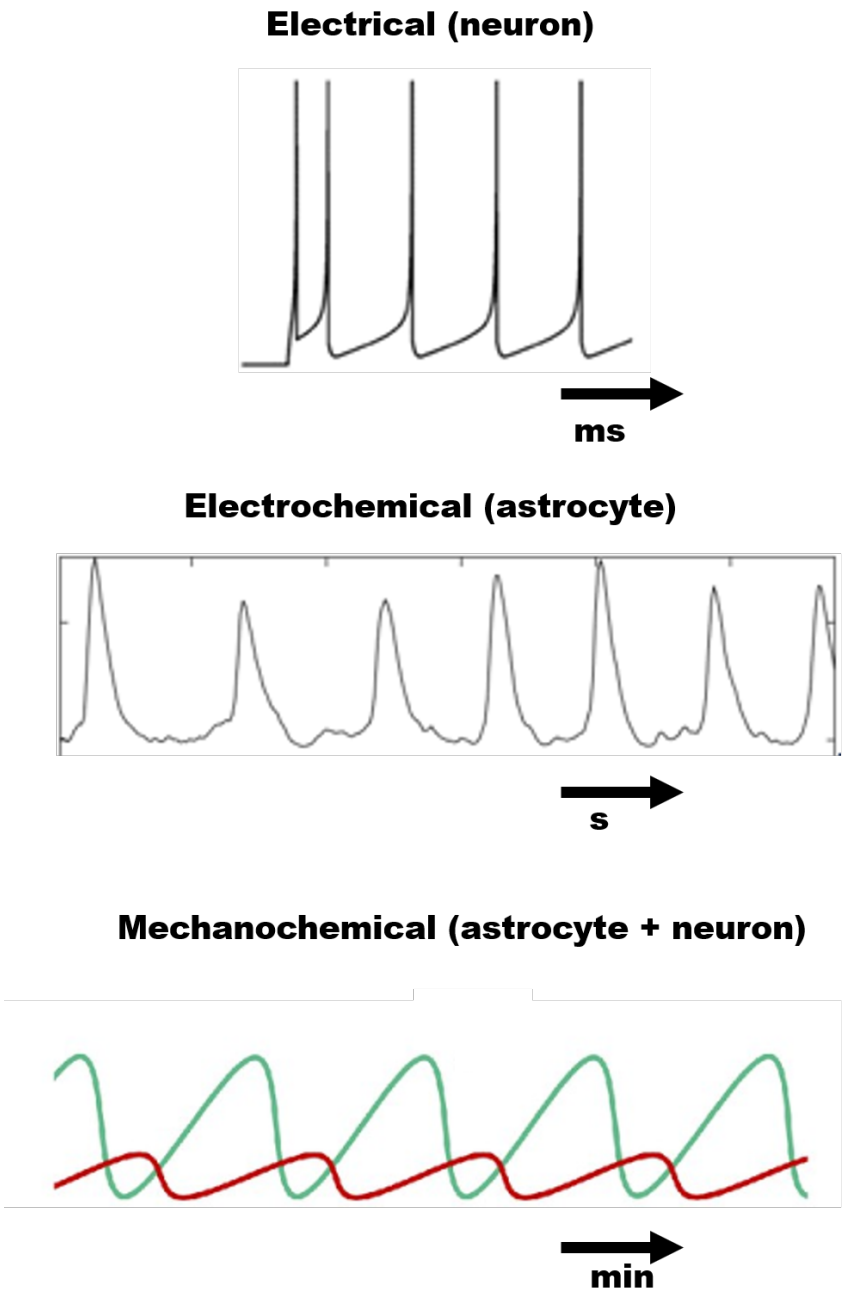

Figure 1.2: Different brain information scales. Only the neuronal axis has been targeted as a source of active contribution to brain functionality. Astrocytes and the cytoskeleton are traditionally viewed as adaptive systems. We reconfigure and adapt the notions presented in Fig. 1.3 to demonstrate the 'modes' of information overlooked. Astrocytes have spontaneous signaling patterns. The cytoskeleton is non-static and has dynamical wave-like patterns. Much like neurons, these naturally active systems are modes of information. Much like neurons, these information modes possess properties that may define brain functionality and cognition. Neuron spiking reproduced from [46], Copyright © 2003, IEEE. Calcium time series taken from N. Mennona. The bottom portion of the figure, actin dynamics, is reproduced under the terms of the Creative Commons Attribution License (CC BY) from [47]. Figure inspired by [44]

1.2 Neuronal/electrical information paradigm

On the order of 100 billion neurons exist in the brain. Each of these neurons possesses on the order of $10^3 - 10^4$ synapses [48]. Due to their electrical activity, neurons have been the only brain cells whose individual and collective signaling patterns have been traditionally researched in depth. The functionality and structure of these connections, coupled with physics and network science, have engendered more mathematically sophisticated models of the brain, as seen by the richness in the spatial, temporal, and topological perspectives of the brain [49] in Fig. 1.3. It is impossible to overstate the contributions made to science in general by studying neurons. Not only has the study of individual neurons yielded insights into behavior patterns and disorders, but neuronal activity is the bedrock upon which artificial intelligence is built.

The most known model of neuronal activity is the Hodgkin-Huxley model [50]. This simple model is arguably one of the most essential models in the scientific community [51]. Hodgkin-Huxley describes the action of electrically active neurons. This model involves a single neuron. The aftermath of neuronal modeling is now defined by 'artificial' versus 'biological' neurons, mainly owing to the success of simplification to neuronal firing on neural networks. For an updated overview of the mathematical modeling distinctions, consult [52]. The impressive growth of neuroscience (separate from computer science) has come about, though, mainly from incorporating big data with applied mathematics and physics-based modeling. Within this incorporation, the collective dynamics of neuronal firing have incurred

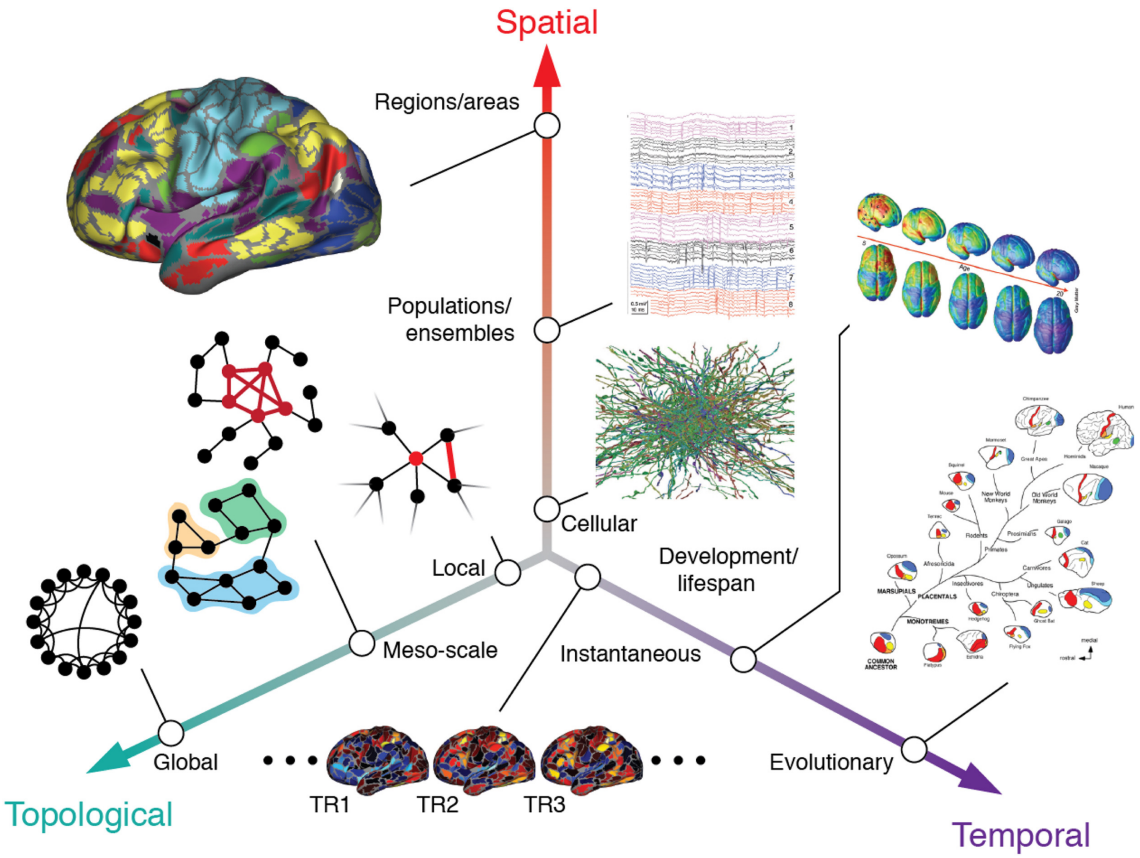

Figure 1.3: Brain networks across spatiotemporal scales. Astrocytes and cytoskeletal interactions are not included in this sophisticated analysis. This figure was adapted from Elsevier [49] under the terms of the Creative Commons Attribution-NonCommercial-No Derivatives License (CC BY NC ND).

the most robust insights into the action of the brain. As the scales embedded in 1.3 show, these data and topologies are derived from solely focusing on neurons.

This complex network-scientific view of the brain is sourced from the electrical information processing neurons perform. Successfully used as a proxy for brain functionality, the electrical activity of neurons has solidified the modern concept of the brain. The tools of information theory have been applied to this electrical information processing whether generally [53–55], in neural coding [56], pairwise population interactions [57, 58], or in the physics of neuroscience [59–70]. Success has been demonstrated by introducing artificial astrocytes into neuronal network

models [71], but the breadth of this subfield is limited. A more focused discussion of future incorporations of information theory into astrocytes is provided in 6. Still, the interested reader should consult [53–70]. In summary, due to the voluminous quantity of research on neuronal information, one may assume these cells are the only active contributors to brain signaling. This notion is incorrect.

1.3 Astrocytes: the hidden contributors to information processing in the brain

Astrocytes, a subset of glia (derived from Latin for glue), are non-neuronal brain cells. Like all living cells, there is a difference between extracellular and cytosolic ion concentrations in astrocytes. Some cytosolic ion concentrations differ from those present in neurons [27]. Functional and heterogeneity of astrocytes is a hallmark of the cell type. The diversity in astrocyte shape lays the groundwork for the work in Chapter 4. Astrocytes have somas and outgrowths consisting of branches, branchlets, and leaflets. Astrocyte endfeet contact the vasculature. Astrocytes are territorial cells located in distinct non-overlapping regions [72]. These branches and branchlets are broadly classified as processes, which are analyzed in Chapter 5. The ratio between astrocytes and neurons is estimated to be 1:1 [73]. This ratio is a topic of active research, but current estimates demonstrate the prevalence of these overlooked cells in the brain. Thus, most of what is known about the brain only considers roughly half of all active participants. Astrocytes are, in fact, active (not passive) participants in information processing due to the discovery of astrocyte communication [74]. One

need not abandon the notion of astrocytes as 'glue.' Astrocytes, despite having active signaling properties, still maintain a vital, immunologically supportive role in the brain. This dissertation does not consider pathologies, but the consequences of pathologies are implied as the reactivity [75] of astrocytes in response to injury plays a key role in Chapter 4. Astrocytes' migratory capabilities throughout development [76] enable the development of the glial scar [75,77], important for axon regeneration [78]. Importantly, the shape-shifting nature of astrocytes, this morphological adaptation is implicated in injury and disease [79–82], such as hydrocephalus [83], epilepsy [84,85], and mood disorders [86,87]. Astrocytes adapt to the environment. This sensing capability is explored in Chapter 2. Computer vision techniques are used to demonstrate preferential angle alignment of differentiated [88] astrocytes toward the cell boundary [89]. Calcium signaling in astrocytes plays a role in ischemic stroke [90]. Astrocytes are coupled via gap-junctions, which, as a counter-part to synapses, allow ion (e.g., K^+ and Ca^{2+}) flow. These signaling aspects will appear in Chapters 4 and 5. The structural plasticity of astrocytes [91] (in part a consequence of astrocyte mechanical sensing) plays a foundational role in the comparative analysis of the signals of three prominent astrocyte classes: polygonal (immature), stellate (healthy), and reactive (injured) astrocytes in Fig. 4. While not shown in this dissertation, I demonstrated using Particle Image Velocimetry (PIV) and dimensionality reduction that astrocyte migratory patterns retain different characteristics as a function of both reactivity and water channel (OAP) knockdown.

Astrocyte signaling properties had not been previously analyzed due to their non-electrical activity. With the improvement of calcium sensors, a new era of

research devoted to understanding how astrocytes signal and the content embedded within these signals has flourished [92]. Astrocytes have been implicated in a recently advanced concept known as the 'Tri-Partite Synapse' [93]. This model, while under debate, is reproduced in Fig. 1.4 As this dissertation does not consider interactions at the 'Tri-Partite Synapse,' it is left to the reader to explore this hypothesis in subsequent chapters. The interest is in the calcium signaling of astrocytes and astrocyte networks themselves. To reorient the reader's thinking regarding astrocyte communication, consider the activity of neurons. Neuronal action potentials are the electrical signals that allow neurons to communicate within networks. The timescale of action potentials is on the order of 10s of milliseconds [95]. Now, astrocytes do not have action potentials. Instead, their signals consist of calcium waves, for which Fig. 1.5 is a representative example. Fig. 1.5 showcases how excitability was discovered and newly introduced into the working definition of astrocyte activity. Notice that the timescale for wave propagation through adjacent astrocytes is 10 seconds, three orders of magnitude slower than neuronal activity. Thus, calcium waves are the counterpart to action potentials (while gap junctions are the counterpart to synapses, linking astrocytes as shown in Fig. 1.5.

While the discovery of astrocyte calcium waves is an important discovery, understanding the properties and characteristics of astrocyte signaling is still an active area of research [92, 97–101]. These contributions to the field of astrocyte excitability regard the complex signaling patterns as responses to exogenous influences rather than inherent properties of astrocytes. Note that the mechanical stimulation of astrocytes (which is how the speed of 25 μm/s for a calcium wave has been established)

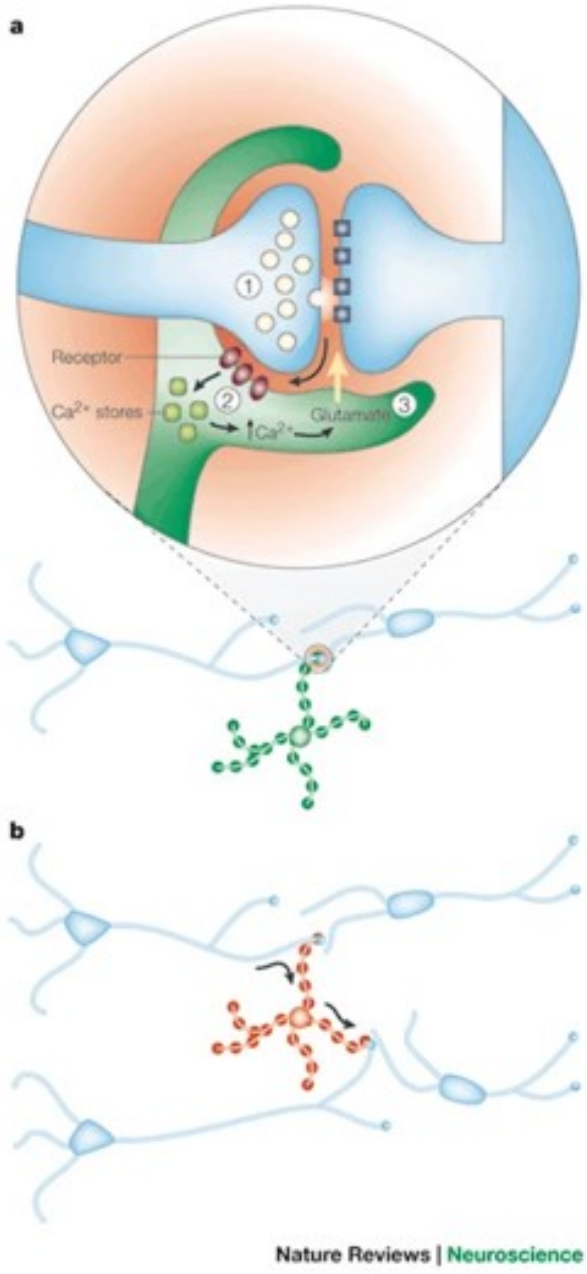

Figure 1.4: The concept of the Tri-Partite Synapse extends the notion of information processing in the brain. Reproduced with permission from Springer Nature. Adapted from [94].

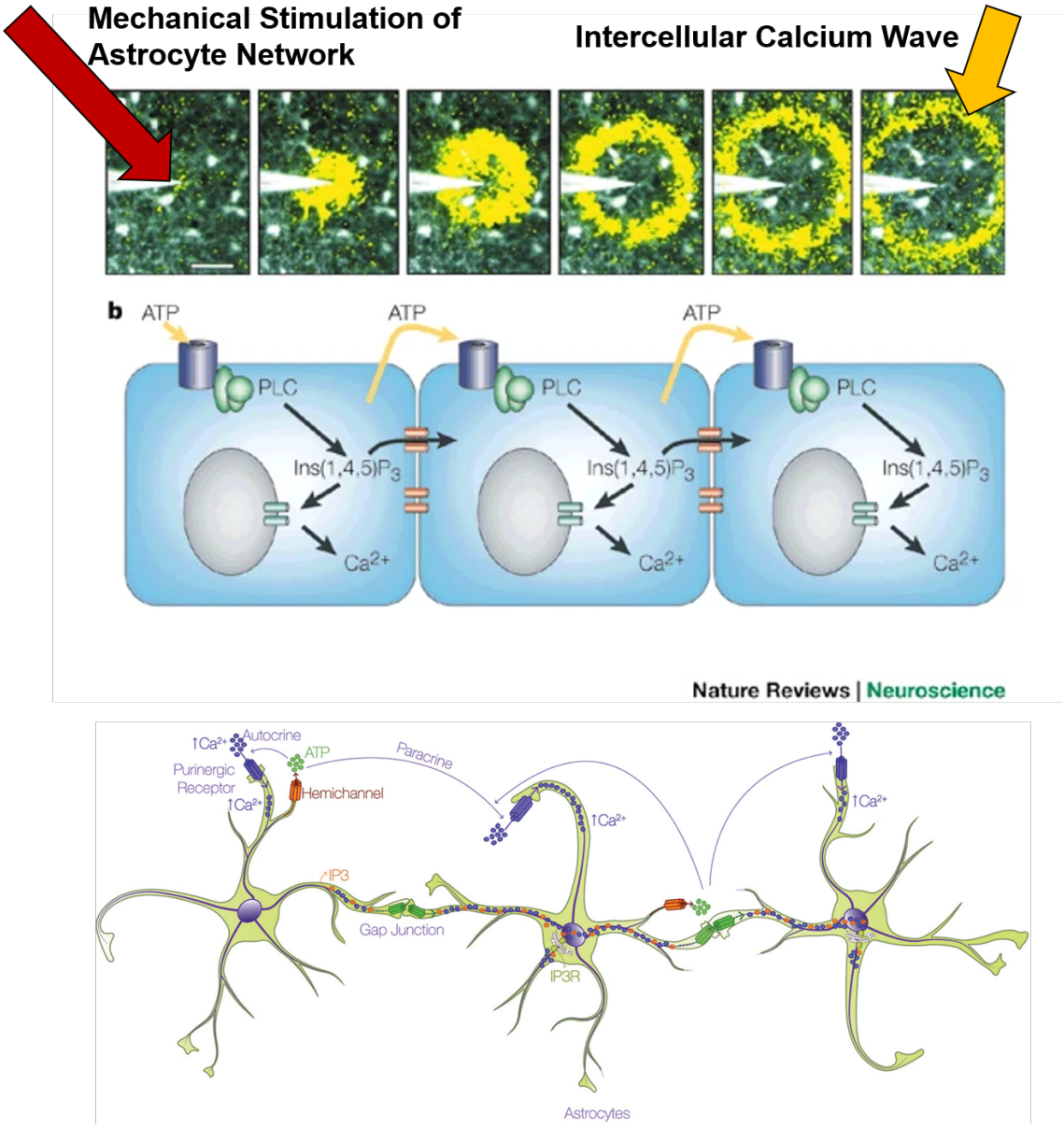

Figure 1.5: Mechanisms described for the Ca^{2+} signaling of astrocytes. Astrocytes intercellularly communicate via calcium waves. White marks in the top row represent individual astrocytes. Reproduced with permission from Springer Nature. Adapted from [94]. The bottom portion of the figure, representing the interconnected astrocyte network through which calcium flows, is reproduced under the terms of the Creative Commons Attribution License (CC BY) from [96].

still implicitly regards astrocytes as passive. It is only with some exogenous factor, such as neurons [102] or mechanical stimulation [74], that astrocytes are considered worthy of investigation. This dissertation posits that natively astrocytes exhibit rich and complex information processing, as seen in Fig. 1.6. Moreover, in contrast to neuronal spiking, astrocyte dynamics are not merely slower but exhibit more properties that render them analog, as opposed to neuronal dynamics, which are readily digitized. In the spatial kymographs, as shown twice in Fig. 1.6, the calcium signaling is not exactly wave-like (for which the fluorescent would follow a straight line in the red-boxed regions). For Fig. 1.6, the complex time-dependent patterning of calcium signals (as shown in the leftmost figure) is transformed to visualize the complex spatiotemporal patterns across an entire image sequence (rightmost figure). Each elliptical yellow region demonstrates the heterogeneity in signal size, duration, direction, and frequency. These patterns are not exactly wave-like, but varying time delays and differing initiating cells are demonstrated by the dynamics embedded in the red boxes in Fig. 1.6. It is not enough to implicate calcium signaling [90] as an important factor; the richness of astrocyte dynamics must be further explored and more rigorously.

1.4 Mechanical character of information in brain cell interactions

Slowly, the interest in the mechanical properties of cells has risen. Even within the context of the brain. The cytoskeleton and its arrangements are implicated in general neurogenesis [103], calcium signaling [104], polarization of cell shape

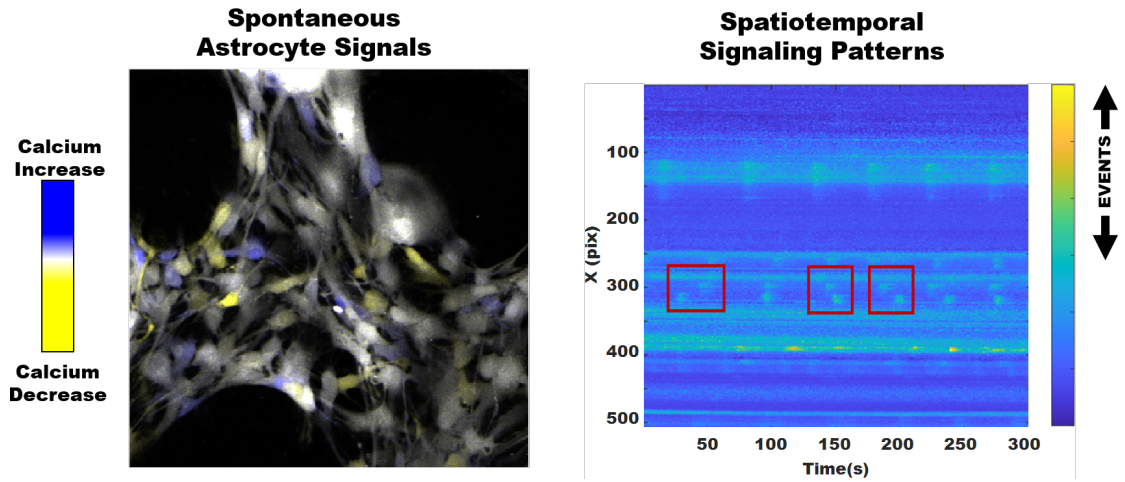

Figure 1.6: The field of astrocyte calcium signaling is growing. This growth benefits our understanding of the brain. More attention must be paid to the active spatiotemporal patterns that exist within astrocyte networks. Here is where the physics of astrocytes may provide as much insight as the physics of neuroscience. Dynamics in red boxes demonstrate synchrony with other regions in the image, as well as the varying patterning over time compared to other comparable red boxes. Data taken from N. Mennona.

[105], axonogenesis [106],synapse structure [107],dendrite formation and memory [108, 109]. Similarly to the previous discussion on calcium signals in astrocytes, a good way of thinking about the cytoskeleton is in thinking about these systems as adaptive and active, containing information-dense spatiotemporal waves and patterns [38, 39, 110–114]. The links between neurons in the brain are synapses. Briefly, neurons are connected via a pre- and post-synapse. Jointly, this synapse allows the passage of neurotransmitters, or the downstream by-product of electrical signaling (via the action potentials) in the brain. Synaptic interactions and synapses themselves have been modeled purely as an electrochemical phenomena. Recently, however, it has been shown that the synapse must additionally be thought of as a site of mechanical interactions [45, 115, 116], as illustrated in Fig. 1.7. Given the nature of the structural plasticity, morphological heterogeneity of astrocytes [86, 91, 117]

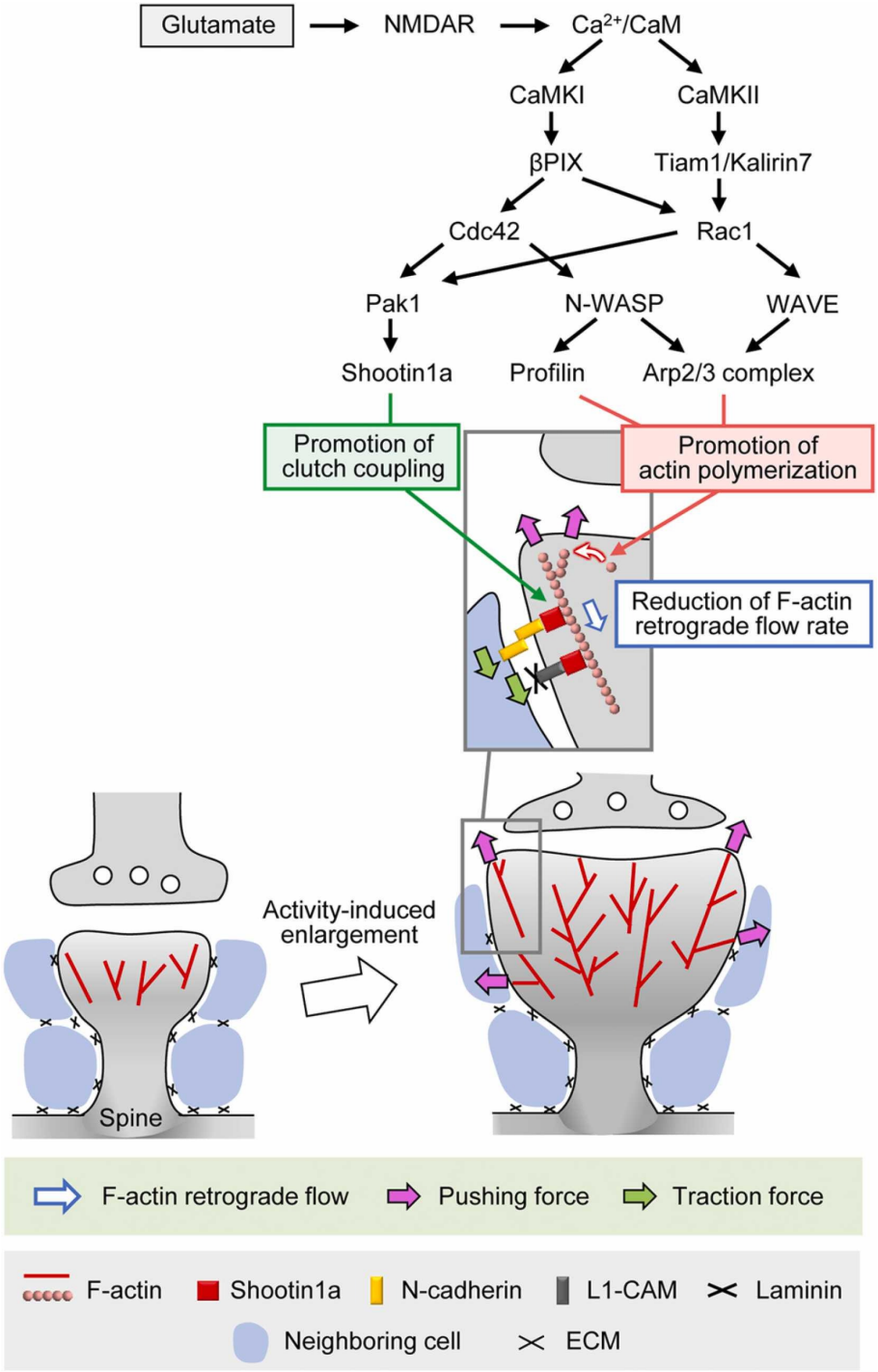

Figure 1.7: The interactions between brain cells are mechanical. The cytoskeletal interactions have been implicated, but to date, there is no causal link between the spatiotemporal dynamics of chemical signals and mechanical oscillations. This figure was adapted from Elsevier [115] under the terms of the Creative Commons Attribution-NonCommercial-No Derivatives License (CC BY NC ND).

and the suggestion of the Tri-Partite synapse [93, 118] as a model for information processing, the implications of these mechanical views of the synapses may provide the key for enhanced understanding of the brain.

1.5 Initial links between mechanical excitability and astrocytes

In following up on the questions raised by Ucar et al. [45], a study out of the Losert lab has profound relevance that will inspire future researchers in the field. The work done for this dissertation from this work is reproduced in Chapter 2. The relevance of the results not done by the author is expressed in his own words.

As previously mentioned, astrocytes are structurally adaptive and morphologically heterogeneous. Such adaptivity and heterogeneity may affect the information processing of brain networks contingent upon the veracity of the Tri-partite synapse. Within this work [89], astrocytes of different morphologies are shown to demonstrate distinct spatiotemporal actin dynamics. Thus, different astrocytes may provide different forcing patterns on neuronal synapses. This result is followed up by work done in co-culture, reproduced in Fig. 1.8. Here, it is shown that astrocytes co-cultured with neurons exhibit stronger and more frequent actin 'hotspots' (actin dynamics above a threshold). This study is the first to follow up the work of [45] with astrocytes while leveraging the benefits of a data-scientific analysis approach to the spatial patterning of actin dynamics.

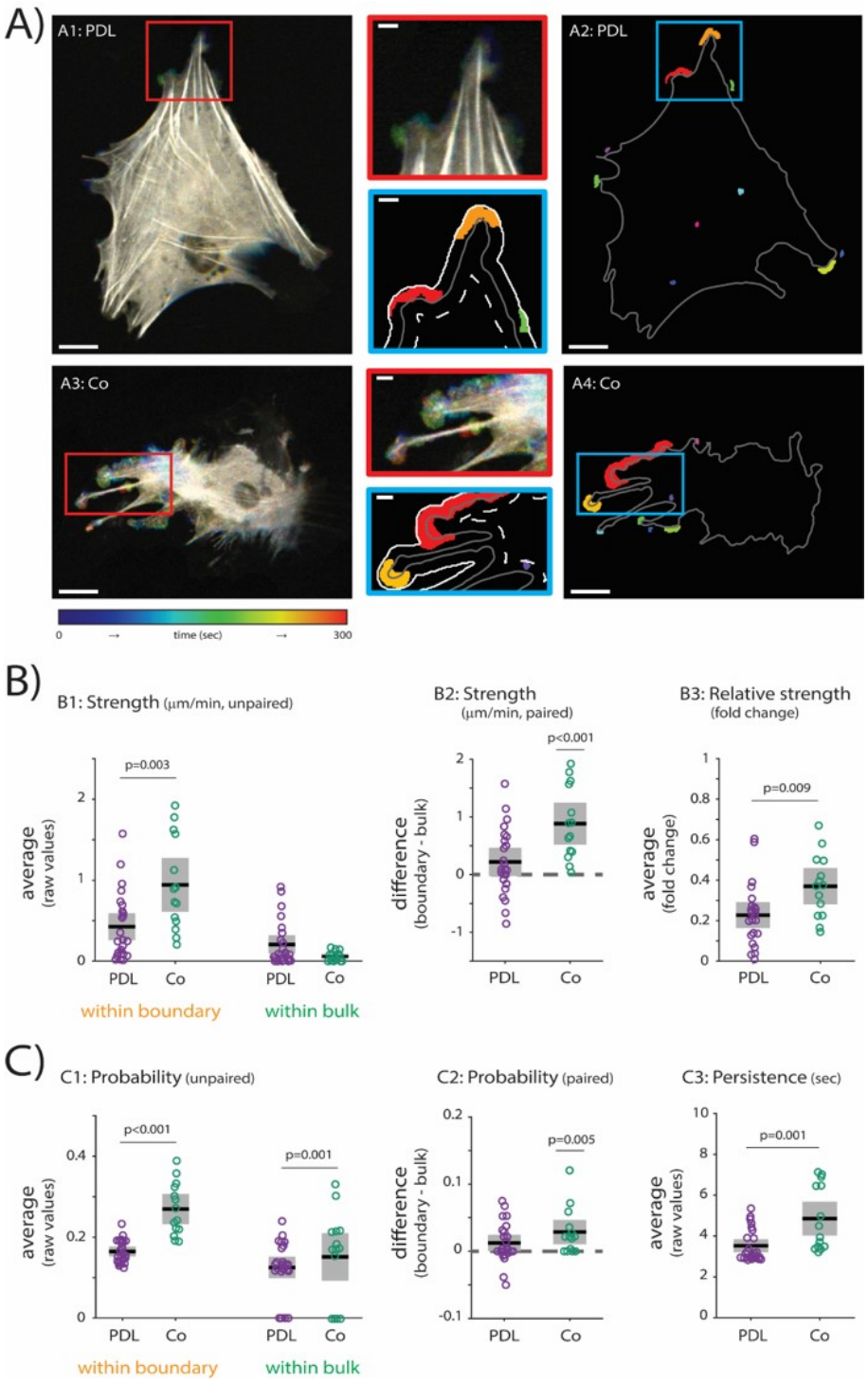

Figure 1.8: Using optical flow to measure small, active actin regions, astrocytes co-cultured with neurons exhibit stronger and more frequent actin events. The effect is pronounced at the boundary where astrocytes may contact neuronal synapses. Reproduced with permission from John Wiley and Sons [89]

1.6 Actin filaments versus Microtubules: A brief aside into imaging cytoskeletal systems

The cytoskeletal work in this dissertation is done on static actin images in Chapter 2 and on microtubule dynamics in Chapter 3. Only super-resolution (STED) is sufficient data to determine the actin angle organization results within that section. Actin filaments are neither as long nor as stiff as microtubules. Persistence length of microtubules is greater than 1 millimeter; actin filaments 10 μm. Microtubules have a diameter of 25 nm and actin filaments 8 nm [119]. The size difference is schematically drawn in Fig. 1.9. Moreover, the thinness of actin filaments requires STED resolution to discriminate between neighboring filaments. Reported literature on STED image sequences of actin are too slow to gain insights into the spatiotemporal patterns of actin [120]. Nonetheless, the results in Chapter 2 demonstrate that there are still insights to be gained from static images with appropriate context provided.

1.7 Computer vision and information theory on astrocyte and cytoskeletal data

1.7.1 Matching computational techniques with biophysical questions

The works herein combine physics, computer vision, and information theory techniques. Various methods and metrics are available for researchers to use within each of these disciplines. As a developing field, there are no standardized ways of

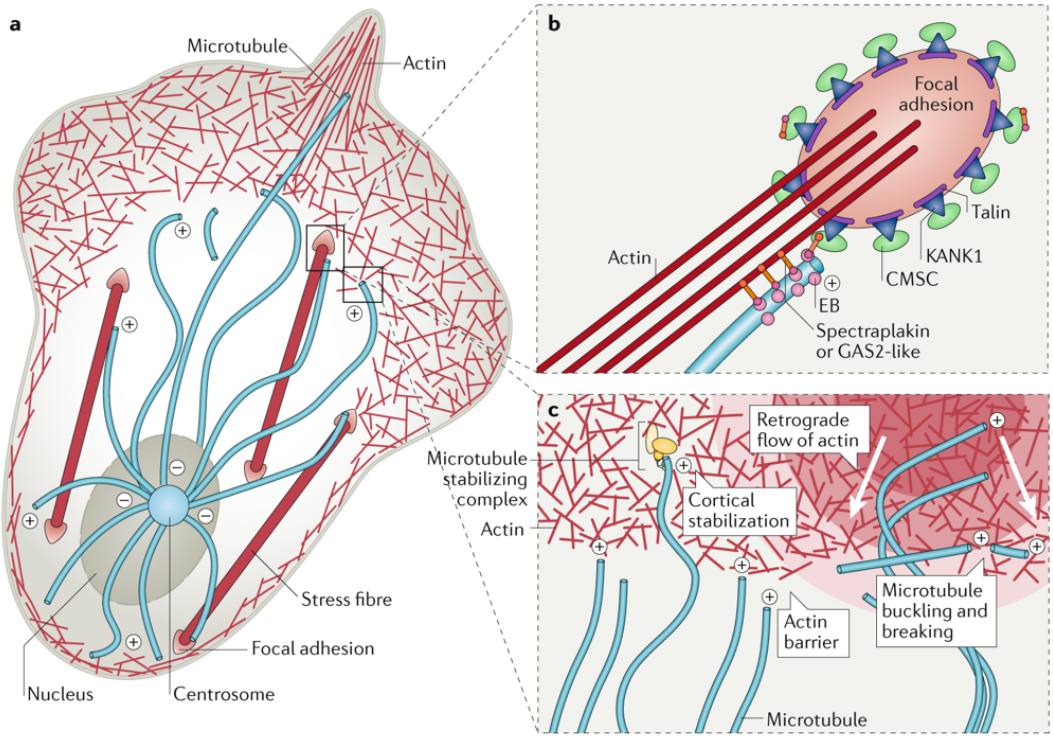

Figure 1.9: Differences in persistence length of actin filaments versus microtubules. Microtubules are longer, stiffer, and more dispersed. Actin filaments are more difficult to visualize absent super-resolution. Reproduced with permission from Springer Nature. Adapted from [121]

practicing research. Indeed, this freedom allows researchers to creatively discover new phenomena (e.g., eigenworm modes). However, this freedom comes at a risk of creating artifacts arising from an improper use of technique. For example, consider that Optical Flow and Particle Image Velocimetry (PIV) vectorize apparent motion in a field of view. Optical flow may prove more suitable for a research question than PIV, and vice versa. Thus, we provide context on the metrics and algorithms contained within this thesis.

1.7.2 Measuring entangled filamentous structures

Laplacian of Gaussian filtering is used in various chapters within this work. It appears in Chapters 2,3, and 5. As an image processing kernel, Laplacian of Gaussian filtering (LoG), an anisotropic filter, specifically 'picks out' rod-like objects within an image. The anisotropy of the filter enables the extraction of 'rod-like' or filamentous objects. As previously mentioned, there are various biophysical differences between the actin cytoskeleton and the microtubule network. However, in an image processing algorithm, both structures are similarly shaped and can thus be picked out from a filter. In Chapter 5, deviating from using LoG filtering for cytoskeletal segmentation, LoG is used for astrocyte process extraction. Essentially, these processes 'look' similar to the same actin and microtubule filaments extracted in Chapters 2,3. The intuition behind using the LoG kernel in Chapter 5 is to differentiate the various structures (which are approximately rod-like and circular for processes and cell bodies, respectively) in stellate astrocyte networks. This differentiation is crucial for

uncovering information flow in the various calcium pathways developed for stellate astrocyte signals.

1.7.3 Characterizing cytoskeletal filament network activity

In Chapter 3, I developed an algorithm for analyzing the lateral motion of microtubule filaments. While most research is devoted to tracking EB-tip, some works analyze the motion of microtubule filament dynamics (cite Arpita). The novelty of the work contained in Chapter 2 is two-fold: (1) by analyzing the lateral (perpendicular) motion of microtubule filaments, we can extract a measure of the active forcing environment of a cell; (2) the use of the Laplacian of Gaussian (LoG) filter enables segmentation of overlapping filaments. The forces (e.g., the pushing and pulling of molecular motors) within cells are numerous. This state of this environment can be read out from the internal mechanical dynamics of dense microtubule networks as a function of this environment. Other methods of filament dynamics are coarse grain and grouping the dynamics of differing filaments [122], but the method in Chapter 2 provides a way to differentiate these overlapping filaments via angle organization. Optical Flow, as a pixel-wise extraction of apparent motion within an image sequence, is thus the appropriate computer vision measure to track the movements of these segmented filaments. Overall, a more nuanced measure of the active forcing environment is available via analysis of lateral dynamics.

1.7.4 Information theoretic tools for analog astrocyte signals

Astrocyte networks in vitro are frequently considered inactive or passive. This is incorrect. With the development of more physiologically relevant protocols that induce differentiation of more in vivo astrocyte profiles, it is crucial to analyze the various active signaling patterns within the three prominent classes of astrocytes. Crucially, astrocyte signals are analog; they are not merely slower than neuronal electrical firing but express different dynamical microstates (e.g., varying rise and decay times). As such, binarizing the calcium events of astrocytes is inappropriate, which is a common practice in neuronal dynamics research. Moreover, these analog dynamics, rich in unexplored patterns, are dynamically distinct from the 'spikes' of neurons; this distinction is why astrocyte signals are regarded as events, not spikes, in this thesis. Thus, peak-finding algorithms typically used for neuronal spiking neglect the rich dynamics present in astrocyte calcium traces. The amplitude-ordering symbolization invoked for Chapters 4,5 is a suitable measure to convert calcium traces into a probabilistic state space in which each state represents a unique dynamical permutation. These permutations are interpretable; for example, a state '12345' can be regarded as a 'rise' as each fluorescent value in a window exceeds the previous value.

Symbolization is the foundational backbone of the astrocyte calcium signaling analysis. This symbolization enables the use of Shannon entropy. Shannon entropy is an interpretable measure for expressing the amount of information, or rather, the occurrence of a diverse (or non-diverse) set of dynamics experienced. We

are interested in understanding how the dynamic patterns in differing astrocyte physiologies are expressed, and such a measure helps distinguish the subtypes. The other measures used are the Hurst exponent, cross-correlation, mutual information, partitioned entropy, and the Wasserstein distance. These methods are explained more in-depth in Chapter 4. Briefly, the Hurst exponent quantifies whether a calcium trace is smooth in its dynamics; cross-correlation and mutual information describe the exchange of dynamics between traces in absolute value and amplitude-ordered space, respectively; partitioned entropy is a method for capturing the time-dependent fluctuations of the amplitude-ordered states themselves within an individual calcium trace; and, as we are interested in distinguishing various physiological profiles via the measures as mentioned earlier, we use the Wasserstein distance, as the 'earth mover's distance,' to quantify the differences in a set of distributions across the studied physiologies for any metric in focus.

Chapter 2: Environmental sensing by primary rodent astrocytes results in nanotopographic dependent actin angle organization

This chapter adapts sections from O'Neill et al [89]. Kate M. O'Neill and Emanuela Saracino collected the data, Kate M. O'Neill performed the optical flow analysis. Barbara Barile collected the STED data. Nick Mennona performed the actin angle analysis on STED actin data. Nick Mennona constructed the figures and wrote most of the sections appearing in this chapter. The actin angle analysis is the subject of this chapter.

2.1 Overview

Astrocytes are key regulators of brain homeostasis, equilibrating ion, water, and neurotransmitter concentrations and maintaining essential conditions for proper cognitive function. Recently, it was shown that excitability of the actin cytoskeleton manifests in second-scale dynamic fluctuations and acts as a sensor of chemo-physical environmental cues. However, it is not known whether the cytoskeleton is excitable in astrocytes and how the homeostatic function of astrocytes is linked to dynamics

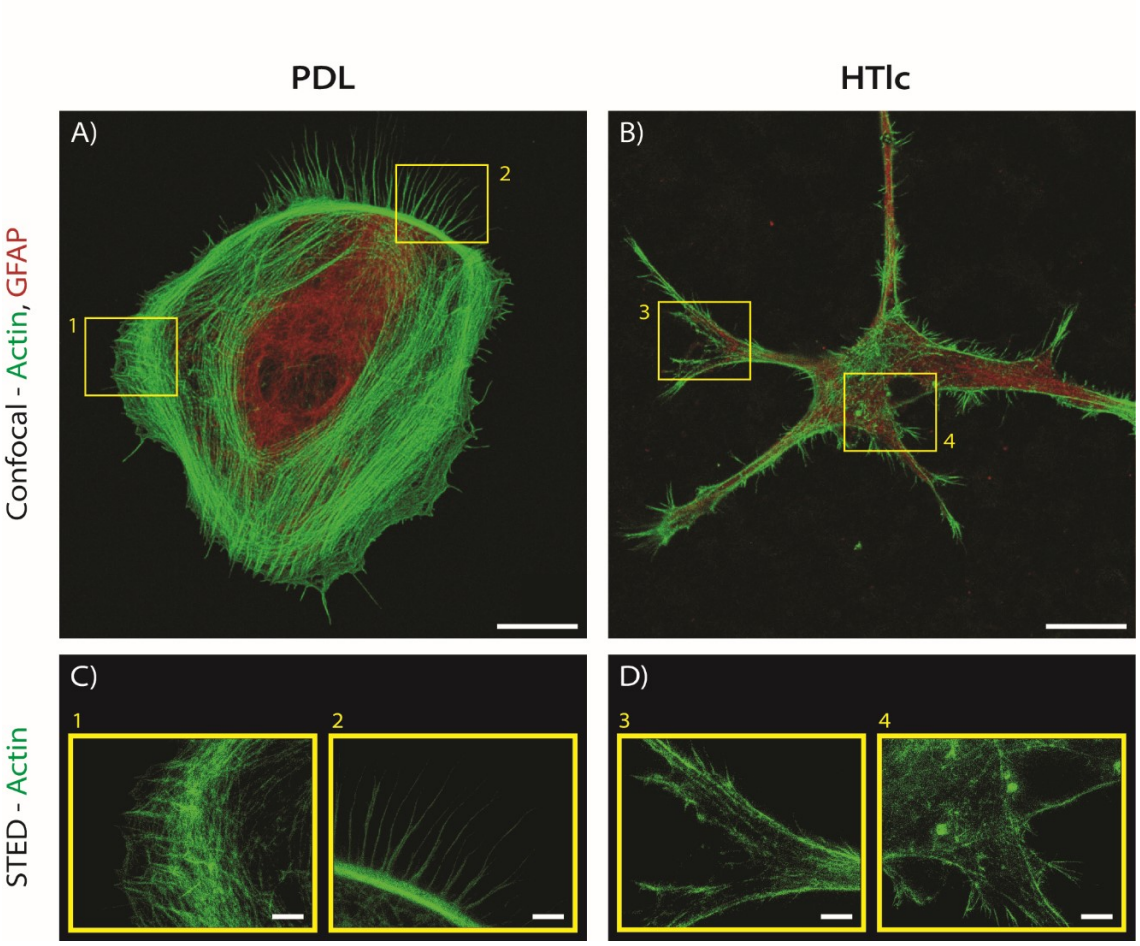

Figure 2.1: STED microscopy visualizes nanoscale actin structure within primary astrocytes grown on PDL and on HTlc A-B) Confocal microscopy images of representative astrocytes grown on PDL-coated glass (A) or on HTlc films (B) for five days, fixed, and stained for actin (green) and GFAP (red). Scalebars indicate 10 µm. C-D) Superresolution images taken via STED microscopy of cells grown on PDL (C) and on HTlc (D) of boxed yellow regions from A and B. Scalebars indicate 2.5 µm.

of the cytoskeleton. Here we show that homeostatic regulation involves the excitable dynamics of actin in certain subcellular regions of astrocytes, especially near the cell boundary. Super resolution images demonstrate that surface topography is also associated with predominant perpendicular alignment of actin filaments near the cell boundary whereas flat substrates result in an actin cortex mainly parallel to the cell boundary.

2.2 Actin Dynamics in primary rat astrocytes plated on PDL and HTlc

The following is an excerpt written in my own words. This excerpt describes the research done by K. O'Neill. The initial portion of the paper [89] describes actin dynamics of primary rat astrocytes. Astrocytes were plated on poly-d-lysine coated glass (PDL) or HTlc (Hydrotalcite-like compounds) nanotopographic films. HTlc induces stellation in astrocytes, a more physiologically healthy astrocyte state, whereas astrocytes grown on PDL display a polygonal morphology. Briefly, to visualize actin dynamics, a baculovirus transduction system was chosen to overexpress actin-GFP due to its low transduction efficiency. This ensured only a single cell was visible in a field of view; cells were plated at 5k cells/well. Using computer vision techniques, it was found that astrocytes plated on HTlc demonstrate more frequent actin events at the boundary of cells but did not display the larger 'hotspot' events observed in polygonal cells. Hotspot events are actin events surpassing a high activity (optical flow magnitude) threshold. For more details, including additional information on the analysis of co-cultured astrocyte dynamics, please refer to [89]. The finding of differences in actin dynamics at the boundary inspired the following work on static actin organization relative to astrocyte cell boundaries using STED.

2.3 Immunostaining and superresolution imaging of fixed astrocytes

2.3.1 Antibodies

For STED imaging, the following antibodies were used: mouse monoclonal Anti-Glial Fibrillary Acidic Protein (GFAP) antibody (diluted 1:200; cat. no. G3893; Sigma-Aldrich, MO, USA) and Goat anti-Mouse IgG (H+L) Highly Cross-Adsorbed Secondary Antibody, Alexa Fluor 594 (diluted 1:300; cat. no. A-11032; Thermo Fisher Scientific, MA, USA) were used as a primary and secondary antibody, respectively, for GFAP immunostaining. Alexa Fluor 488 Phalloidin (diluted 1:500; cat. no. A12379; Thermo Fisher Scientific, MA, USA) was used for direct labeling of actin.

2.3.2 STED immunostaining

Immunofluorescence for gated STED (gSTED) was performed as indicated in the Quick Guide to the STED Sample Preparation (www.leica-microsystems.com), with some slight adjustments as previously reported [123,124].Astrocytes were plated on the PDL and HTlc-treated coverslips and cultured for five days. On the fifth day of culture, cells were fixed with 2% paraformaldehyde (cat. no. P6148; Sigma-Aldrich, MO, USA) in phosphate buffered saline (PBS) for 10 min, washed with PBS, and permeabilized with 0.3% Triton X-100 (cat. no. T8787; Sigma-Aldrich, MO, USA) for 10 min. After blocking with 0.1% gelatin in PBS, fixed astrocytes were incubated with GFAP-primary antibody for 1 hr at room temperature. Cells

were then rinsed with 0.1% gelatin-PBS and co-incubated with Alexa Fluor 488 Phalloidin and Alexa Fluor 594-conjugated secondary antibody for 1 hr at room temperature. After washing with PBS, coverslips were mounted on microscope slides by using the ProLong Glass Antifade Mountant (cat. no. P36980; Thermo Fisher Scientific, MA, USA) without DAPI, as indicated in Leica official guide, and imaged with both confocal and STED microscopy. To avoid artifacts in cell morphology and/or actin orientation due to dehydration, our fixation protocol does not involve dehydration with alcohols.

2.3.3 STED imaging

Confocal and STED images of fixed astrocytes grown on PDL and HTlc were acquired using a Leica TCS SP8 3X microscope, provided with AOTF and AOBS, white light laser (WLL), Hybrid Detectors (HyD), and two STED lasers (592 nm, 660 nm) [124]. A Leica HC PL APO 100x/1.40 NA Oil STED White objective and Type F Immersion liquid with a refractive index of 1.5 were used. Before starting imaging, the excitation and the doughnut-shaped STED beams were switched on (WLL set laser power= 70%; STED-592 nm set laser power = 98%), aligned, and allowed to reach operating temperature. The beam alignment was repeated whenever necessary. Excitation of the Alexa Fluor 488 dye was achieved using a continuous-wave 488 nm laser line (NKT Photonics supercontinuum laser). For superresolution imaging of actin, g-STED was performed using the continuous wave 592 nm-emitting STED fiber laser. More detailed acquisition settings are reported in [89]. All confocal and

STED images were acquired at a set room temperature of 20 °C under constant Acquisition Mode settings (Format scanning resolution: 1024x1024 pixels; Scan Speed: 100 Hz).

2.4 Analysis of STED images of fixed astrocytes

2.4.1 Laplacian of Gaussian (LoG) filtering to segment actin

To characterize the organization of the actin meshwork in STED images of fixed cells, as shown in Figure 2.1, we performed several image processing techniques. Prior to processing, all STED images were adjusted using a contrast-limited adaptive histogram equalization. The resolution of the STED images is 16.18pix/nm. Next, each image was convolved with an anisotropic, rotating Laplacian of Gaussian (LoG) kernel. The exact kernel parameters were determined through trial and error to approximately match the cylindrical shape of actin as visualized by Phalloidin-488 staining. The number of angles through which the LoG kernel was rotated was chosen to balance computational time and segmentation accuracy. For each pixel, the best match angle was chosen via the maximum value resulting from convolving that pixel with all rotations of the filter, and a threshold was applied to ensure a high-quality match. This processing resulted in a filtered image that highlighted both the actin organization and the angle associated with each filament extracted from kernel (see Figure 2.1A1). The angles associated with the extracted actin were defined in terms of the Cartesian coordinate system, which is not biologically meaningful. To establish the angle at which the actin organized relative to the

cellular boundary, we manually drew a boundary for each cell. The number of pixels per boundary varied on a cell-to-cell basis. For each pixel, we derived the angle of that pixel's actin relative to the closest boundary point. This transformation generated angles in the range of 0 to $\pi/2$. We then applied an additional threshold at an arbitrary value to only segment the longest actin (Figure 2.1A2); doing so greatly reduced the noise in our processed data. We analyzed at least 15 individual cells per nanotopographic surface, and the morphologies of the imaged areas varied from cell to cell. Thus, the boundaries were generated to normalize the distributions of the relative angles across the data sets. We noticed that for the STED images taken of astrocytes grown on HTlc, there was more total boundary per unit-area. Thus, the boundaries from which the relative angles were calculated were drawn to coincide with only the leading edge of the cell (see Figure 2.1B for representative examples).

2.4.2 Cluster analysis of relative angles

To understand how astrocytic actin organization differs when the cells are grown on different nanotopographies, we use a hierarchical cluster analysis. From the relative angle distributions across both PDL and HTlc (22 individual cells and 15 individual cells, respectively), we group the distributions into "parallel" (angles between 0 and $\pi/6$) and "perpendicular" (angles between $\pi/3$ and $\pi/2$), as shown in Figure 2.1B. As inputs to the clustering algorithm, we use the fractions of "parallel" and "perpendicular" actin of the 37 individual cells but do not include information

about the corresponding nanotopographic surface. We [then ... generate] predictive clusters of the input data.

2.5 Astrocytes sense nanotopographic cues through actin orientation near the boundary

Inspired by our analysis of actin dynamics in live astrocytes, we sought to understand i) why certain "hotspots" of actin dynamics are more prevalent in cells grown on PDL than in cells grown on HTlc and ii) whether the characteristics of actin dynamics are related to the underlying actin structure. To this end, we cultured primary rat astrocytes on PDL-coated glass or on HTlc films and performed STED microscopy on fixed cells stained for F-actin and the intermediate filament protein glial fibrillary acid protein (GFAP). Representative images are shown in Figure 2.1. HTlc preferentially induces stellate morphology characteristic of differentiated astrocytes, whereas astrocytes cultured on PDL-coated glass display the polygonal shapes characteristic of undifferentiated astrocytes grown in the absence of neurons [123–130]. Finally, we chose not to use astrocytes co-cultured with neurons in this portion of our study because overlapping protrusions would have been visualized via immunostaining due to the density of the co-culture, thus preventing robust single-cell analysis. Cell density did not present a technical or analytical challenge for our dynamics data because transduction efficiency is low enough to obtain single cells in the field of view. Confocal images of F-actin labeled astrocytes reveal that there is a marked tendency for cells grown on PDL (Figure 2.1A) to display a polygonal and dynamic

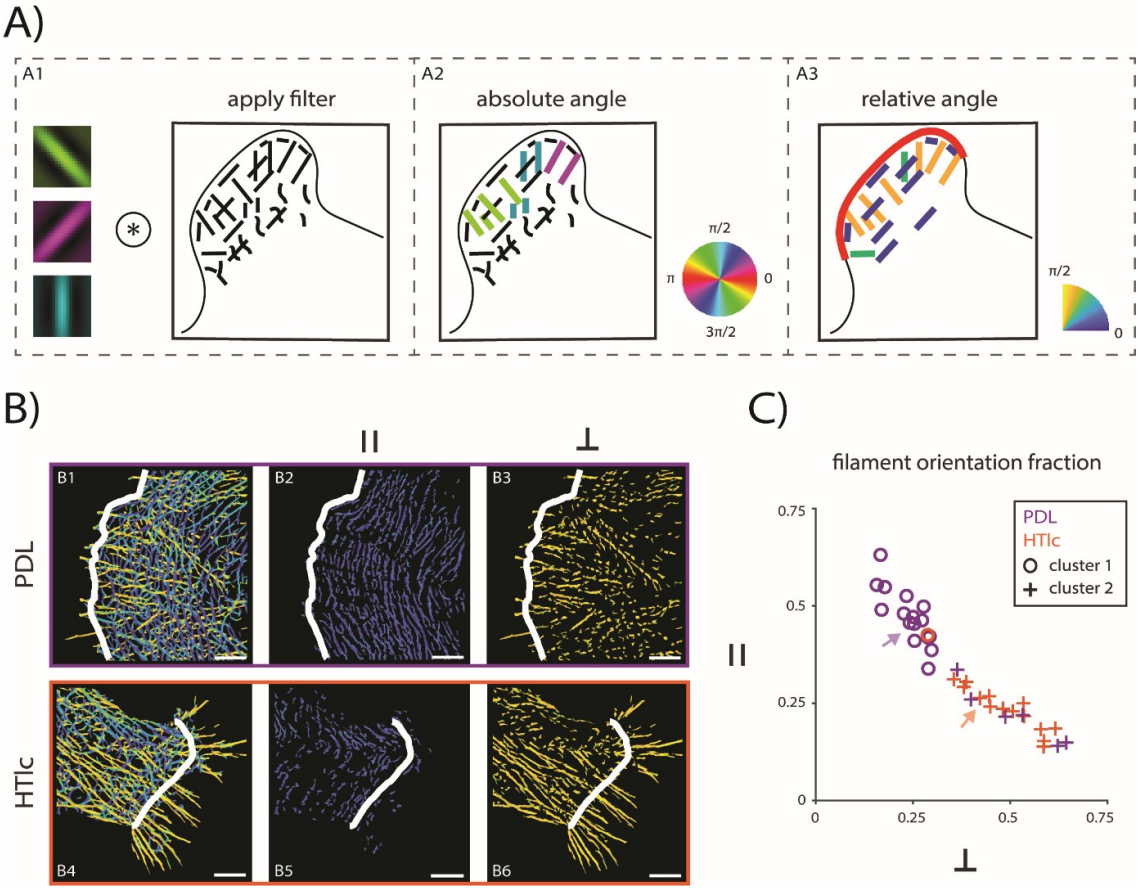

Figure 2.2: Filtering STED images with a rotating, anisotropic LoG kernel reveals differences in nanoscale actin structure for astrocytes grown on PDL versus on HTlc A) Extraction of relative angle information from actin filaments. A1) STED images are convolved with a rotating, anisotropic LoG kernel. A2) Filtering extracts actin bundles and a best match angle that is relative to the MATLAB frame ("absolute angle") with a range of $[0, 2\pi]$ (shown as full colorwheel). A3) A leading edge boundary (red) is drawn manually and is used to transform actin angles to be relative to the closes boundary point ("relative angle") with a range of $[0, \pi/2]$ (shown as a quarter colorwheel). B) Output from A for representative cells (PDL in B1-B3, HTlc in B4-B6). All relative angles, parallel angles only (range of $[0, \pi/6]$), and perpendicular angles only (range of $[0, \pi/3, \pi/2]$) for representative PDL (B1, B2, B3, respectively) and HTlc (B4, B5, B6, respectively) cells. Solid white lines indicate leading edge boundary. Scalebars indicate 2.5 μm. C) Parallel (y-axis) vs. perpendicular (x-axis) fractions of actin detected within PDL (purple) and HTlc (orange) astrocytes. A hierarchical cluster analysis reveals two distinct clusters (cluster 1: open circles, cluster 2: crosses). Arrows indicate representative cells. n=22 cells for PDL, and n=15 cells for HTlc.

phenotype with distinct leading and trailing edges and several motile structures (i.e. lamellipodia, filopodia, stress fibers; Figure 2.1C). Conversely, in the "star" shaped cells grown on HTlc (Figure 2.1B), the same motile elements that would indicate direction of propagation are not clearly visible (Figure 2.1D). Moreover, the astrocytic actin is seen to "burst" out of the actin cortex in HTlc cells (Figure 2.1D). This bursting or "flaring" behavior is indicative of a functional microdomain, known to be present in differentiated astrocytes grown on HTlc [126]. Although many regions in the representative HTlc cell display this microdomain morphology, the actin dynamics of astrocytes plated on HTlc is of lower strength than that of astrocytes grown on PDL (refer to Figure 3B [in the original text [89]]). Therefore, we chose to investigate how astrocytic actin senses the different mechanical environments presented by PDL-coated glass and HTlc films and analyze the subsequent cytoskeleton remodeling at a nanoscale level via superresolution imaging. We used a method for quantitative, semi-automated analysis of the actin bundles' preferential orientation to assess the involvement of actin organization in sensing the local mechanical environment around astrocytes [131]. Image analysis was performed by combining segmentation via an anisotropic, rotating Laplacian of gaussian (LoG) kernel with a hierarchical cluster analysis (see Figure 2.2A for a schematic overview and Materials and Methods for a detailed description). These image processing techniques allow for the analysis of actin angle organization and the determination of fractions of actin roughly parallel versus roughly perpendicular to the leading edge of the cell boundary (Figure 2.2B). From our clustered data, we determine that PDL astrocytic actin is oriented more parallel relative to the leading edge of the astrocyte, whereas HTlc astrocytic actin is

oriented more perpendicular (Figure 2.2C). The difference seen between the actin of cells grown on PDL versus on HTlc is significant as the cluster algorithm identifies two clusters within the data. Moreover, we see the cluster groups largely correspond with the chosen nanotopography, with an error of seven out of 37 cells: one HTlc cell is misclustered, and six PDL cells are misclustered (i.e., six PDL cells can be found in the cluster of predicted HTlc actin fractions). While the differences in dynamics at the micron scale between astrocytes grown on HTlc and those grown on PDL do not necessarily correspond to the differences seen in structure at the nanometer scale, our analytical approach reveals that the underlying nanoscale organization of actin within astrocytes does indeed change when the cells are exposed to different nanotopographic surfaces. Future work will optimize our co-culture approach and determine how the nanoscale structure of astrocytic actin changes when astrocytes are in contact with neurons.

2.6 Discussion

The polygonal phenotype of astrocytes grown on PDL is indicative of an immature state, compared to the astrocytes grown on HTlc, which have prominent processes protruding from the cell body (Figure 2.1B and 2.1D). When in an immature state, it is possible that astrocytes in vivo are more likely to explore their neighborhood for potential neuronal connections [132, 133]. This might in turn cause stronger actin dynamics in immature cells than in differentiated astrocytes[...] Our STED data might also provide the key to understanding why polygonal astrocytes

display more robust cytoskeleton dynamics: a more parallel and dispersed organization of actin fibers into a meshwork underneath the cell membrane is likely to confer mechanical plasticity to the plasma membrane compared to differentiated cells grown on HTLc, where actin fibers are packed into "actin rails" and not only maintain the cell shape (especially in the cellular processes) but also might cause membrane stiffness or resistance to motility. In support of our hypothesis, a recent study demonstrated increased stiffness at the leading edge of migrating astrocytes using live STED and atomic force microscopy [134]. We also hypothesize that this distinct actin structure will lead to differences in the interaction with neighboring cells. As stellation enables communication with other cell types, perpendicular actin may ensure processes are directed along the proper axis for communication. Indeed, recent work implicates membrane-bound integrins, specifically astrocytic integrin-engaged Thy1, in interacting with the neuronal cytoskeleton to promote astrocyte-neuron communication [135]. Moreover, our finding that almost all cells cultured on HTlc have actin structures perpendicular to the boundary affirms the ability of HTlc to encourage stellate morphology and differentiation of astrocytes [136]. Our analysis also hints that some cells grown on PDL have actin structures that "look" like the actin structures of stellate, differentiated cells grown on HTlc, consistent with previous observations that growth of astrocytes on PDL delays but does not fully suppress spontaneous or gliotic differentiation that might occur in standard cell culture [136–139]. We postulate that these mechanical differences may enable different types of astrocytes to respond more efficiently to neuronal activity.

Chapter 3: Filament displacement image analytics tool for use in investigating dynamics of dense microtubule networks

This chapter is adapted from Mennona et al [140]. Some sentences modified for thesis formatting. Nick Mennona performed the analysis and wrote the paper, and Anna Sedelnikova collected the data based upon instructions provided by Mennona during his summer 2021 internship with the Air Force Research Laboratory (AFRL).

3.1 Overview

The fate and motion of cells is influenced by a variety of physical characteristics of their microenvironments. Traditionally, mechanobiology focuses on external mechanical phenomena such as cell movement and environmental sensing. However, cells are inherently dynamic, where internal waves and internal oscillations are a hallmark of living cells observed under a microscope. We propose that these internal mechanical rhythms provide valuable information about cell health. Therefore, it is valuable to capture the rhythms inside cells and quantify how drugs or physical interventions affect a cell's internal dynamics. One of the key dynamical entities inside cells is the microtubule network. Typically, microtubule dynamics are measured by

end-protein tracking. In contrast, this study introduces a new, easy-to-implement approach to measure the lateral motion of the microtubule filaments embedded within dense networks with (at least) confocal resolution image sequences. Our tool couples the computer vision algorithm optical flow with anisotropic, rotating Laplacian of Gaussian filtering to characterize the lateral motion of dense microtubule networks. We then showcase additional image analytics used to understand the effect of microtubule orientation and regional location on lateral motion. We argue that our tool and these additional metrics provide a fuller picture of the active forcing environment within cells.

3.2 Introduction

Microtubules (MTs) are stiff tubular filaments that comprise one of the main mechanical structures within eukaryotic cells, similarly to the actin cortex. Much research concerning MT dynamics focuses on the biochemical interactions involved with single filaments or in vitro networks of microtubules [141–148]. However, MTs form cargo networks within a cell body (due to their high relative stiffness); in other words, MTs, enmeshed within a cell, must be regarded as a system from which information regarding entire cell functionality and health can be extracted. Indeed, quantifying this mechanical network is of interest since mechanical disruption of these 'highways' affects cellular functionality [142, 144, 149–151]. In addition, other aspects of cellular mechanoregulation are assumed to functionally depend upon MT deformation [150, 151]. One way to create such mechanical disruption is through the

major chemotherapy drugs that aim to prevent cell division by targeting microtubules, most notably Nocodazole and Paxitaxel, which destabilize and stabilize microtubules, respectively [152–154]. Electric fields are also known to affect microtubule structure, since tubulin heterodimers are polar [155]; it is unknown whether electric fields drive oscillatory behavior of MT networks.

Typically, the analysis of MTs in cells requires labeling end-tip (EB) proteins. EB proteins are the end-proteins of MT filaments that form comet-like trajectories; the straight trajectories of these ends allow one to quantify the dynamical instability (polymerization/depolymerization) which characterizes MT behavior [156]. Moreover, algorithms exist, for example PlusTipTracker [157], which allows one to quantify the trajectories of such comets. However, analysis of the dynamics of the microtubule filaments themselves in the literature has not been well studied. Efforts have been made to analyze the coarse-grained dynamics of filaments in a specific region [122]. Such efforts provide large-scale insight but do not address the perpendicular motion of individual filaments (in an overlapping mesh network), which reflects internal forcing. Given that the MT network is contained within a forcing environment (MTs respond to shear forcing, hydrodynamic forcing, cytoskeletal force generation from kinesin and dynein; due to the high persistence length of MTs, thermal forcing is negligible [141–148]), the motion of the filaments will reflect the overall active forcing environment around the MT network within the cell. As a result, we retain a fuller picture of the internal rhythms of cellular mechanics than just focusing on the growth mechanics of microtubules themselves.

Here we introduce a filament displacement image analysis method (FIDI)

for quantifying lateral dynamics of microtubules that form a dense network. The image processing algorithms combined in this method are: anisotropic Laplacian of Gaussian filtering (LoG), a second order edge detection algorithm, and Optical Flow (OF), a computer vision technique used to quantify local motion at close to the pixel scale [158,159]. In previous work we used each of these tools separately. LoG filtering identified orientation organization in static actin filament networks [89] while optical flow quantified the dynamics of polymerized actin [110]. In this paper, we combine these algorithms (LoG+OF) for analyzing the dynamics of dense microtubule filament networks. Although super-resolution has shown to benefit researchers investigating cytoskeletal filaments [89, 160], with just confocal imaging our tool is still able to capture the motions of MTs embedded within the active forcing environment.

FIDI is distinct from other tools used for understanding bending dynamics of cytoskeletal filaments. Previous algorithmic tools have been developed to track filaments along their lengths and model the dynamics to quantify the persistence length and bending rigidity of cytoskeletal filaments. Indeed, other studies have devoted attention to the physical modelling of these filamentous networks [161, 162]. Even if the density of the network renders individual filament tracking impossible, lateral motion of the constituent filaments in the MT network is still visible by eye. OF is not sufficient alone to quantify this motion since motion of two crossing filaments (frequently encountered in dense filamentous networks) will generate artifacts in the optical flow field. As we are not tracking filaments over time, LoG provides us with pixels belonging to a MT filament while OF measures the movement of detected pixel over time. In summary, we pre-filter our data with LoG and then further measure

with OF, which allows us to (1) identify pixels associated with MT filaments (2) group filamentous pixels with similar angles, and then subsequently measure the lateral motion of such detected objects. Using additional image processing tools, we can separately analyze the motions of MT filaments depending upon the filament angle (generated as output from LoG filtering) and the region within cells.

3.3 Experimental Methods

3.3.1 Cell Culture

Rodent neuroblastoma-glioma cells (NG108-15 (108CC15) ATCC HB-12317, Manassas, VA) were cultured at 37 °C in a humidified 95% air, 5% CO2 atmosphere in Dulbecco's Modified Eagle's Medium (DMEM, 11965-092, Invitrogen, Carlsbad, CA) containing no sodium pyruvate, 10 % Fetal Bovine Serum (FBS), 1 I.U./ml penicillin, 0.1 μg/ml streptomycin, 0.1 mM hypoxanthine, 400 nM aminopterin, and 0.016 mM thymidine. Cells were harvested between passages 20 and 30 and plated at a density of 104 cells/cm^2 on Poly-D-Lysine (100 μg/ml, Sigma P7886) precoated glass-bottomed dishes (MatTek) in serum-free medium consisting of DMEM, 1 mM dibutyryl cyclic AMP (Millipore-Sigma), and antibiotics. Differentiation was induced 24 hr after cell plating by replacing the growth medium with a differentiating medium in which the FBS had been substituted with B27 (Gibco 17504044) and supplemented with 1 mM dibutyryl cAMP (Tocris 1141). The differentiating medium was replaced every 48 hr. Cells were used for experiments after 7-14 days of differentiation. Differentiated cells exhibited spontaneous APs, evoked by current injection in 50 % and 70 % of

the cells at 10 days post differentiation. Chinese Hamster Ovarian-K1 (CHO-K1) was obtained from ATCC (Manassas, Virginia). CHO-K1 cells were cultured in F12 K medium supplemented with 10 % fetal bovine serum, 2 mM l-glutamine, and 100 U/mL penicillin/streptomycin at 37 °C with 5 % CO2 in air. Plasmids and Cellular Transfection L304-EGFP-Tubulin-WT, which specifically labels tubulin, was a gift from Weiping Han (Addgene plasmid #64060; http://n2t.net/addgene:64060; RRID:Addgene_64060). Plasmid DNA was prepared using a Qiagen Plasmid Plus Maxi Kit (12963, Qiagen, Germantown, MD). For the lentiviral construct (L304-EGFP-Tubulin-WT), the plasmid was packaged into lentivirus and amplified to 108 infectious units (IFU)/ml.

3.3.2 Generation EGFP-Tubulin expressing lentivirus

L304-EGFP-Tubulin-WT construct was packaged in pseudoviral particles in 293TN producer cells (SBI, LV900A-1), supernatant containing pseudoviral particles was collected at 48 hr. post transfection, filtered at 0.45 µm PVDF filters and centrifuged at 50,000Xg, 90 min at 4 °C. Then pseudoviral containing precipitate was re-suspended in TNE buffer (50 mM Tris, pH 7.8, 130 mM NaCl, 1 mM EDTA), virus was stored in 100 µl aliquots at -80 °C. Relative pseudoviral titer was determined by transducing cells and by counting the number of cells expressing EGFP-Tub, allowing 72 hours for expression to start.

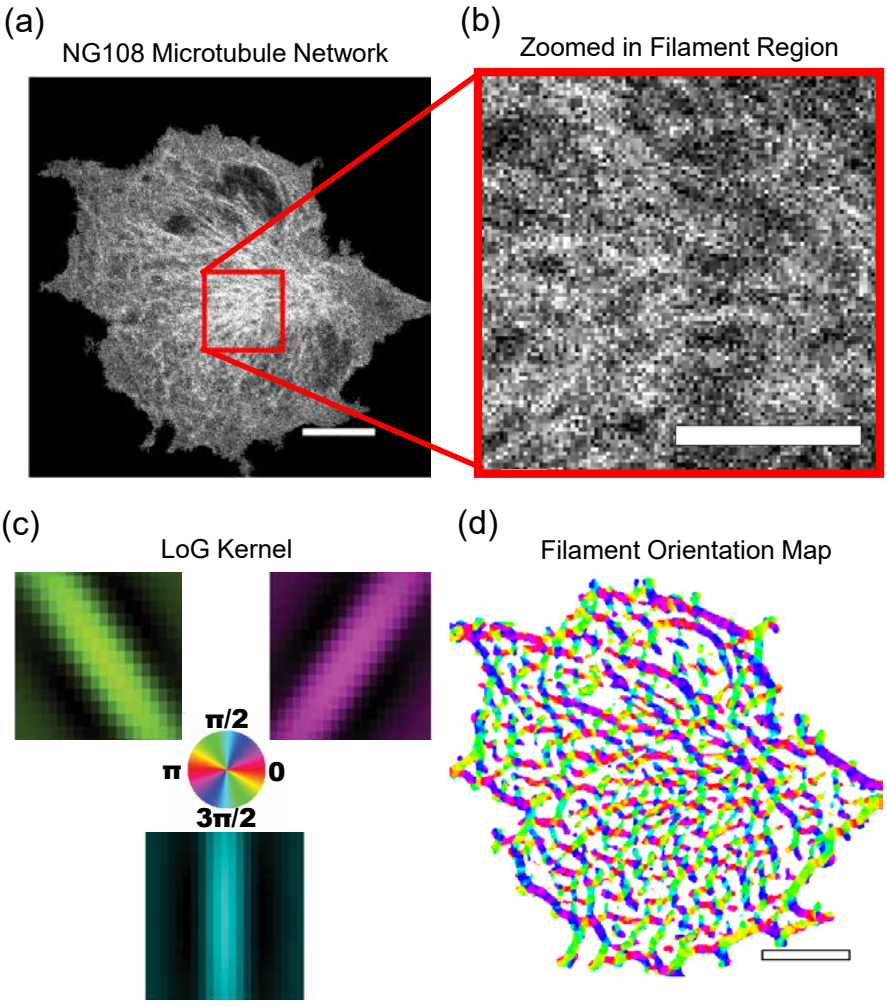

Figure 3.1: LoG algorithm extracts MT filaments in every frame. (a) NG108 cell line with fluorescently labelled microtubule filaments. This confocal image displays a MT network with representative density of filaments. (b) Cytoskeletal networks containing filaments oriented in different directions. Even with the relatively low image resolution, the variety of microtubule orientations (some filaments are tilted while others are horizontal) is apparent. (c) Anisotropic, rotating Laplacian of Gaussian (LoG) filter with some rotation steps. The rods (right leaning, left leaning, and vertical) in each of the three images represent the LoG kernel with angle prescribed as the closest area on the colorwheel (different shading represents different angles). These rods resemble the shapes of microtubules, which showcases how microtubules are detected. Note, that once microtubule pixels are found above a threshold, each pixel is ascribed an associated angle belonging to which kernel causes maximal value in the max projection step. (d) Filament Orientation Map output from convolving data in (a) with kernel in (c). This final output shows all microtubule filaments detected. Note that the there are spatial homogeneities with neighboring pixels which amounts to filament detection. Moreover, note that there are regions of white (corresponding to pixels not valued as microtubules) within the image; areas not white (different colors and shades) represent regions where the algorithm has identified a filamentous pixel and has prescribed an angle for this pixel. We found that LoG paramters of [1, 7] for the sigma in $\hat{x}$ and $\hat{y}$ as well as 30 rotations to work well with our data. Our scripts are provided in the GitHub link at the end of the manuscript. Scale bars are 10 µm for (a) and (d); scale bar is 5µm for (b).

3.3.3 Microscopy

Image sequences were acquired using the Leica® TCS SP5. Confocal microscopy was performed with magnification of 40x water immersion objective. Conversion ratio from pixel to micron ranged from 0.04 to 0.15 microns/pix. Image sequences were acquired every 1.1 seconds, which is faster than previous studies [161]. Images analyzed were of 'strips' of cells with image dimensions of 40x1024.

3.4 Results

3.4.1 Anisotropic Laplacian of Gaussian filtering highlights MT filaments

The data used for prototyping the algorithm contains image sequences of Tubulin-GFP transfected NG108 cells as seen in Fig. 3.1(a). Within these cells, we observe by eye a dense network of microtubule filaments. These filaments are oriented in several different directions within the cell body as shown in the zoomed-in region in Fig. 3.1(b). After preprocessing with a Gaussian filter, we convolve these data with a rotating, anisotropic LoG kernel. Examples of rotations of the kernel are shown in Fig. 3.1(c) (different orientations, i.e. left-learning, right leaning, vertical, in addition to different shades/colors correspond to different angles). Due to the bidirectional nature of the kernel, we rotate the kernel through π radians (as opposed to 2π radians) at a discrete number of angles, a parameter chosen for accuracy and speed. Given data with N columns and M rows, the convolution results in a matrix

with n columns and m rows, where n,m = N-p, M-p (p is defined as the padding size used to avoid artifacts). Edge effects occur when convolving close to the edges of data frames where the convolution is likely to extend beyond the image frame. We fix the padding at 6 pixels based upon observation of edge anomalies. Due to the nature of our data, as discussed later, we desire to retain as much filament information as possible. The kernel for this convolution is described in Eq. (3.1).

$$L(x,y) = \frac{-y^2 + {\sigma_y}^2}{{\sigma_y}^4} \exp\left(\frac{-x^2/{\sigma_x}^2 - y^2/{\sigma_y}^2}{4\pi\sigma_x\sigma_y}\right) \tag{3.1}$$

The anisotropy of the LoG kernel results from the quadratic pre-factor and the different sigma parameters in the Gaussian. To achieve a rod-like object for extraction of filament-like objects, we induce anisotropy in the minor axis ($\hat{y}$) by penalizing for extending in that direction. Indeed, notice that higher values of y corresponds to lower values of L in Eq. (3.1). This anisotropy causes the rapid drop off as seen in Fig. 3.1(c) (notice the color/shade of the rod remains relatively constant while areas far away from the rod in the perpendicular direction are darker). Additionally, the different sigma parameters, σ_x and σ_y regulate the width of the kernel in $\hat{x}$ and $\hat{y}$, which can vary the thickness of the rod furthering the anisotropic effect. After convolution, a matrix with dimensions n,m,a results (where a is defined as the discrete number of angles chosen for kernel rotation); we have then 'a' (N-p)x(M-p) frames and we take the max projection of this matrix in the 'a' dimension to arrive at our final output matrix. Finally, we threshold these maximal values to ensure they correspond to filaments. This output matrix contains pixels which (1) have been

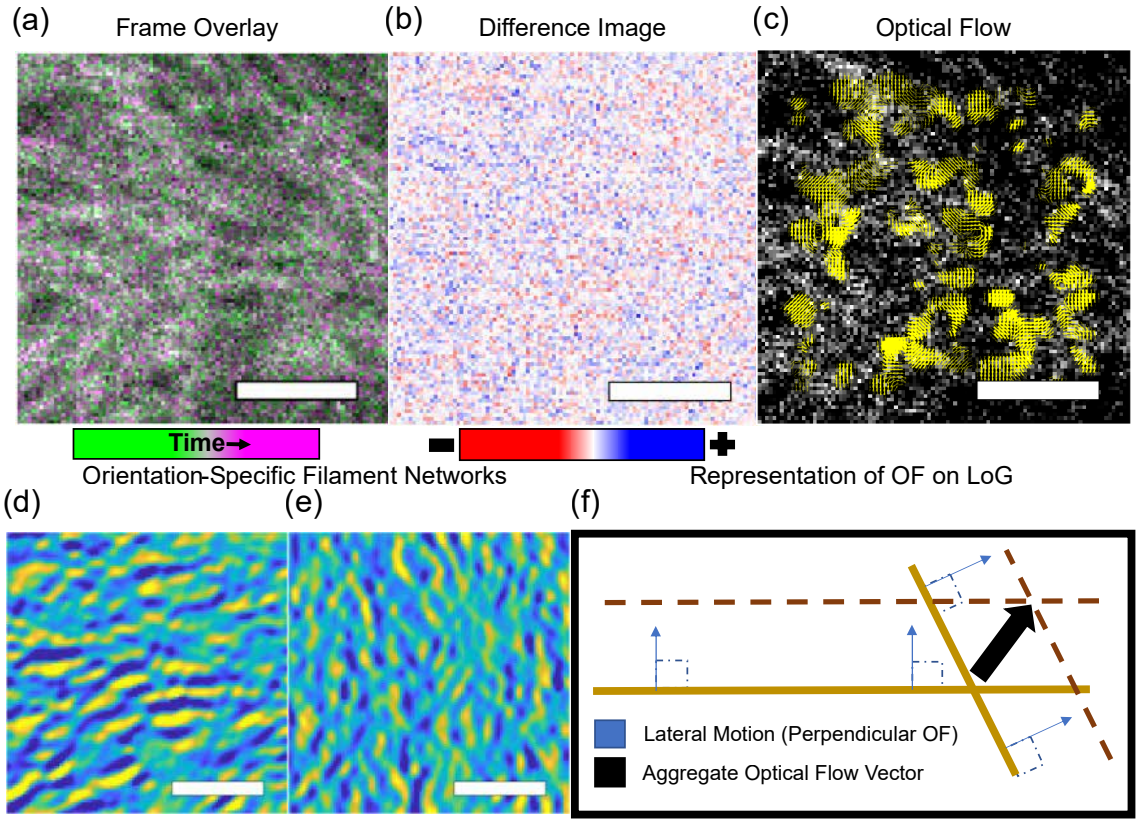

Figure 3.2: Lateral motion of detected filaments is quantified by coupling OF with LoG. (a) Two frames separated by time are shown overlaid on top of each other. The minimal differences between the frames are shown by the green and magenta pixels (grayer shades–lighter from one frame, darker for the other–correspond to differences in either frame, white regions are pixels shared by both frames). (b) The frame overlay in (a) can be better represented as a difference image (a frame earlier in time subtracted from a frame later in time) where the pixels now correspond to the magnitude of intensity changes over time. (c) Using the equation in Eq. (3.2), we generate vectors of motion as represented by the yellow arrows (lighter regions with 'clusters' of activity/arrows). Similarly to LoG, we find local neighborhoods for assessing motion. For our results, we use a kernel width, in both $\hat{x}$ and $\hat{y}$, as 5. (d),(e) These masks showcase horizontal and vertical filaments, respectively. Notice that with our rotating LoG kernel, we are able to separately partition filaments to focus on specific orientations for analysis. (f) This schematic shows filaments in one frame (tan undashed lines) and a subsequent frame (brown dashed lines). Due to the crosslinking of filaments, the overall OF motion would normally be quantified by the larger black arrow. However, since we have access to the filament information (for which the two tan undashed lines are oriented in different directions) we can decompose that larger black vector into components perpendicular to each filament as shown by the smaller blue (lighter) arrows and analyze them separately (and we have access to the different filaments despite the crosslinking based upon the different orientations output). In this regard, we overcome the difficulty of analyzing dense MT networks and assess lateral motion. Scale bars are 3.5 µm.

detected above the threshold, and (2) have an angle, initially in the range [0, 2π], associated with them. An example output is seen in Fig. 3.1(d), where the colors (shades) correspond to the angles in the color wheel in Fig. 3.1(c). Our LoG filtering detects filaments on a pixel basis. The use of pixel-by-pixel detection foregoes the difficulty in tracking a filament with fluctuating length and changing position over time. In this sense the algorithm measures changes in motion but is agnostic as to which filaments are moving or had previously moved. Moreover, our pixel detection method allows us to detect with (sub) pixel accuracy microtubule fluctuation (even for a filament with fixed length). We optimize our filter threshold to select those pixels which belong to noticeable filaments, and to minimize the detected edges which do not belong to filaments in the output data.

3.4.2 Capturing lateral motion of detected MT filaments in dense networks using Optical Flow

We apply the Lucas-Kanade optical flow algorithm onto the preprocessed data. Optical Flow measures the spatial changes in image intensity over time, an example of applicable data for this algorithm is shown in Fig. 3.2(a). The algorithm detects pixel intensity changes between frames, as shown in Fig. 3.2(b), and spatially defines these intensity changes; as such we are given vectors that describe the motion. The OF output for the data shown in Fig. 3.2(a) is produced in Fig. 3.2(c). In this way, we can assess apparent motion within the fluorescently labelled cells. Outputs from OF are a magnitude and orientation matrix, which allow us to understand the

speed of the motion as well as its direction. For a more detailed explanation of OF, please consult [110]. The equation for OF is referenced in Eq. (3.2). We store the magnitude and orientation output from convolution of the dataset with OF. We use the filaments detected by LoG as a mask overlaid upon the OF magnitude matrix. Additionally, we can further partition our LoG output to specific angles of focus, as seen in the horizontal and vertical detected filaments shown in Figs. 3.2(d,e). Only those pixels which contain values (i.e. not NaN values) in both LoG and OF output correspond to bending motion. The metric for bending is calculated by taking the portion of the OF vector perpendicular to the detected filament, as this measures lateral motion. To restate, from the OF vector, we are only using the component of the OF vector that is perpendicular to those filaments detected in LoG (regardless of the orientation of the filaments given from the previously described LoG output). The process is shown in schematic, and the ability to overcome crosslinking filaments is further explained in Fig. 3.2(f). For this reason, we claim we are capturing the lateral motion of microtubules. We achieve this by taking the sine function of the angle between the filament's orientation and the OF vector (i.e. we take the cross product).

$$-\vec{\nabla} I \cdot \vec{v} = \frac{\partial I}{\partial t} \tag{3.2}$$

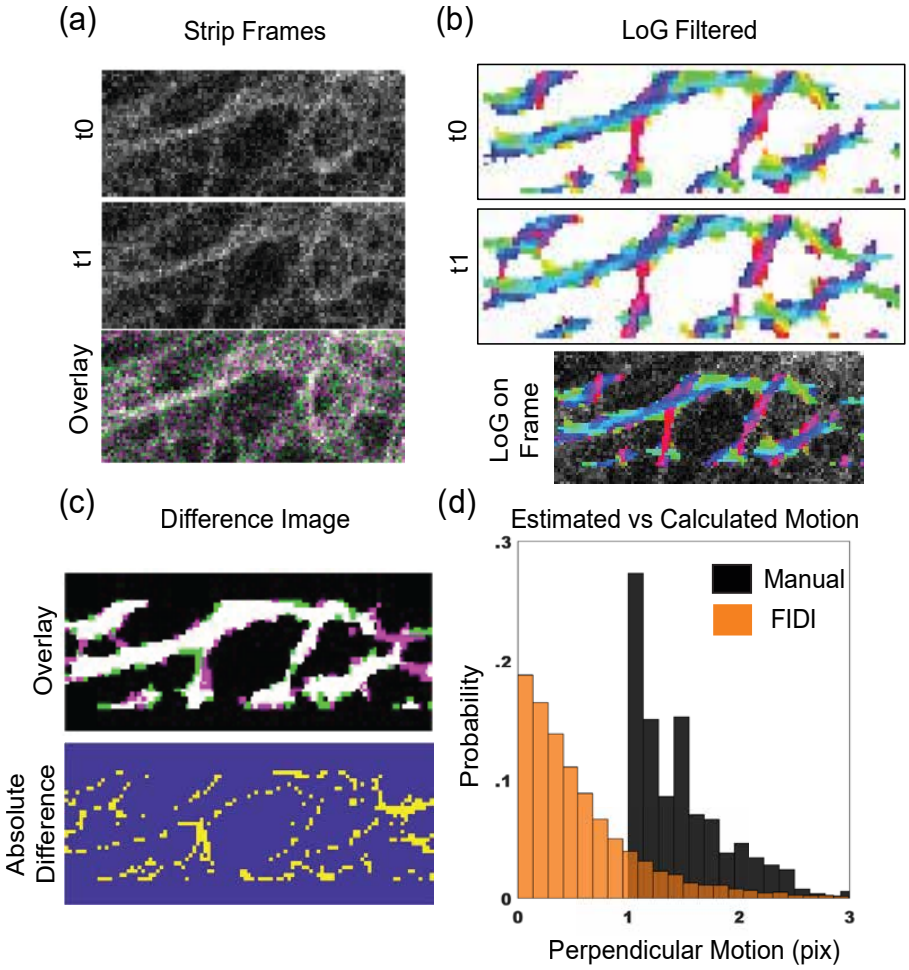

Figure 3.3: Manual verification of FIDI. Comparison of the strips of CHO filaments reveals the small (sub) pixel level movements of these clearly defined filaments. (a) Two frames at difference time points, t0 and t1 separated vertically. The overlay of the two frames shows the differences in movement. Most of this movement is small; pixels from t0 and t1 are identified as green and magenta, respectively (shades more gray but not dark represent regions of activity from either frame; white represents regions of overlap. See (c) for more detail.). (b) For the t0 and t1 frames shown in (a), we show the LoG generated output (different colors and shades represent different angles). The slight heterogeneity of angles within the filaments is due to our pixel level detection of filaments. Overall, however, the general angle of the filament is well-defined by eye. The LoG output overlaid below t1 showcases the agreement of our kernel parameters with the actual data. (c) In order to verify whether our algorithm is assessing motion with realistic output, a difference image of the detected filaments (using the LoG outputs from (b)) is generated. We further notice subpixel level differences. We quantify the area of these objects, which correspond to motion, and take the square root to mimic perpendicular motion relative to a filament. (d) We compare the values of our algorithm with a manual calculation of the square root of difference 'objects' found. We notice that FIDI captures with sub-pixel level accuracy the movements of filaments across frames.

3.4.3 Manual Comparison of Detected Motion

To assess the reliability of our detection of the microtubule lateral motion, we verify outputted values with a manual estimation of movement. As shown in Fig. 3.3(a), the movement of the strips of data collected for CHO cells results in differences that are on the (sub) pixel level. Furthermore, the differences in between the LoG output generated from slices t0 and t1 in Fig. 3.3(a) are minimal, but these differences can still be seen by eye, see Fig. 3.3(b) and Fig. 3.3(c) for comparison. To properly verify FIDI, we binarize the difference image (those values shown in neither white nor black in Fig. 3.3(c)) to arrive at an absolute difference image. This absolute difference corresponds to overall movement of filaments. From this difference image, we use MATLAB's regionprops function to extract an area estimate of all 'objects,' i.e. detected objects correspond to movements of filaments across frames. Since we are interested only in the perpendicular motion of the filaments, we estimate the motion by taking the square root of all objects detected by the regionprops algorithm. We notice that our algorithm accurately captures a majority of the movement in a sub-pixel regime (note, the lower bound of the region props area values is 1). We conclude that the majority of the movements correspond to the curve generated by manual estimation. See Fig. 3.3(d).

3.4.4 Quantifying lateral motion to assess active forcing environments

We use our FIDI tool to assess the active forcing environment of MTs within cells. To achieve the best possible results with our tool, we use strips of areas of

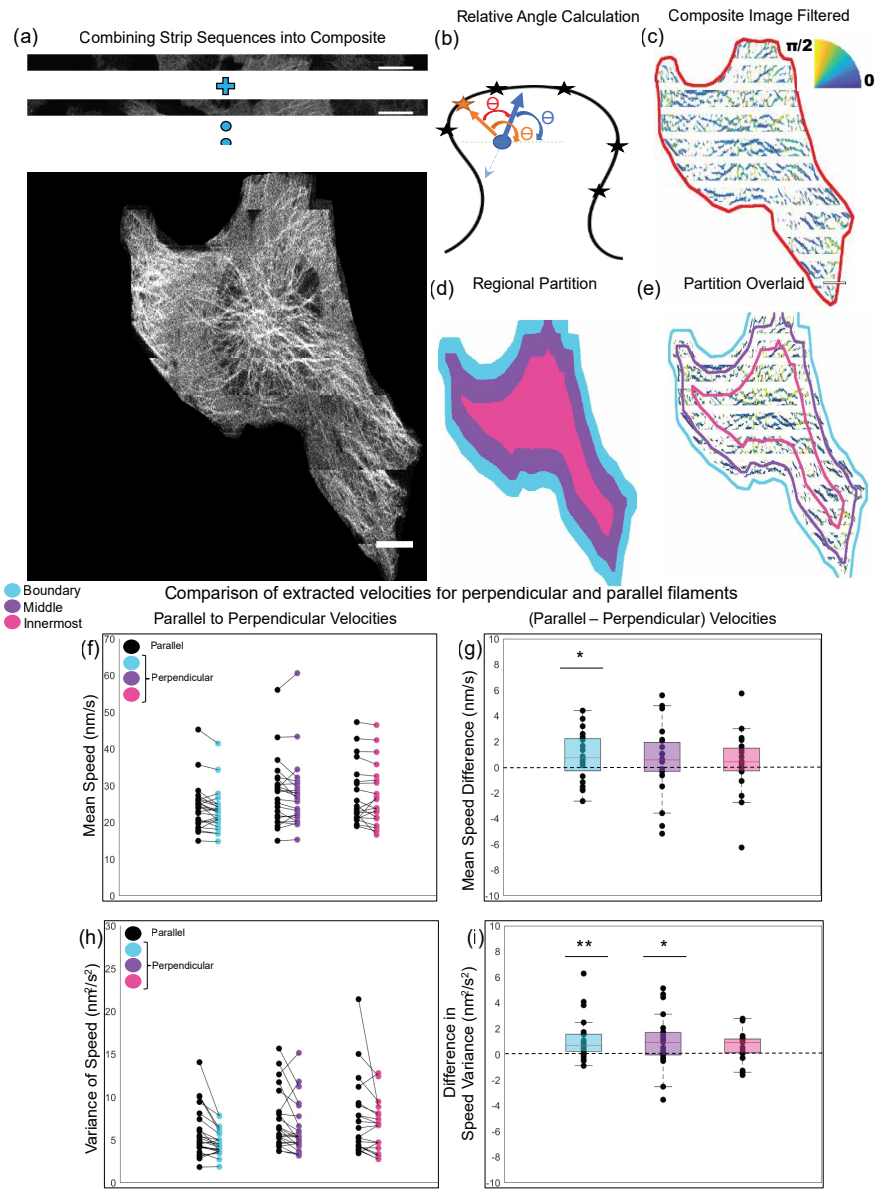

Figure 3.4: Composite dynamic microtubules in CHO cells reveal differences in lateral motion based upon orientation and location. (a) Strips of CHO microtubules are taken. These strips have a higher frame rate and resolution than standard confocal imaging. We concatenate the strips as each strip contains different information of microtubule dynamics. (b) We find each filament's orientation relative to its closest boundary point. Given a pixel's LoG outputted angle, we find the relative angle between the angle created from the vector normal to the boundary and the unit vector created from the LoG angle. (c) The relative angle output from the composite image in (a) is shown. The color wheel displays angle colors corresponding to $[0, \pi/2]$ (d). The composite cell image is used to generate a mask from which angles relative to the boundary of the mask are generated. These regions are not meant to be extact, but to provide a qualitative assessment of regional differences. (e) We show the boundaries of the regions in (d) overlaid on the output in (c). (f) We compare the mean speed of lateral motion for filaments that are considered parallel to the boundary versus filaments considered perpendicular to the boundary. (g) We find that only in the boundary region is there a significant difference. Filaments that are oriented parallel have a higher motion than those perpendicular. (h) We assess the variability of the mean speed across differently oriented filaments for both parallel and perpendicular filaments. (i) We compute the difference in this variability and find a statistically significant difference in the boundary and middle regions. Scale bars are 10 µm.

CHO-K1 cells. This filament motion analysis on dense microtubule networks requires us to use approximately one second frame rates and at least diffraction limited pixel resolution. These strips are small (40 pix x 1024 pix in dimension), and are not taken simultaneously. Since the cells themselves do not change shape significantly during the imaging time, and since the average location of microtubules does not shift very rapidly, we combine strips corresponding to the same cell into an aggregate composite image sequence, as seen Fig. 3.4(a). Since each strip contains different information, we analyze each strip separately while gathering information about the entire object. This step is not a necessary step in the FIDI algorithm. Given our strips of data, we are able to generate 24 composite CHO-K1 cells across 9 independent experiments for this study.

In order to further demonstrate the effects of the forcing environment on cells, we convert the angles of detected filaments to contain more biological relevance. Previous work has indicated that analyzing the orientation of filaments relative to the nearest cell boundary can determine phenotypes within a dataset [89]. For each pixel, we identify its closest boundary point, and then use this boundary point to determine the relative angle between the filament orientation $\theta_{filament}$ and the vector pointing to the nearest boundary $\theta_{boundary}$. The schematic for this conversion is shown in Fig. 3.4(b). Because the filament orientation is bidirectional, we choose angles smaller than or equal to 90 degrees, as shown in the example output in

Fig. 3.4(c).

$$\theta_{\text{relative}} = \min(\{\theta_{\text{boundary}} - \theta_{\text{filament}}\}, \{\theta_{\text{boundary}} - \theta_{\text{filament}} - \pi\}) \tag{3.3}$$

As the strips provide a qualitative depiction of the overall cell shape, we manually create a boundary mask for the composite cell. This allows us to quantify the overall cell boundary using this hand-drawn mask of the cell, which is used to determine the angle and distance to the nearest boundary point. The strips are analyzed separately, which limits the pixels for which we can carry out LoG filter analysis to fewer than 40 pixels wide, resulting in regions of the composite image for which we cannot determine filament orientation, as previously described. We erode the boundary mask to generate smaller regions within the composite cell so we can identify generally where the microtubules in each strip belong globally. Each region generated for this study comprises 1/3 the area of the total composite cell. Each region is depicted with a different color in Fig. 3.4(d). The overlay of these regions on the relative angle output is shown in Fig. 3.4(e). Note, this regional analysis is not necessary for the overall use of FIDI, but we argue that analyzing the microtubules in this fashion leads to more biologically meaningful results.

We analyze the motion of parallel and perpendicular filaments in 3 distinct cellular regions. We take the median value of all filaments of interest (we define perpendicular filaments as filaments whose angles relative to the cell boundary are between 60-90 degrees; parallel 0-30 degrees) for every frame in the composite image sequence, and then compute the mean of the transverse filament speeds for all the frames. Fig. 3.4(f) shows a cell-by-cell comparison of transverse filament speeds for 24

cells, contrasting motion of filaments oriented parallel or perpendicular to the nearest boundary point vector. For each cell we compute mean difference between these mean filament speeds for each region of the cell. As shown in Fig. 3.4(g), we find a small but statistically significant difference in mean lateral motion in the boundary region (p=0.0305). The variability in motion, measured from the variance in the mean distributions is shown in Fig. 3.4(h). Across each region, we notice a more prominent downward trend in speed variability between parallel and perpendicular filaments. In Fig. 3.4(i), we compute the difference in speed variance for each of the three regions in the composite cells. We find that there is a small but statistically significant difference in speed variance in both the boundary (p=0.0028), and middle regions (p=0.0306). These results carry biological importance in understanding that the active forcing environment may change depending upon location within a cell and may differently affect filaments of different orientation (e.g. in the case of torques generated within a cell acting on microtubules).

3.5 Conclusion

The microtubule network of a cell is highly dynamic mechanical structure within the cell that contains vast information regarding cellular properties. The dynamics of this information network need not be limited to the tip dynamics typically studied. As a simple readout of the dynamic state of the microtubule network, we have introduced a method for measuring lateral motion of microtubule networks that can be applied to dense networks. We argue that the lateral motions captured reflect

the active forcing environments generated within a cell body. We can read out the nature of this environment via the MT network. Our method for motion analysis leverages both a rotating, anisotropic Laplacian of Gaussian filtering and Optical Flow in a novel way by analyzing the perpendicular motion of filamentous pixels detected. We propose useful downstream analysis measures to ascertain whether angle-specific regimes work collectively or in competition with each other. We applied the technique to measure microtubule dynamics in CHO-K1 cells and prototyped the method on NG108 cells. We find that standard confocal microscope images have high enough spatial resolution to reveal microtubule orientation, but must be acquired rapidly enough to capture microtubule dynamics. In CHO-K1 cells, we find statistically significant differences between the dynamics of microtubules that are tangent or normal to the closest boundary point. We also find that the dynamics depends on the distance of the microtubule from the cell edge.

FIDI is useful for detection of changes in microtubule mechanics, which is readily perturbed by a variety of chemical, mechanical, and electromagnetic probes. While our analysis cannot differentiate changes in microtubule stiffness from changes in active forcing due to motor proteins, FIDI provides a robust approach to characterize the cytoskeleton, complementing traditional biomechanical measurements that focus on forces and stresses such as AFM. The statistics of microtubule motion are also directly comparable with cellular scale simulations and can serve as an important calibration point for simulations of dynamic biomechanical structures.

Chapter 4: Astrocytes are active: An information theoretic approach reveals differences in Ca^{2+} signaling patterns among distinct astrocyte subtypes

This chapter is adapted from a submitted work by Mennona et al [163]. Nick Mennona performed the experiments, did the analysis, and wrote the paper. Barbara Barile performed the Western Blot verification of different astrocyte physiologies and added to sections on the physiological profiles of the *in vitro* cultures and Western Blot analysis.

4.1 Overview

The discovery that astrocytes are an active, rather than a passive, component of the brain has ushered in a paradigm shift in thinking about how the brain processes information. Although the mechanisms by which astrocytes integrate information from neurons are still debated, such discourse should not distract from the importance of more completely understanding how astrocytes communicate via signals amongst themselves. This work aims to study how different astrocytes signal within their own networks. We investigate group calcium (Ca^{2+}) dynamics in polygonal, stellate, and

reactive astrocytes. These distinct and important astrocyte subtypes are present in the brain to varying degrees at different physiological states. We use an information-theoretic framework to quantify the dynamics embedded in the Ca^{2+} traces within astrocyte networks; specifically, we employ the Hurst exponent, cross-correlation, mutual information, and partitioned entropy to assess differences in the astrocyte signals across subtypes. To gain insights into the ability of astrocyte networks to respond to changes in the extracellular environment, we probe the networks with perturbations affecting their cytoskeletal dynamics (Latrunculin B) and energetic levels (Adenosine triphosphate). Overall, these three classes of astrocytes behave differently and respond idiosyncratically to their extracellular environment. We find that polygonal astrocytes are not quiescent, stellate astrocytes respond most strongly to ATP, and reactive astrocytes are uniquely perturbed by Latrunculin B. Interestingly, despite these distinct differences in behaviors, we find a uniform speed of information transport regardless of subtype or perturbation; this uniformity is maintained when using both cross-correlation and mutual information to assess this speed. We conclude that the differential ways astrocytes signal within our measured framework yield important insights into how astrocytes communicate and contribute to this pressing issue of understanding astrocyte information processing.

4.2 Background

Astrocytes are the most numerous glial cell type in the brain. They are important for physiological functions including K+ clearance [164] , glutamate

homeostasis [165] , and extracellular volume regulation [88] (reviewed in [166]). Since astrocytes carry out these known supporting functions and lack electrical excitability, most studies have overlooked the potential active role of astrocytes in information processing. In contrast, neuronal dynamics has become synonymous with information processing [12, 22, 23, 167–169].

Nevertheless, recent work has provided strong indications that astrocytes do play an active role in information processing. As a counterpart to neurons, astrocytes also form their own networks, linked together via gap junctions composed of connexins, including Cx43, one of the main connexins in astrocytes [98, 101]. Within these networks, astrocytes signal to each other via slow Ca^{2+} waves [74]. IP_3 triggers intercellular (Ca^{2+}) waves [74] which propagate through astrocyte networks via the aforementioned gap junctions. Recent studies reveal that these waves can occur spontaneously, with excitable dynamics similar to action potentials, although on a slower timescale of seconds [92]. Thus, astrocytes can have an active role in information flow, with calcium waves functioning as non-electrical communication signals. In single astrocytes, these calcium waves are heterogeneous [170] and flow through astrocyte processes and microdomains [41, 100, 171]. Methods such as the machine learning tool AQUA now enable robust intracellular analysis of astrocyte calcium [170] for ex-vivo and in vivo analysis of astrocyte activity.

One way active astrocytes may contribute to neuronal information processing is through the tri-partite synapse, by which an astrocyte couples to a synapse, allowing astrocytes to impact information transfer in the brain directly [93]. Indeed, the tight coupling of astrocyte excitability and neuronal activity has become increasingly

recognized and confirmed [172–174]. By linking to multiple synapses, astrocytes could integrate and encode information and modulate neuronal networks and brain cognition by extension [97,175,176]. Astrocyte gliotransmission (information transfer from astrocytes to neurons) has been modeled for synaptic plasticity, memory, and learning [99,118,173,177]. Although gliotransmission has added to the fundamental picture of communication within the brain, much is still unknown about the methods with which astrocytes decode functional transients, [177] and their role in brain function [99,118]

Our work focuses on information flowing directly between active astrocytes and the network scale implications, which have been unexplored [92]. Here, we focus on information flow within astrocyte networks independent of neurons, utilizing physics-based information-theoretic techniques. The current study contrasts three physiologically relevant subtypes of astrocytes, focusing on their collective (ensemble) dynamics within in vitro networks. These *in vitro* cultures remain a powerful tool [92] for analyzing astrocyte dynamics, especially since the current study focuses on how individual astrocytes contribute to the ensemble.

Following established protocols, we study *in vitro* models of polygonal (immature), stellate (healthy), and reactive (immature) astrocytes. Intracellular and extracellular ionic changes are reported to occur upon several physiological and pathophysiological events, including regulation of the activity of chemical synapses, glial scarring [96], synapse plasticity [178], and formation upon neurodevelopment [179]. Anisosmotic challenges are counterbalanced by water flows, which are predominantly mediated by the water channel aquaporin-4 (AQP4) in brain astrocytes [180]. AQP4

is reported to be polarized and enriched in astrocyte endfeet where it plays a key homeostatic role. By modulating water influx/efflux, it ensures a fine regulation of astrocyte cell volume and morphology, thus preserving brain integrity and functionality [180]. In this view, it is not surprising that AQP4 is found to be co-expressed or functionally coupled in astrocyte membranes with ion channels, including potassium (i.e. Kir4.1 [181]) and calcium (i.e. TRPV4) channels [180, 182]. On the other hand, connexins are shown to take part in astrocytes' response to injury upon the stimulation of pro-inflammatory cytokines, including TGF-beta [183]. An increase in the levels of Cx43 in reactive astrocytes is proposed to act as a supporting mechanism that helps maintain astrocytes' gliotic phenotype and maximize the coordinate intervention of these cells and their communication for the injury resolution [184,185].

The astrocyte networks – polygonal, stellate, and reactive – are broadly classified as immature, healthy, and injured, respectively, and have distinct physiological behavioral profiles [41, 75, 186–188]. A key readout of these distinct subtypes is their unique and stark morphologies. The differing structures and morphologies of astrocytes in general have been implicated in brain functionality [86,91,186] and the cell-cell signaling of astrocyte networks [117].

With the goal of broadening our understanding of astrocyte-specific signaling, we quantify the collective dynamics, both spontaneous and perturbed, of these astrocytes. We perturb these in vitro cultures with low-dose Latrunculin B (LATB) and Adenosine triphosphate (ATP) as these represent basic perturbations to the cellular cytoskeleton [189–191], and cellular energy [192–195], respectively. Due to the slow and heterogeneous characteristics of astrocyte calcium signaling, astrocyte

signals are more analog than digital. Neuronal signals are often treated as digital, 1 (firing) or 0 (not firing). Astrocyte signaling is too slow for such binarization. Thus, information-theoretic methods that extract information without digitizing the signal are used. We employ amplitude ordering symbolization with an embedding window large enough to encapsulate the dynamics of astrocyte calcium events, which are mostly on the order of 1-5.5 seconds [92]. Amplitude ordering, rather than binarizing via the mean, is more appropriate for quantifying the dynamic properties of these nonlinear signals. This nonlinearity allows us to elucidate information characteristics and information speeds across polygonal, stellate, and reactive astrocytes in a comprehensive manner.

4.3 Methods

4.3.1 Imaging

Experiments were performed between 14 to 21 (DIV14-DIV21) days after dissection [196]. At this time, astrocytes were trypsinized from flasks and plated into PDL-coated (Sigma-Aldrich) 35 mm dishes (MatTek). Dishes containing cultured astrocytes were incubated with 5μM CalBryte 590 AM (AAT Bioquest) for 30-60 min at 37°C prior to imaging. Dishes were then washed with PBS. Astrocytes are plated at densities such that they proliferate to roughly 500k cells/well on the day of imaging (a final density of approximately 10k cells/mm^2), and imaging was performed on a spinning disk confocal microscope (PerkinElmer). Image acquisition occurred for approximately 15 minutes at roughly 1 frame per second with 100 ms of

exposure time per frame. The University of Maryland Imaging Core maintains the PerkinElmer spinning disk confocal microscope used for this research. The image sequences were taken by the equipped Hamamatsu ImagEM X2 EM-CCD camera (C9100-23B), which records 16 bit images. Sequences were taken from an air 20x objective (0.75 NA; 0.717 μm per pixel) and under temperature (37°C), CO2 (5%), and humidity control.

All experiments are performed in NeuroBasal media (Gibco). We use this media to simulate a neuronal environment, and we found that it allows for spontaneous activity in unperturbed wells (over DMEM). For simplicity, throughout this manuscript this environment is referred to as spontaneous (control). ATP (Sigma-Aldrich) and Latrunculin B (Sigma-Aldrich) were applied immediately upon imaging and at low-dose concentrations of 1.5μM for ATP and 0.5μM for Latrunculin B. Unlike Latrunculin A, the slower depolymerization rate of Latrunculin B allows for perturbation of actin without drastically dissociating the entire astrocyte network. The value of Latrunculin was found based upon testing whether our astrocyte networks were maintained (expressed minimal disassociation) for the 15 minutes duration at the chosen imaging setting (e.g. laser intensity). For simplicity, throughout the rest of this work we refer to Latrunculin B as LATB.

4.3.2 Cell Culture

Primary astrocytes were obtained from Sprague Dawley rats housed at the University of Maryland (in concordance with the recommendations of and approval

by the University of Maryland Institutional Animal Care and Use Committee; protocols R-FEB-21-04). Astrocytes were prepared from 0-to-2 day postnatal (P0-P2) Sprague Dawley rat brains as described previously [89]. Briefly, cortical tissue from each pup was separately dissociated via trituration, filtered, and plated into T25 flasks containing DMEM (ThermoFisher), 15% fetal bovine serum (Benchmark), and 1% pencillin-streptomycin (P/S). After roughly 7 days, in order to generate stellate and reactive astrocytes, the media was changed to either (1) stellate media, which includes Neurobasal (ThermoFisher), 2% B27+ (GIBCO), 5 ng/mL HB-EGF (TOCRIS BioSciences) [41] or (2) reactive media, which is serum-free DMEM to which 10 ug/mL of TGF-B1 was added after 5 additional days in vitro [197]

4.3.3 Cell lysis and Western Blot

Protein samples were obtained as previously described with some slight changes [88]. Briefly, astrocytes grown for 7 days in control, stellate and reactive media were washed in ice-cold phosphate-buffered saline (PBS) and scraped with 300 μL of RIPA lysis buffer (10 mM Tris-HCl, pH 7.4, 140 mM NaCl, 1% Triton X-100, 1% Na deoxycholate, 0.1% SDS, 1mM Na3VO4, 1 mM NaF, 1 mM EDTA and 1× Protease Inhibitor Cocktail). Lysates were vortexed every 5 minutes for 30 minutes and centrifuged at 22,000 for 30 minutes at 4°C. Supernatants were collected and Pierce™ BCA Protein Assay Kit was used to dose the protein content. 5 μg of proteins/lane were dissolved in Laemmli Sample Buffer (Bio-Rad, Hercules, California, USA) added with 50 mM dithiothreitol, heated to 37°C for 10 min and resolved by SDS-PAGE in

10% (for Cx43 detection) and 12% (for AQP4 and GFAP detection) gels prepared with Mini-PROTEAN TGX Stain-Free Precast polyacrylamide solutions (Bio-Rad, Hercules, California, USA). gels were then activated for 5 minutes on a Chemidoc imaging system (Bio-Rad, Hercules, California, USA) and transferred to polyvinylidene fluoride (PVDF) membranes (Merck Millipore, Burlington, Massachusetts, USA). Stain-free signal of transferred blots was collected. Membranes were incubated with blocking solution and incubated overnight with primary antibodies, rinsed, then incubated with the appropriate peroxidase-conjugated IgG secondary antibodies. Protein-specific bands were revealed using enhanced chemiluminescent Clarity Western ECL Substrate (Bio-Rad, Hercules, California, USA) and visualized on a Chemidoc imaging system. The densitometric analysis was performed in Image Lab software 6.1.0 by normalizing the bands to the stain-free blot signal. The Western blot analysis of Cx43, AQP4, and GFAP for the polygonal, stellate, and reactive astrocytes confirms three distinct phenotypes; reactive upregulate Cx43 and AQP4, stellate upregulate AQP4, and polygonal cells do not express any of these markers significantly.

In this work, we investigate astrocytes of three physiological types; a prominent distinguishing characteristic of the differences is seen in the morphological differences. Fig. 4.1 (top) provides representative images of the three classes of astrocytes analyzed in this study. Each astrocyte network does not contain a mix of different cell types and is cultured to maintain a singular physiological expression. For these astrocyte types, we investigate collective Ca2+ dynamics as illustrated in Fig. 4.1 (middle), where multiple frames are overlaid to demonstrate the distribution

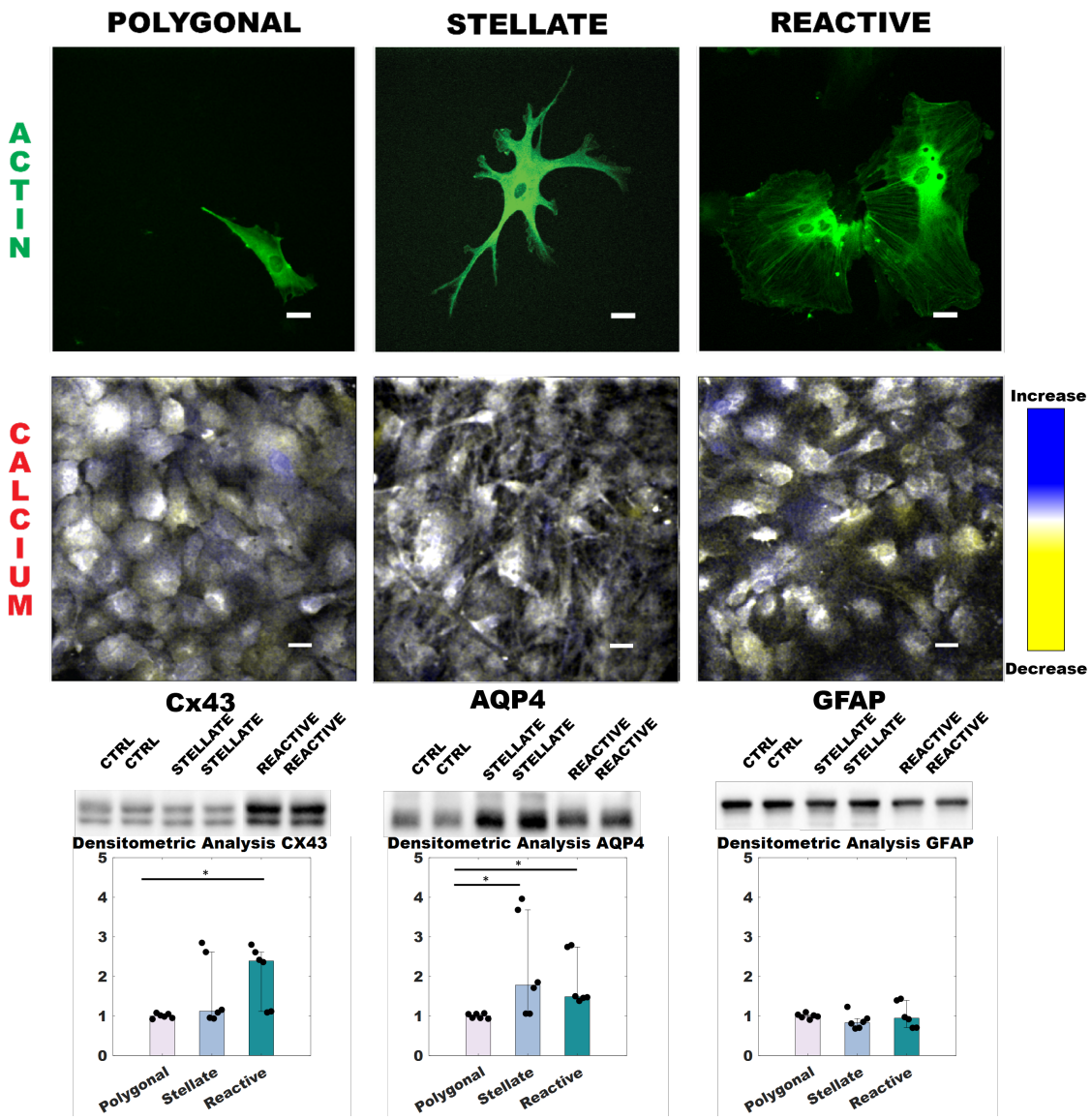

Figure 4.1: Astrocyte morphologies (polygonal, stellate, and reactive). The phenotypes correspond to different morphologies, as shown in green via actin images. Images of actin are acquired with 488nm light of astrocytes that express BacMam Actin-GFP. We record the calcium signaling channels of these dense astrocyte networks with 561 nm light of astrocyte networks stained with CalBryte 590. It has been noted that, regardless of protocol, different media formulations result in different morphologies for astrocytes [41] We use time overlays to show the different manifestations of calcium propagation in the distinct morphological conditions of astrocytes. Blue corresponds to an increase in Ca^{2+} during this frame, yellow a decrease, and white means that this frame contains values similar to the previous timepoint. Western Blot analysis of Cx43, AQP4, and GFAP in polygonal, stellate, and reactive astrocytes. The upper panels show Cx43 (band at $\sim$ 43kDa), AQP4 (band at $\sim$30-32 kDa), and GFAP expression (band at $\sim$50 kDa) in primary rat astrocytes. Using a Kruskal Wallis Dunn's multiple comparison test, we find statistical significance for polygonal compared to stellate (AQP4) and reactive (Cx43 and AQP4). $*p < 0.05$; $**p < 0.01$. Scale bars are 25 μm.

of Ca^{2+} fluctuations (rising calcium in blue, diminishing calcium in yellow) in a network. Through Western blot analysis, we evaluated the expression profiles of 1) Cx43, one of the major isoforms forming astrocytic gap-junctions involved in calcium-mediated cell-to-cell communication, as a molecular marker of intercellular connectivity within astrocytes networks; 2) AQP4, the most abundantly expressed water channel in brain astrocytes, and GFAP, the predominant intermediate filament of the astrocyte cytoskeleton in the CNS, as proxy markers of cell differentiation and reactivity [88, 198, 199].

AQP4 and its supramolecular level of organization in larger-sized assemblies have been reported to correlate with the morphological and functional maturity of astrocytes in CNS postnatal development [200] as well as in in-vitro models of astrocyte differentiation [88]. Therefore, the overexpression of AQP4 in stellate astrocytes is likely to be referred to the morphological differentiation of this cell type in the experimental conditions. The overexpression of Cx43 in the reactive conditions might be ascribable to the acquisition in vitro of the in vivo-like reactive state that makes astrocytes more prompt to tissue healing and wound repair. As for GFAP, besides the number of studies that identified a positive role for these canonical hallmarks of astrogliosis, just as many provided opposite evidence. On one hand, it was previously found to be downregulated in similar or even different models of astrogliosis (i.e., TNF and IL-1 [201–203]) and LPS-treated astrocytes [204]. On the other hand, its upregulation was associated with beneficial and neuroprotective effects (i.e., enhancing neuronal regeneration through protein re-localization; increasing the membrane retention of glutamate transport GLAST in astrocytes, which protects

surrounding neurons from glutamate excitotoxicity [205]); providing scaffolds for new neurites [206]. In the present study, no changes were detected in the three conditions, although we could detect differences in other markers in response to inflammatory (i.e., Cx43) and differentiation stimuli (i.e., AQP4; Cx43). We, therefore, anticipate that GFAP might not be a reliable maker to assess astrocytes' degree of astrogliosis or differentiation.

Western blot analysis shows that the three cell types have distinct expression profiles of the aforementioned astrocyte proteins. Of note, we found that Cx43 is upregulated in the reactive state compared to control and stellate astrocytes (Fig.4.1, bottom left panel), while AQP4 is overexpressed both upon stimulation with TGF-beta and in star-shaped astrocytes, differently from controls (Fig.4.1 , bottom middle panel). GFAP was equally abundant in the three conditions with no statistical significance (Fig.4.1, bottom right panel).

Overall, while illustrating that the proteins undergo distinct changes in their profile expression in response to the different external stimuli provided under culture conditions, these results also provide evidence that the three cell types can be regarded as distinct "phenotypes" from the molecular perspective.

4.3.4 Analytical Methods

To analyze the calcium dynamics of astrocytes, we first segment individual astrocyte objects within our imaging datasets using the morphological watershed algorithm FogBank [207]. Manually, we refined parameters per each imaging sequence

such that segmented boundaries roughly correspond to the distinctions made by eye. FogBank preserves the unique heterogeneity of astrocyte bodies rather than using the cell center with an arbitrary radius, as is typically done with neuron-imaging analysis [208]. See the Appendix for a representative FogBank example. All image sequences are jitter corrected, and Gaussian smoothed in the spatial domain before further analysis. For each frame in a dataset, we take the median fluorescence value from all the pixels identified within the astrocyte object, as shown in the five objects in Fig. 4.2A. We compute relative fluorescence measure (Δ F/F0), where ΔF=F-F0, for each astrocyte object. F0 is computed using a window of approximately 30s (30 frames, 15 back, 15 forward) where F0 is the average of the fluorescence values below the 50th percentile of values contained within the window [209]. This is called a trace. Throughout the paper, we address this fluorescence measure as DF/F for convenience. As seen in representative traces, peaks in calcium dynamics are broad and not well-defined. The sliding window is chosen based on an inspection of the data and does not meaningfully change the dynamic properties of the traces. Please consult the Appendix for more details. We chose this window size based on experimental observation of astrocyte calcium event duration. Examples of such traces are shown in Fig. 4.2B. Recall that astrocytes are not neurons, so it is inappropriate to call the activity of our traces 'spikes.' Instead, we use the term 'calcium event' to describe the smooth rises and falls exhibited by traces in Fig 4.2B.

Our goal is to use traces that show persistent calcium signals and to distinguish them from random fluctuations of signals in the networks. Our goal is to define traces that exhibit smooth and meaningful rises and falls (see red, darker curves

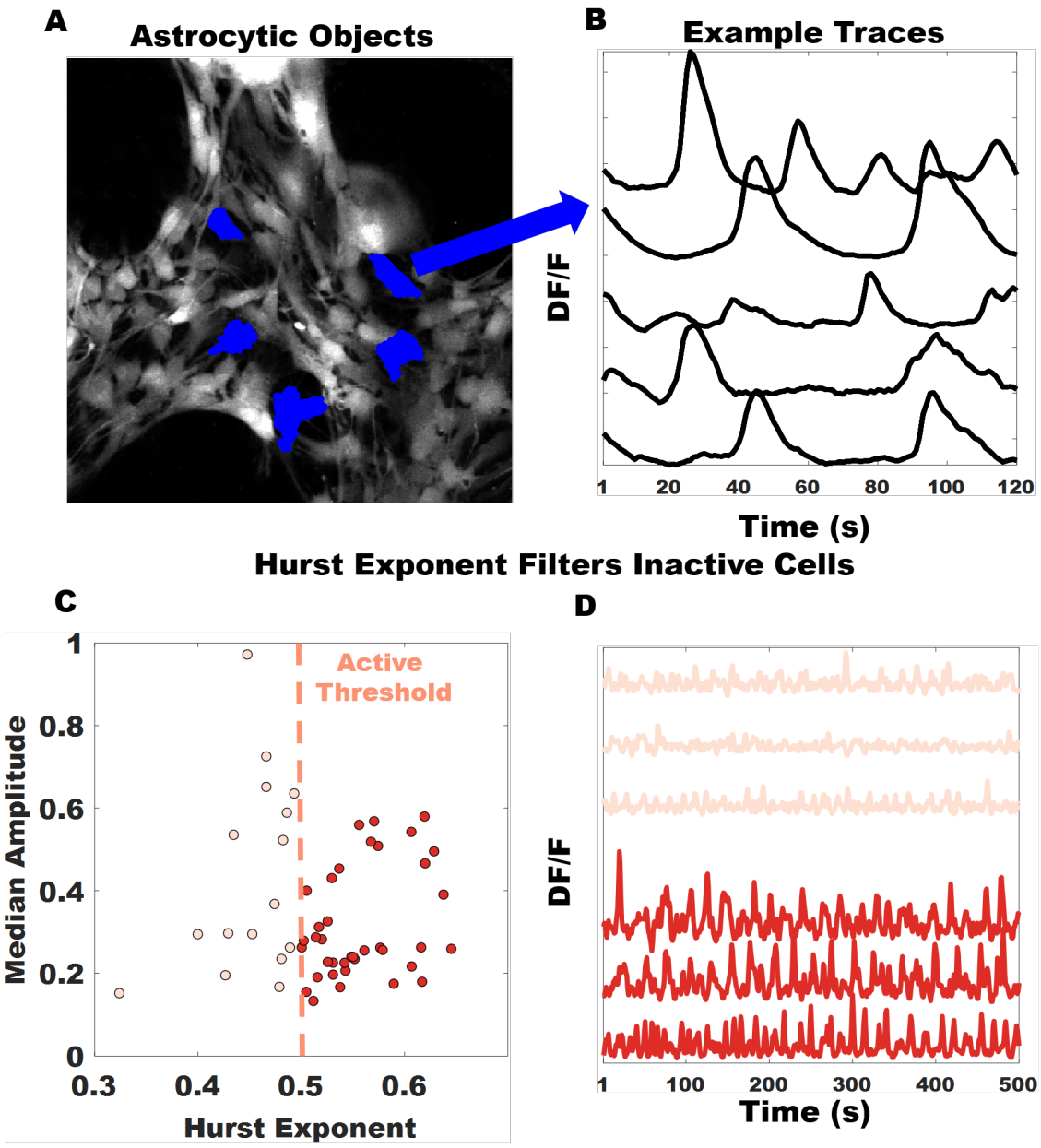

Figure 4.2: Astrocytes traces extracted and filtered using Hurst exponent. (A) Given a dense astrocytic network, astrocytic elements are segmented using FogBank. Examples of astrocytic elements extracted. (B) DF/F traces of the five objects extracted in blue (dark pixelated objects) are shown. (C) Hurst exponent measures memory in a time series, which filters out inactive cells or poorly segmented objects. Inactive (salmon, light) versus active (red, dark) cells plotted. Only time series with Hurst exponents greater than or equal to 0.5 are used. (D) From the example points, we plot representative inactive and active traces.

in Fig. 4.2D) as 'active,' regardless of the intensity values. The Hurst Exponent (defined as H) allows us to carry out this analysis. H is defined for a given time series $x(t)$ as:

$$< |x(t+\tau) - x(t)|^2 > \sim \tau^{2H} \tag{4.1}$$

We find that the Hurst exponent provides a robust and reliable way of filtering out noisy traces due to poor segmentation or weak calcium signals. Hurst exponent values below a threshold of 0.5 represent random activity, and the corresponding traces (e.g., the salmon, lighter colored curves in Fig. 4.2D) are excluded from the analysis [210,211]. The importance of correlations in neuronal encoding is well-cited in the literature [212–215]. The study of correlation in the brain relates to the collective activity of neuronal ensembles in relation to information encoding and processing in the brain. This level of mathematical rigor has not been applied to astrocyte-only networks, and the study of correlation within astrocyte networks has only been viewed in the context of neuronal activation [102]. Given the success of using these methods on neurons and the absence of their use in analyzing astrocytes, we argue that our use of these methods should yield comparable success and insight. Correlations allow us to understand the global characteristics of an ensemble of active nodes (in this case, astrocytes). However, we can alternatively view the dynamics in our astrocyte networks as a dynamical system that is affected by individual astrocytes, i.e., the local dynamics of one trace affecting the global dynamics observed. Since our Western blot analysis confirms cell-cell coupling, we argue that these readouts provide a fairly accurate representation of the information processing performed by these collections

of astrocytes. This approach has been well-documented experimentally (e.g., with neuronal MRI data) and theoretically [216–223]. A limitation of correlations is that the global characteristics of a network are studied by assessing each cell's connections to others in the network. Information theory helps overcome such limitations. An information theoretic approach can analyze a network for each astrocyte rather than for pairs of cells. Thus, this approach provides a robust metric for assessing each individual astrocyte's contribution to the mean field or the group characteristics of the network.

To implement this approach, from the extracted traces, we convert the traces into states using symbolization [216, 224]. This symbolization enables the interpretation of changes in calcium as an analog signal; traces that exhibit lower entropy correspond to traces with more periodic fluctuations. We take the time traces shown in Fig. 4.3A, the amplitude order of each timepoint in a window, and convert this set of timepoints into a state (an example suite of states is available in Fig. 4.3B), and then convert the traces into symbol sequences visualized in Fig. 4.3C. As an illustrative example with a manageable number of states, m=3 has been used (number of states = m!). From the resulting symbol sequence, we can find the probability distributions of states (Fig. 4.3D). The probability of states, in turn, allows us to compute an information entropy for this representation of calcium traces. Amplitude ordering entails choosing two parameters, m, and l, where m defines the embedding dimension [216, 221] (the symbol set size that functions as a coarse-graining window) and l denotes the time lag [221]. A more comprehensive review of this symbolization method can be found in Refs [216, 217, 220–225]. We

choose m to smooth out noise without losing actual spikes in the data. Based on our experimental observation of the duration of calcium events in our data, we chose m=5 and l=1. As m takes the role of the coarse-graining window, l can be kept at its minimum (l=1) to prevent further information down-sampling. Given that we have converted these time series into symbol series, we can perform time-delayed mutual information methods. Time-delayed mutual information is the symbolized equivalent of cross-correlation. Moreover, given that astrocyte signals are nonlinear, mutual information is a more appropriate method than Granger causality [226]. While there are some similarities between mutual information and cross-correlation, we emphasize that mutual information discusses the dynamics of symbols (with embedded dynamics) from a probability distribution. Cross-correlation looks at the absolute fluctuations from the mean for traces. In some regards, then, symbolization can be viewed as the differential expression of trace dynamics. Lastly, from both of these measures, we can quantify the speed of information transport [227]. We can measure speed from the measured distances between astrocytes and either the cross-correlation time lag or the time lag associated with the mutual information measurement.

Additionally, we analyze the information content of astrocyte networks with partitioned entropy. Partitioned entropy $h_a(\tau)$ is a useful metric for understanding the time-evolution of states over a certain window [225]:

$$h_a(\tau) = -\sum_{i=1}^{m!} \rho_{ai}(\tau) \log \rho_{ai}(\tau) \tag{4.2}$$

where $p_{ai}(\tau)$ represents the probability that the system evolves from state a to

state i at τ timesteps. Partitioned entropy differs from canonical entropy as it is a function of time. We employ this approach to better understanding how the ramps and falls of these calcium fluctuations evolve differentially for all of the cells within the unique networks. A schematic for understanding partitioned entropy is shown in Fig 4.3E. We validated this analysis on both regular and chaotic time series data [225]. See Appendix for details. As a clarification, we note that the symbolization, as described, enables analysis of Shannon entropy. The rest of the analysis refers to Shannon entropy and the dynamics therein, e.g., partitioned (Shannon) entropy.

4.4 Results

4.4.1 Astrocyte Speed of Information Transport

An important metric for assessing how astrocyte transport information is information speed. This ad-hoc (average) metric is extracted for free by any time lag calculation. We do not track calcium flow, but can track the exchange of information as a function of time and distance between cells. This method has been used for mutual information [227]; we extend it for cross correlation since the time lag associated with maximal cross correlation is similarly extracted. Our measure of speed is average (v= DIST/τ), it coarsely reveals the rate at which these pairwise quantities are absolutely maximized, reflecting the nature of the timescales associated with astrocyte calcium events. Additionally, the maximal time lags found are rate-limited by the acquisition speed, which is 1 Hz. Due to the 1 Hz frame rate and other coarse graining involved (e.g. distance is computed from center of mass

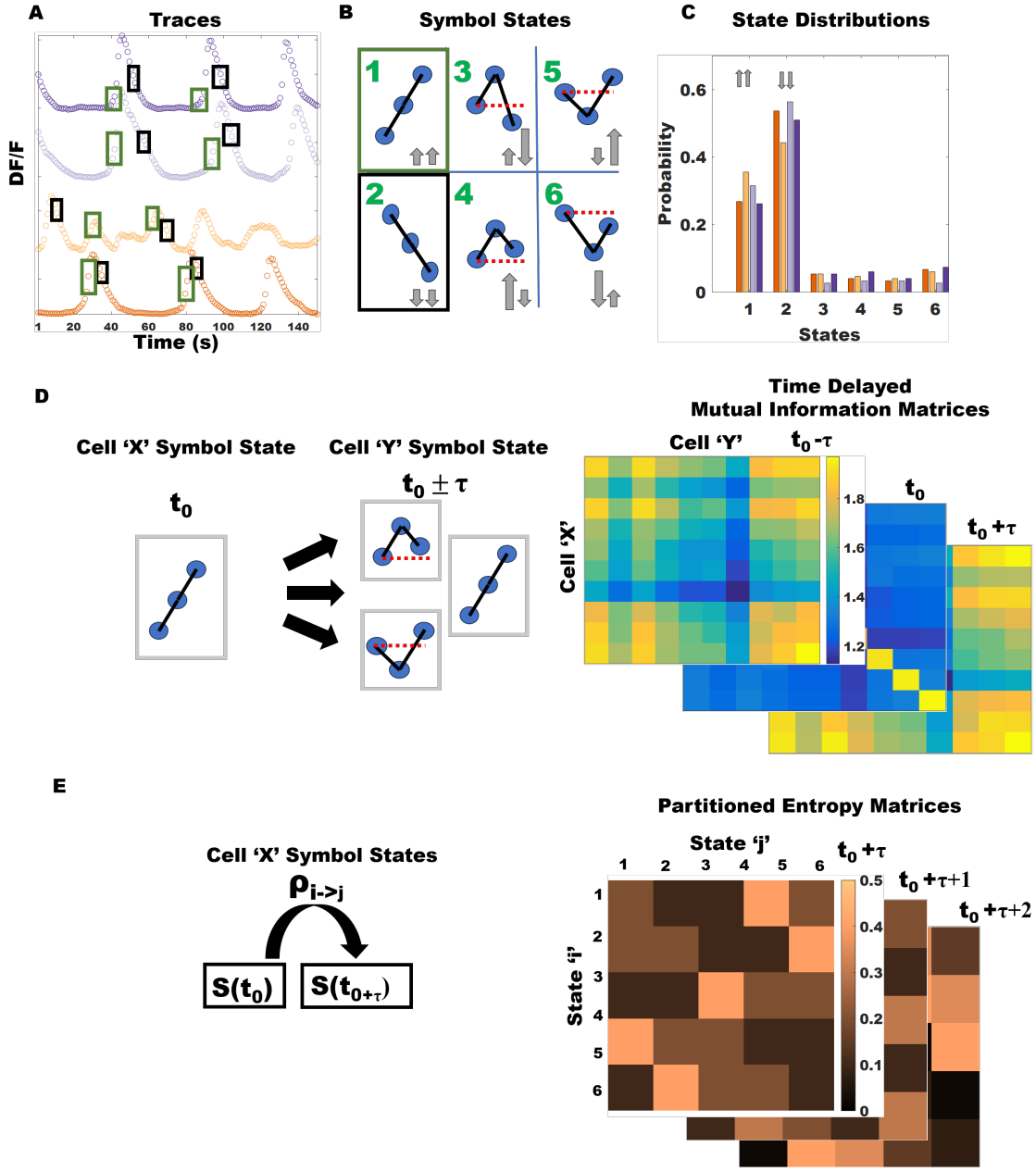

Figure 4.3: Methods for Information Theoretic Approach to Collective Astrocyte Dynamics. (A) Astrocyte traces. Different shaded boxes correspond to example symbol states. (B) Symbol states. Shaded boxes are those previously overlaid on traces. In this figure, have used an m of 3 as this corresponds to 6 possible states for every time window ($m! = 6$). We note, using grey arrows, the physical dynamics behind each state (for states 1 and 2, the same size for the arrows is for visual purposes). (C) Symbol sequences for the traces shown previously. (D) Visualization of Time-Delayed Mutual Information. (E) Example subset of transition probabilities from states to future states for some given tau for any particular state 'i'. See Equation 4.1 for more details. This subfigure represents partitioned entropy.

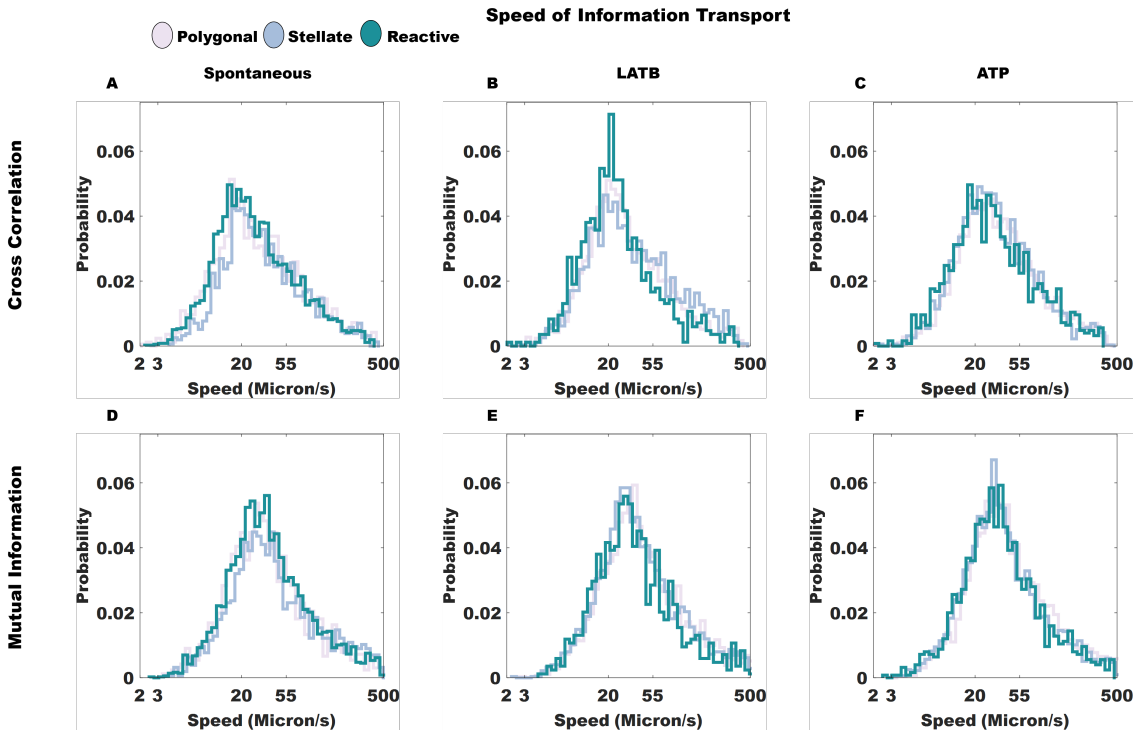

Figure 4.4: Figures shown for all distinct subtypes of astrocyte. Cross correlation speeds are shown for (A) spontaneous, (B) ATP, and (C) LATB affected networks. Mutual information speeds are displayed for (D) spontaneous, (E) ATP, and (F) LATB affected networks. Due to the skewed nature of all distributions, these distributions have been log-normalized. We find the speed of information transport is invariant across astrocyte subtype and extracellular environment.

points in a segmented image), this measure is an average metric. Thus, we conclude that a few micron per second difference is not significant to ascertain any meaningful discrepancy from a biological perspective.

We describe the cross-correlation speeds first. The distributions are modelled as a lognormal distribution to obtain the mean speeds to follow as shown in Figs 4.4A-C. Outliers at infinity are removed (which may happen for time lags of zero). We report the mean of these distributions modeled under lognormal assumptions. The spontaneous speeds are: for polygonal 25 μm/s, for stellate 28 μm/s, for reactive 23 μm/s. Under LATB, for polygonal 25 μm/s, for stellate 27 μm/s, for reactive 21 μm/s. With ATP, for polygonal, 29 μm/s, for stellate 28 μm/s, for reactive 25 μm/s. As expressed in Figs. 4.4A-C, these distributions are not symmetric (not entirely lognormal). Given that the order of difference between stellate and other networks is 5 μm/s at most, and the distributions themselves retain similar characteristics (the distributions peak within this 20-30 μm/s range consistent with experimental studies), we conclude that the speed of information transport is invariant across astrocyte subtypes and conditions.

Next, we report the mutual information speeds. The spontaneous speeds are: for polygonal 28 μm/s, for stellate 32 μm/s, for reactive 30 μm/s. Under LATB, for polygonal 34 μm/s, for stellate 32 μm/s, for reactive 29 μm/s. With ATP, for polygonal 34 μm/s, stellate 30 μm/s, and reactive 29 μm/s. These mean values are reported from modeling the distributions as lognormal. We conclude that the apparent differences between the reported mean values are minimized for mutual information speeds. The speeds are slightly higher than those of cross

correlation. All speeds are in the 30-35 μm/s. This range is roughly consistent with the cross-correlation speeds (at the higher end), and is consistent with the reported literature.

Largely, we find a constant speed of information transport across conditions and types. Using this metric (defined as the distance between objects divided by the time lag associated with the maximization of pairwise quantity), we find that all distributions sharply peak similarly within the reported experimental range for calcium wave speeds. The nature of these distributions across both subtype and conditions suggests an invariance of the speed of information transport in astrocyte networks using this coarse approximation. The similarities in the relationships between the distributions for the quantities (mutual information and cross-correlation are similar but differently formulated) reflect that the aggregate relationships between calcium signals for astrocytes are independent of subtype and perturbation. This counter-intuitive result suggests that astrocytes regulate ions' flow despite cellular state, and maintain homeostasis in stressful environments to maintain signaling speeds.

As a final remark, we comment that the time-lags associated with either maximal cross-correlation or mutual information may come from a symmetric peaking in a time-lag curve (i.e. bimodal peaks about the y-axis). We argue that many of the time lags reflect a maximal value over a relevant physiological window. All other lags reflect a mode within the time-lag curves themselves. This argument is expanded in the Supplement.

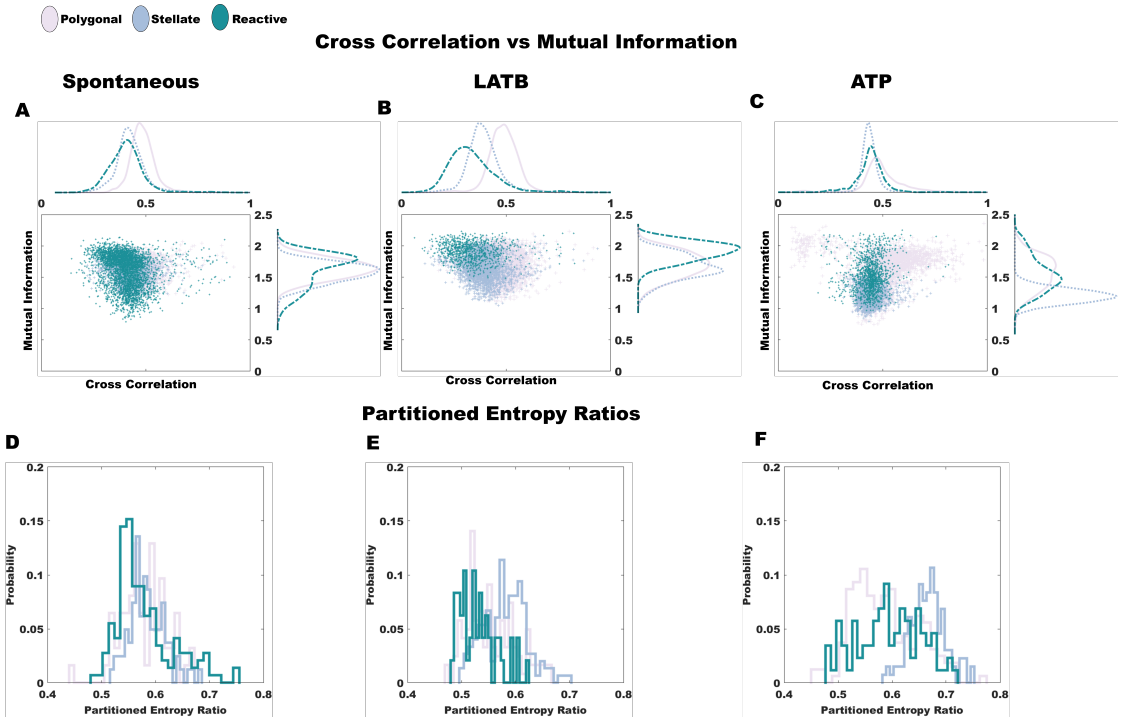

Figure 4.5: Cross correlation versus mutual information, and partitioned entropy comparisons. We compare the distributions of both maximal cross correlation and maximal mutual information across time for (A) spontaneous, (B) LATB-induced, and (C) ATP-enhanced astrocyte networks. Each point represents the cross correlation (x-axis) and mutual information (y-axis) for the same pair of cells. We then look at the dynamics of individual traces using partitioned entropy for (D) spontaneous, (E) LATB-induced, and (F) ATP-enhanced networks. Partitioned entropy ratio is the average of the partitioned entropy divided by the entropy.

4.4.2 Information exchange of signaling amongst active astrocytes

Next, we assess how the traces in astrocyte networks can be used to infer relationships across pairs of cells. Given a time window of 31 frames (roughly 31 s), we find the maximum cross-correlation and mutual information values. These relationships are shown in Figs. 4.5A-C. First, we discuss the cross-correlation distributions. In spontaneous conditions, polygonal astrocyte pairs have higher cross correlation subtype, but stellate and reactive pairs demonstrate comparable distributions (Fig. 4.5A). When LATB is introduced into the astrocyte networks; the distributions are separable indicating that the breakdown of the actin cytoskeleton causes idiosyncratic (i.e. each astrocyte network varies its distribution relative to its spontaneous profile) changes to astrocyte subtypes (Fig 5B). When ATP is introduced, all distributions curves aggregate (Fig. 4.5C). The effect of ATP suggests a minimization between the global differences in astrocyte populations. This minimization is reflected in the strongly overlapping distributions.

Next, we discuss mutual information. In spontaneous conditions, we find that the distributions for the astrocyte polygonal and stellate astrocytes are similar (and lower than reactive). These results suggests that spontaneously polygonal and stellate astrocyte behave more independently than reactive astrocytes (Fig. 4.5A). When LATB is introduced, all mutual information curves are shifted higher with reactive astrocytes retaining larger values while polygonal and stellate astrocyte pairs are similar (Fig. 4.5B). Interestingly, this result indicates that a breakdown in the cytoskeleton causes uniformity in local behavior in astrocyte interactions (i.e. higher

values of mutual information reflect less independence). When ATP is introduced, stellate astrocytes respond the most strongly (Fig. 4.5C). Stellate astrocytes become strongly independent in terms of their local behavior. While stellate astrocytes respond the most strongly, all astrocyte subtypes become more independent (lower mutual information) when exposed to ATP.

4.4.3 Partitioned entropy highlights temporally local dynamics

We look at the partition entropy ratios for astrocytes in networks. Unlike with cross correlation and mutual information, partitioned entropy is a method for analyzing the dynamics of individual traces themselves (i.e. it is not a pairwise analysis method). Moreover, it provides more ability for understanding of information dynamics than entropy alone. Partitioned entropy ratios are calculated by finding the average partitioned entropy across some time window (in this paper we chose to start at $\tau = 10$ and end at $\tau = 150$, see Supplement for details). Values of partitioned entropy closer to 1 are classified as chaotic whereas values closer to 0.5 are deemed limit cycles. Classifying astrocytes in this way is beyond the scope of this work, but it useful for further distinguishing dynamical profiles of the subtypes.

We find that spontaneously, astrocytes retain similar individual characteristics, as demonstrated in Fig. 4.5D. This result is surprising given the numerous reported physiological differences in these subtypes. Coupled with some similarities across subtypes in the pairwise interactions results, we argue that, in spontaneous conditions, when astrocytes signal it is similar. This result suggests a universal characteristic

to spontaneous astrocyte calcium events. LATB, comparable to the distinct effects in pairwise interactions, causes reactive astrocyte to behave more sinusoidally (Fig. 4.5E). Stellate astrocytes respond with higher partitioned entropy ratios. Lastly, where LATB induces the strongest separation in cross-correlation distributions, ATP seems to induce a comparable outsized effect in the partitioned entropy curves shown in Fig. 4.5F. The different perspective (focusing solely on the individual embedded dynamics) provided by partitioned entropy complements the results mentioned above in ascertaining the nuanced differences in astrocyte calcium signaling.

4.4.4 Wasserstein distances enhance interpretability of comparisons

We use the Wasserstein distance (Wasserstein-1) for enhancing the interpretability of the distribution differences shown in Fig 4.5. Wasserstein-1 quantizes the differences in distribution by calculating the average of the minimum amount of distance needed to shift each point in a distribution to match another. This Wasserstein distance can be considered an 'earth mover's distance. Consider histograms as piles of dirt in which some displacement must occur such that both piles look identical. The Wasserstein distance quantifies such displacement. It is useful for understanding the differences in collective dynamics across distinct physiological subtypes of astrocytes. The Wasserstein distance is more robust than the Kullback-Leibler divergence as the former is symmetric (e.g., the difference between entropy distributions for polygonal and stellate astrocytes is identical to that for stellate and polygonal astrocytes) whereas the latter is not. For the results in Fig. 4.6, we bootstrap results from the

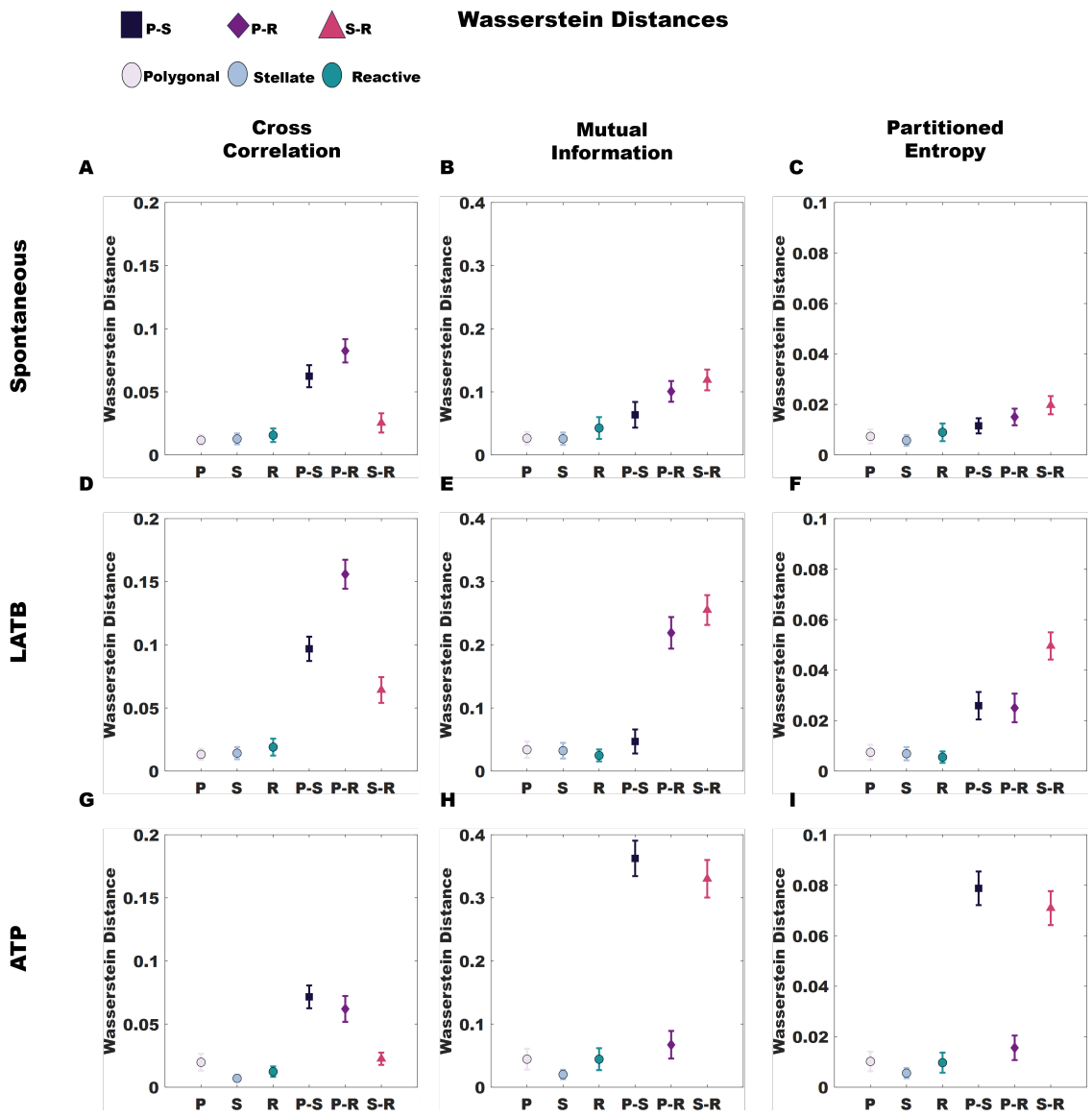

Figure 4.6: Wasserstein distances for the three classes of distributions shown in Fig 5. Astrocytes types are grouped; three pairs exist as highlighted by the dark (polygonal-stellate), purple (polygonal-reactive), and pink (stellate-reactive). We contrast these groups against the natural variance within the individual subtype distributions. We find the Wasserstein distances for: spontaneous (A) cross correlation (B) mutual information, and (C) partitioned entropy distributions, LATB exposed (D) cross correlation (E) mutual information, and (F) partitioned entropy distributions, and ATP induced (G) cross correlation (H) mutual information, and (I) partitioned entropy distribution. Results are bootstrapped.

aggregate distributions. Bootstrapping was performed with a sample size of 100 and 10,000 iterations. We proceed starting with the Wasserstein distances under spontaneous conditions.

Under spontaneous conditions, polygonal cross correlation values are the most distinct (Fig. 4.6A). Using symbolization, we find that the differences between the P-S and S-R Wasserstein distributions are significant relative to each other for mutual information (Fig. 4.6B) and partitioned entropy (Fig. 4.6C). Thus, we conclude that on a global interaction perspective, polygonal dynamics behave the most uniquely, on a local level (using the embedded symbol states to understand dynamics) we find that spontaneously stellate astrocytes have a unique dynamical profile relative to the other subtypes. The ability of information theory to tease out this result is significant. Both stellate and reactive astrocytes possess branches [72]. The process formation could have implicated such processes in the similarities seen in their cross-correlation distributions.

Relative to spontaneous conditions, LATB increases the differences in the distributions for cross-correlation (Fig. 4.6D), mutual information (Fig. 4.6E), and partitioned entropy (Fig. 4.6F). Where again, we see that polygonal astrocytes on a global level are the most distinct relative to stellate and reactive astrocytes (Fig. 4.6D), we find that in the mutual information distributions, P-R and S-R, reactive astrocytes separate the most strongly relative to these subtypes. This suggests reactive astrocytes are more susceptible to cytoskeletal perturbation. The strongest separation in terms of individual trace dynamics is seen in S-R (Fig. 4.6F) suggesting a strong difference in effect when healthy versus unhealthy astrocytes are exposed to

LATB.

Lastly, it is interesting that the highest reported Wasserstein distances for mutual information (Fig. 4.6H) and partitioned entropy (Fig. 4.6I) are found under exposure to ATP. The lowest differences are attributed to the cross-correlation (Fig. 4.6G). Unlike previous results, this suggests that although ATP may cause an entire network to become energetic (i.e. hyper-active), reflected in the cross-correlation similarities, information theory enables a more nuanced readout of dynamical differences. Surprisingly, the lowest Wasserstein differences (across all conditions) are reported for P-R. Indeed, this result indicates that stellate astrocytes are the most susceptible to ATP intervention whereas polygonal astrocytes share the unhealthy characteristics of reactive astrocytes.

4.5 Discussion

Collective astrocyte dynamics are rich in information distinct from neurons and previously overlooked. Starting from filtering out inactive traces with the non-biased Hurst exponent, we employed cross correlation, mutual information, and partitioned entropy to ascertain the dynamical properties of collections of maturing (polygonal), healthy (stellate), and injured (reactive) astrocytes. This behavior characterization extends to these astrocyte networks defined by distinct states (subtypes defined by differences e.g. in molecular expression, morphology) and when either the energy (ATP) or biomechanics (LATB) of the system is altered. Interestingly, this focus on information differences allowed us to demonstrate uniformity in the speed of informa-

tion transport across astrocyte subtype and extracellular environment (ATP/LATB). Our analysis on these astrocyte networks handles the complex spatiotemporal patterns present in these data. Not merely regarding the calcium signaling of astrocytes as an adaptive mechanism, our work argues that the spatiotemporal patterns embedded in these networks are active. That these patterns themselves are sources of dense information rivaling neuronal networks. The spatiotemporal patterning of spontaneous astrocytes is shown in the Appendix.

A principal finding of this work is the corroboration of astrocyte signaling (Ca^{2+} waves) speed using information theoretic methods. Using cross correlation and mutual information on analog astrocyte traces, aggregating traces from independent image sequences, we find an invariance of the speed of information transport. We discovered that for all conditions investigated, the speed of information transport is approximately 25-40 μm/sec, consistent with the speed of Ca2+ waves measured directly in prior studies [196, 228, 229]. These findings are independent of astrocyte subtype and chemical milieu, which strongly indicates that Ca^{2+} waves are the primary mechanism of astrocyte-to-astrocyte information exchange, i.e. Ca^{2+} dynamics is a dominant form of communication in astrocyte networks for all states and environmental conditions investigated despite differences in molecular expression, information processing, and the biochemical cell-cell coupling machinery (AQP4, Cx43). Given that we will subsequently discuss the differences in information dynamics, this result is even more startingly. Confirmation of the speed of information transport with previously reported values lends confidence to using these methods for understanding astrocyte signals.

We preface subsequent interpretation of our results with subtle distinction between the competing pairwise information theoretic concepts in this work. Correlation (of which cross is the most appropriate for astrocyte signals, see Supplement for more details) deals with the specific similarities of mean field fluctuations of the traces. One way to understand this subtle concept is that pairwise correlation values relate to the absolute coarse-grained differences between points in a time series. Accounting for the time lag to maximize correlation, in the context of astrocyte signals, it describes how similar the calcium events look; the average area overlap of all calcium events. Mutual information, supported by symbolization, is more focused and able to provide more local descriptions of how symbol state influences across time series71Both are important, and our results, such as the marked separation between cross-correlation LATB distributions, indicate that both provide a holistic ability to compare astrocyte dynamics. Indeed, an externality of these results, including the use of partitioned entropy for comparative analysis, is a demonstration of the varied insights that are gained by using this complete set of information theoretic tools.

Importantly, polygonal astrocytes in control conditions (spontaneous), which have been regarded as quiescent, [41] exhibit information processing; in other words, polygonal cells are not inactive cells and have complex signaling patterns. The difference between these polygonal cells, and stellate and reactive astrocytes at first lies in the global correlation structure amongst polygonal astrocytes. As shown in Figs. 4.6A,D,G, polygonal cells are the most distinct with higher cross correlation values than stellate and reactive astrocytes. As correlation is a global averaging of time values, this suggests that the mean field behavior of polygonal cells is more coupled

than those of stellate and reactive astrocytes. In other words, polygonal astrocytes broadly have more global network synchrony. These insights are counterintuitive as the higher expression of the astrocyte markers regulating cell-cell coupling, AQP4 and Cx43, seen in stellate and reactive astrocytes (Fig. 4.1) suggest that these cells would couple more closely in their information processing. One possible explanation is that the lower expression of coupling proteins limits the signal propagation to fewer polygonal neighbors and thus, paradoxically, these polygonal networks are globally more aligned. Future studies will investigate this possibility.

Locally, we gain additional insights into stellate and reactive signaling dynamics using symbolization which embeds the dynamics. We conclude that reactive astrocytes respond most strongly to cytoskeletal perturbation (LATB) whereas stellate astrocytes react most strongly to additional energy (ATP). These results are consistent with the role of the cytoskeleton and ATP in reactive and stellate astrocytes, respectively. Reactive astrocytes must have a dynamic cytoskeleton as they migrate to form the glial scar, an adaptive function in response to injury or disease [79, 86]. Stellate astrocytes communicate via more localized contacts, and ATP is suggested to be an important extracellular messenger for specifically stellate-like calcium waves [230, 231].

The science of causality is a burgeoning field due to the pioneering works of Judea Pearl [232]. The rungs or levels of causation are classified as associative (probabilistic), interventional (manipulative), and counterfactual (imaginative). Our pairwise calculations are associative. The partitioned entropy calculations upon ATP and LATB stimulation are interventional. Interventions for pairwise calculations

could include fixed staining after calcium imaging to assign known gap junction connected cells. Counterfactual association could include specific biomarker knockdowns or additional gliotransmitter incubation (e.g., calcium imaging upon exposure to GABA).

Overall, our work shows that applying information theoretic tools to *in vitro* astrocyte networks lends insights into the collective action of astrocytes. Generally, our work has analyzed the complex spatiotemporal characteristics of polygonal, stellate, and reactive networks. We find that polygonal astrocytes are not quiescent, stellate astrocytes respond most significantly to ATP, and reactive astrocytes are affected by LATB. Our study also provides a systematic baseline of three complementary astrocyte states and key perturbations supporting future studies of astrocyte network function in health and disease. The successful demonstration of our method across numerous astrocyte conditions and microenvironments suggests broad applicability and promise for these tools to study analog astrocyte dynamics.

Chapter 5: Partitioned informational interactions within stellate astrocyte networks: An in-depth analysis of rising and falling entropy

This chapter is based on a work in preparation by N.Mennona.

5.1 Overview

The heterogeneity of calcium (Ca^{2+}) signaling in stellate astrocytes has been developed via the advance of calcium markers and machine learning techniques. The use of information theory to understand the physical dynamics encoded within astrocytes as both a metric for comparison and for understanding of astrocyte signals has only recently garnered interest. Here, we focus on the information embedded within stellate astrocytes across their cell bodies and processes. Stellate astrocytes in vitro are rich in enchanting morphology which shows marked networks of entangled processes and cell bodies. We develop an understanding of information propagation through both 'regular' and 'time reversed' partitioned entropy. In addition, we 'group' entropies from 'calcium events' by modifying amplitude-ordered symbol sequences to provide more interpretable variations of symbol states that contain

biological relevance. It is found that information varies between processes and cell bodies for stellate astrocytes. Given that most research in both neuroscience and 'astrocytescience' focuses solely on information (e.g. correlations) for cell bodies, the implications of this study provide insights for both understanding the differences in signaling networks, and future development and design of experiments and theory for astrocyte signaling.

5.2 Background

The brain, using both astrocytes and neurons, performs information processing. Given the incredible increases in image resolution and more sophisticated sample preparation, researchers are now endowed with a remarkable level of cell-scale detail. This detail has enabled investigations into the rich structural heterogeneity within both astrocyte and neuron morphology. It is imperative to use these intracellular scales now afforded in image sequences to understand better how astrocytes process information.

At a high level, neuronal networks sense and integrate information across networks via their somata (cell bodies), synapses (links between soma), and dendrites (long, thin processes protruding from the soma). Within neuroscience, the information processing and interactions are largely focused on two main components: cell bodies and synapses. Within ex-vivo and in-vivo imaging sequences, neuronal soma can be modelled as point particles using difference of gaussians filters, which confer a circular region of activity [233]; resultant correlations are based solely on the

dynamics of neuronal cell bodies. The introduction of synaptic links between somata has generated immense development in neural networks. With the goal to understand how the brain abstractly generates representations [234], neural networks can "learn" (have memory) through these connections between neurons represented as nodes [235]. Recently, it has been called into question whether somatic activity is driving the dynamics of these networks; are synaptic dynamics, modelled by link weights (strengths), the driver? [236]. None of these important studies focus on the information embedded within the rich heterogeneity of these cells. There is a small but growing body of work devoted to understanding how the intracellular excitability of neurons contribute to the information processing within these networks. Neuronal dendrites are thin processes emanating out of neuronal soma. And this body of work demonstrates, both experimental and computationally, that these thin processes perform information processing in idiosyncratic ways relative to somata. Fascinatingly, dendrites are different in their dynamic; the whole neuron is not isotropic. Dendrites compartmentalizes electrical signals differently relative to neuronal cell bodies. [237, 238] Accordingly, their calcium signaling is equally distinct [239, 240]. This noted uniqueness of dendrites has been used to argue that the computational processing credited to the somata-synapse duality may result more from the dynamics of dendrites. [241–244] Acknowledging the hidden information embedded in dendrites, astrocyte processes may contain an equally important role in the information processing of astrocyte networks.

Astrocyte processes have been implicated in synaptic modulation, with occurrence of processes at postsynaptic sites outweighing presynaptic sites [245]. Some

progress has been made in analyzing the differences between astrocyte soma and proccesses [246], and modelling the Ca2+ signaling in fine processes [247]. The integration of astrocyte processes into synaptic dynamics is not the goal of this work. Not only is little known about the dynamics of astrocyte networks independently of neurons, but there remains ongoing debate regarding the tripartite synapse and how astrocytes functionally integrate neuronal information [92]. In short, all research reviewing and describing the state of astrocyte research argue that more techniques are needed to shed light on what is actually going on within astrocyte processes and, generally, within astrocyte networks as a whole. [100]

Advances in understanding the compartmentalization of astrocyte networks are ongoing. Independently of processes, the calcium dynamics embedded within astrocyte microdomains, within these subcellular regions, are under investigation in terms of their role in astrocyte signaling heterogeneity. Advances in images and research methodologies as in the case of the machine-learning based algorithm AQUA [170] have enabled questions regarding the role of subcellular astrocyte dynamics and their integration in cognition. Overall, healthy, stellate astrocytes have an arborization comparable to neuronal dendritic geometry. This arborization as a network, and the information contained within this network are underexplored. An important technique needed to understand astrocyte information processing better is information theory, and the technique of symbolization to encode the dynamical representations of complex astrocyte Ca^{2+} events.

Building upon the work [163], we study stellate astrocyte networks in vitro at a higher magnification than our previous study; our interest is not single subcellular

dynamics, as we are interested in the collective dynamics of astrocyte processes. Leveraging and modifying amplitude-ordering symbolization for understanding astrocyte processes, we describe, quantify, and contrast stellate astrocyte bodies and processes.

5.3 Materials/Methods

5.3.1 Imaging

Experiments were performed between 14 to 21 (DIV14-DIV21) days after dissection [196]. At this time, astrocytes were trypsinized from flasks and plated into PDL-coated (Sigma-Aldrich) 35 mm dishes (MatTek). Dishes containing cultured astrocytes were incubated with 5μ M CalBryte 590 AM (AAT Bioquest) for 30-60 min at 37degC prior to imaging. Dishes were then washed with PBS. Astrocytes are plated at densities such that they proliferate to roughly 125k cells/well on the day of imaging (a final density of approximately 2.5k cells/mm^2), and imaging was performed on a spinning disk confocal microscope (PerkinElmer). Image acquisition occurred for approximately 60 minutes at roughly 5 frames per second with 100 ms of exposure time per frame. The University of Maryland Imaging Core maintains the PerkinElmer spinning disk confocal microscope used for this research. The equipped Hamamatsu ImagEM X2 EM-CCD camera (C9100-23B) took the image sequences, which records 16-bit images. Sequences were taken from an oil 40x objective (1.3 NA; 0.36 μm per pixel) and under temperature, CO2, and humidity control. All experiments are performed in NeuroBasal media (Gibco) for reasons previously

described [163].

5.3.2 Cell Culture

Primary astrocytes were obtained from Sprague Dawley rats housed at the University of Maryland (in concordance with the recommendations of and approval by the University of Maryland Institutional Animal Care and Use Committee; protocols R-JAN-24-01). Astrocytes were prepared from 0-to-2 day postnatal (P0-P2) Sprague Dawley rat brains as described previously [89]. Briefly, cortical tissue from each pup was separately dissociated via trituration, filtered, and plated into T25 flasks containing DMEM (ThermoFisher), 15% fetal bovine serum (Benchmark), and 1% pencillin-streptomycin (P/S). After roughly 7 days, in order to generate stellate and reactive astrocytes, the media was changed to stellate (AWESAM) media, which includes Neurobasal (ThermoFisher), 2% B27+ (GIBCO), 5 ng/mL HB-EGF (TOCRIS BioSciences) [41].

5.4 Results

5.4.1 Correlation as segmentation

An important result found is that using Pearson correlation in an a priori known region of acitivty (i.e. an active astrocyte located by the researcher upon observation of the data), one can generate segmentation maps, as illustrated in Figs. 5.1A,B. These segmentation maps are generated by finding an active region in Fig. 5.1A. Such a region is shown by the black circle in Fig. 5.1B. From here, a pixel-wise

Pearson correlation is performed. This calculation is between the mean valued time series generated by the values in the assigned black region, and every pixel in the entire image sequence. Interestingly, the correlation can pick up well defined regions corresponding to astrocyte bodies and processes. Next, we downsample the pre-existing image sequence (Fig. 5.1). This method acts as both a smoothing step in addition to an averaging for pixel-wise Pearson correlation. Since Pearson Correlation is a simultaneous measure, we perform the calculations for several windows in an image sequence. As of these windows are max projected (Fig. 5.1D. Notice how the upper cell body noted by negative correlation in Fig. 5.1B is now red in Fig. 5.1D due to this maximal projection over several windows. Using a Difference of Gaussian (DoG) filter coupled with an anisotropic Laplacian of Gaussian filter (LoG), cell bodies (Fig. 5.1E) and processes (Fig. A.1F) are differentially extracted. Unlike in studies on the different calcium expressions intracellularly [41], we normalize the areas contributing to these analog signals. The various colors in Figs. 5.1G,H show different regions within segmented objects. For both cell bodies and processes, we construct sub-regions of 9 pixels in total for both of these objects in order to ensure proper comparison of signals (i.e. signals extracted from more pixels by definition will be more smoothed than signals from small regions).

5.4.2 Rising and Falling State entropy differences

Next, we modify the symbol states used in the literature [163]. We do this in order to separately extract rising and falling dynamics from an analog time series.

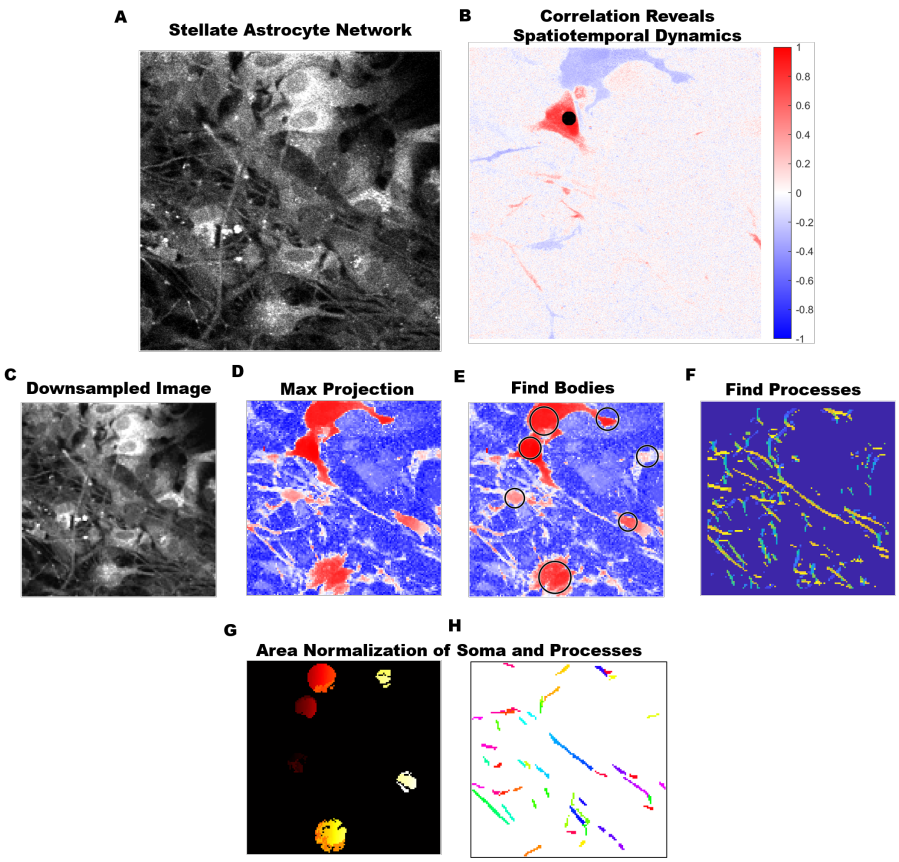

Figure 5.1: Pearson correlation dynamics within several windows allows segmentation of cell bodies versus processes. Cell bodies and processes are extracted with a difference of Gaussian (DoG) filter and LoG filter, respectively.

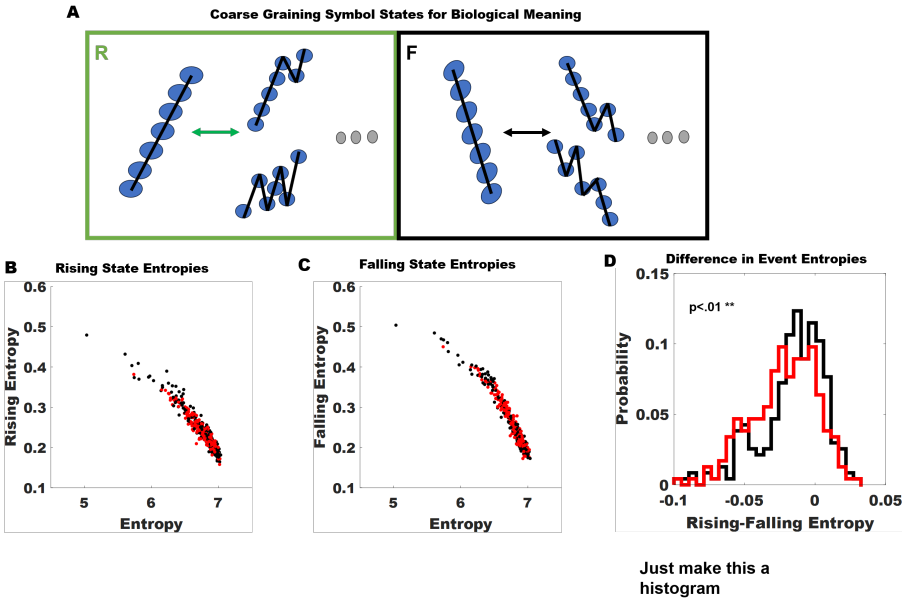

Figure 5.2: Modifications to the embedded states reveal differences between the rising and falling dynamics of stellate cell bodies and processes.

These states are of interest as they define the complex spatiotemporal patterns of astrocyte dynamics. A 'rise' state is defined as all embedded states in which the first point is the lowest and the last point is the largest in an embedded window; 'falling' states are the opposite. Using this analysis, we can extract the entropy associated with rising and falling from any time series (Fig.5.2A).

We extract the rising (Fig. 5.2B) and falling (Fig. 5.2C) entropies for normalized area regions within stellate bodies and processes. We find that processes have a significantly larger falling entropy (Fig. 5.2D), suggesting that the ways in which calcium decreases in processes are more varied.

5.5 Discussion

Pearson correlation provides another simple method for segmentation. Without minimal thresholding, cell bodies and processes can be extracted in order to understand how the different components contribute to the overall information processing of stellate networks.

We have found that stellate processes have a larger falling entropy than stellate bodies suggesting that the dynamical shapes of analog process time series are more varied than those of stellate bodies.

5.6 Conclusion

We have modified symbolization to generate symbol states with biologically interpretable meaning. We have extended these to astrocyte stellate cell bodies and

processes. We have found that the rising and falling entropies of these components within a stellate network differ.

Chapter 6: Summary and Future Directions

6.1 Concluding discussion of works contained

In this dissertation, data scientific insights from image sequences of cellular collections demonstrate the information content of astrocyte and cytoskeletal dynamics. As a result, this dissertation highlights the collective characteristics of astrocyte and cytoskeletal networks regarding organization, morphology, lateral motion, and signaling patterns. Astrocytes and the cytoskeleton contain unique dynamics. These insights were generated from computer vision, statistical methodology, physics-based techniques, and information theory. Chapters 2,3,4, and 5 discuss data-driven techniques to uncover the slow signals of astrocytes and the filamentous dynamics or arrangement of the cytoskeleton. Similarly, these chapters showcase improvements to our understanding of complex biological systems. As astrocytes are the main object of interest in this work, it has been shown repeatedly how the brain, one of the most–if not the most–popular complex biological systems, contains collective astrocyte and cytoskeletal dynamics. The next research steps will be to incorporate these dynamics and account for the resultant interactions with previously studied dynamics, e.g., the electrochemical firing of neurons. What follows is a short, detailed summary of the chapters.

6.1.1 Astrocyte insights generated

The information modalities of astrocytes have been overlooked, not purposefully, but as a result of their importance in supporting brain health. As a reminder, glia is derived from Latin, meaning glue. Astrocytes, as a subset of glia, provide critical physiological help to the brain in previously described areas. Indeed, astrocytes are regarded as the brain's immune cells, e.g., in their ability to migrate and perform wound healing. This wound healing is often referenced as a glial scar. This physiological support's downstream effect is seen via astrocytes' morphological plasticity. This plasticity is a repeated pattern in this dissertation. We first began this discussion on plasticity by demonstrating that astrocyte actin organizes differently depending on environmental cues. Astrocytes mechanically sense their environment. Some of the consequences of this functionality are differentiation of physiology and shape and migratory ability. Building upon the work demonstrating the differential dynamical response of astrocytes functionally dependent upon the presence of unique topographies and neuronal cells, I demonstrated that astrocyte actin filaments organize with a different angle relative to the cellular boundary when on various surfaces. I analyzed this using a rotating, anisotropic Laplacian of Gaussian (LoG) filter. This predictive ability has implications for linking astrocyte geometry to functional interactions within astrocyte networks and mechanical interactions with other brain cells.

In addition to the vital sensing and supportive functions, astrocytes signal. To avoid confusion with neurons, we do not call such signals 'firing.' The calcium

(non-electrical) events of astrocytes are orders of magnitude slower than neurons. Motivated by the differentiation caused by the mechanical sensing of astrocytes, the signals generated by the three significant classes of astrocytes were investigated. Information-theoretic tools found that although the speed of information transport is unaffected by subtype and extracellular environment. The indifference of speed is contrasted against the differences in the information-theoretic measures. Cross-correlation, mutual information, and partitioned entropy were the measures used. This work was followed up by narrowing my focus to stellate networks to ascertain partitioned entropy differences between processes and cell bodies.

6.1.2 New technique to study lateral motion of filaments

Building upon the work done with the LoG filter, I combined Optical Flow and LoG to capture the lateral dynamics of microtubule filaments. Due to previous difficulties in analyzing tubulin in image sequences, tracking EB-tip proteins became the standard analysis method for microtubule activity. This filament displacement tool provides a methodology to study the intracellular forcing environment via microtubule lateral motion. Future studies will complement EB tip tracking with this filament motion method.

6.2 Future Directions

The following sections provide an overview for future researchers to build upon the foundations provided and questions raised in this dissertation.

6.2.1 Applying information-theoretic techniques to cytoskeletal dynamics

Optical flow and LoG filtering are practical computer vision techniques for extracting and analyzing cytoskeletal dynamics. Optical flow has successfully revealed the underlying wave structure of actin dynamics. Further use of the Filament Displacement tool described in Chapter 3 should inspire readers for microtubule work.

In the optical flow patterns discussed, including in the work motivating investigation of astrocyte actin organization [89], there is an averaging of pixels for some ROI. Even in the case of Chapter 3, the results described are magnitudes contained within pixels; these magnitudes do not reveal any embedded dynamics within these cytoskeletal structures.

A future project worthy of investigation is to convert cytoskeletal dynamics data into time series. After this conversion, researchers can quantify the embedded dynamics, taking the analysis approaches introduced in Chapter 4 into account. For example, symbolization of microtubule fluctuations data extracted as described in Chapter 3 under some perturbation may elucidate the effects of these perturbations.

Any cytoskeletal analysis involving ROIs constitutes an averaging of dynamics; pixel-level dynamics are lost for quantification purposes. There is an opportunity for researchers interested in studying image information theory to ask several questions about cytoskeletal dynamics. The field is in its infancy, and therefore, one may investigate how best to leverage both information theory with the high-dimensional,

high-resolution datasets to achieve a more nuanced understanding of the embedded dynamics [248–250].

6.2.2 Causal linking calcium signals with cytoskeletal dynamics

Calcium signaling and the actin cytoskeleton (and its possible dynamics) have been linked for both neurons and astrocytes [251–258]. The reader is reminded to reference Chapter 1 for a refresher on the non-static nature of both of these systems; i.e. these studies would benefit from a re-investigation utilizing the information-dense spatio-temporal patterns embedded within these systems. The motivation behind the project in 4 is the salient morphological differences observed across the three physiological classes of astrocytes. Representative examples of these differences are represented in 6.1. Referencing the previous section as motivation, causally linking cytoskeletal dynamics to calcium signaling in astrocytes remains an ambitious undertaking. One may ask: are stellate astrocyte actin dynamics related to their differential calcium signaling profile? Studies have demonstrated effects on calcium signaling following cytoskeletal perturbation [114]. Applying time-delayed mutual information [226] to both information channels to 1) better understand the timescales for this interaction and 2) incorporate models or generate new ones from these data insights. Furthermore, comparable to the comparative framework of 4, motivating a comparison of understanding how differing cytoskeletal dynamics in structurally plastic astrocytes may precipitate differing calcium dynamics is of interest. A project summary is shown in Fig. 6.1.

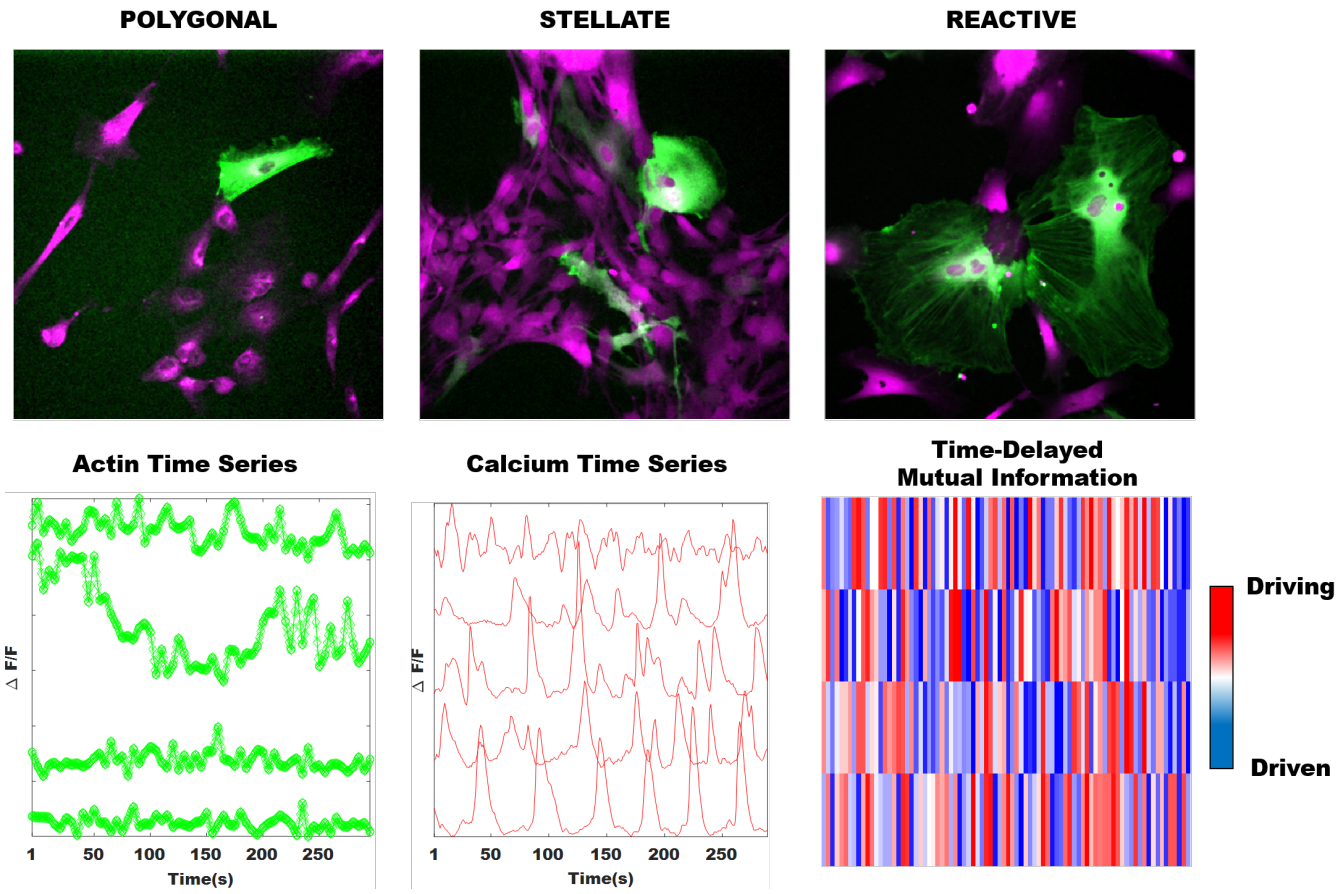

Figure 6.1: Motivation behind the comparative analysis of information processing of astrocyte subtypes. Actin cytoskeletons manifest different morphologies for polygonal, stellate, and reactive astrocytes. Actin is labeled green, and calcium is labeled dark red. Linking the actin and calcium time series via time-delayed mutual information proves a worthwhile starting point.

6.2.3 Non-stationarity of astrocyte signals and parameter

For this section, the reader is encouraged to revisit the discussions of partitioned entropy as outlined in Chapter 4. It is noted that the time series present suffers from a lack of a large number of time points (unlike in neuronal signals within the millisecond timescale). This is a result of the discussed slower time scale of astrocyte dynamics (relative to neuron dynamics on the millisecond timescale). Partition entropy has proven helpful in this dissertation for comparative analysis. However, the time series for astrocyte signals in Chapters 4 (and in 5) are not stationary. An investigation of the chaotic nature of astrocyte signaling dynamics is outside the scope of this work. The conclusion remains that astrocyte dynamics (regardless of physiological subtype) are close to limit-cycle dynamics. However, the dynamics expressed in the partitioned entropy curves (Fig. 6.2) resemble the partitioned entropy curves of well-known chaotic time series. A more theoretically oriented project investigating the properties of astrocyte signals is of interest. Tools and research on quantifying and discriminating chaotic signals exist, and good starting points are referenced here [225, 259–268].

The parameters described in Chapters 4 and 5 are non-trivial. Careful tuning of parameters, such as the time-delay parameter l, may provide researchers with more substantial results for understanding the unique characteristics of astrocyte signals. Indeed, further modifications to the time delay, l, may prove fruitful. m, l were chosen after careful consideration of the parameter selection discussion in both applied and theoretical studies [217–225]. However, as discussed, the applied work

done in the literature is focused on neurons except works provided in this paper. Updating the works described herein with a robust discussion of parameter selection specifically for astrocyte calcium dynamics is of interest.

6.2.4 Water transport as a slow mediator of astrocyte information

Water flows in the brain are implicated in central nervous system health and disease or injury [77, 269, 270]. As a specific example, Aquaporin-4 (AQP4) is implicated in brain edema [271]. AQP4 is the main water channel in the brain. It is almost exclusively expressed by astrocytes [77] similarly to Connexin 43 (Cx43) [185] (itself an important link in the migratory function of astrocytes). Moreover, it is known that astrocytes migrate in response to injury (forming the glial scar) [96], and upregulated water channels affect the success of astrocyte response [77]. Using calcein as an imaging marker, water dynamics are shown to follow comparable fluctuations to calcium. Leveraging information theory on these signals provides a pathway to analyze astrocyte networks from a pathology perspective. Moreover, sample datasets of GL-261 wound healing coupled with water transport imaging are of interest to better establish causal links. As an example, using mutual information to understand the driving channel (whether cytoskeletal or water transport) in migration by measuring shape dynamics [272] of migrating cells with water dynamics with add to the body of literature which still analyzes the pathological implications of astrocytes. Example data is shown in Fig. 6.3.

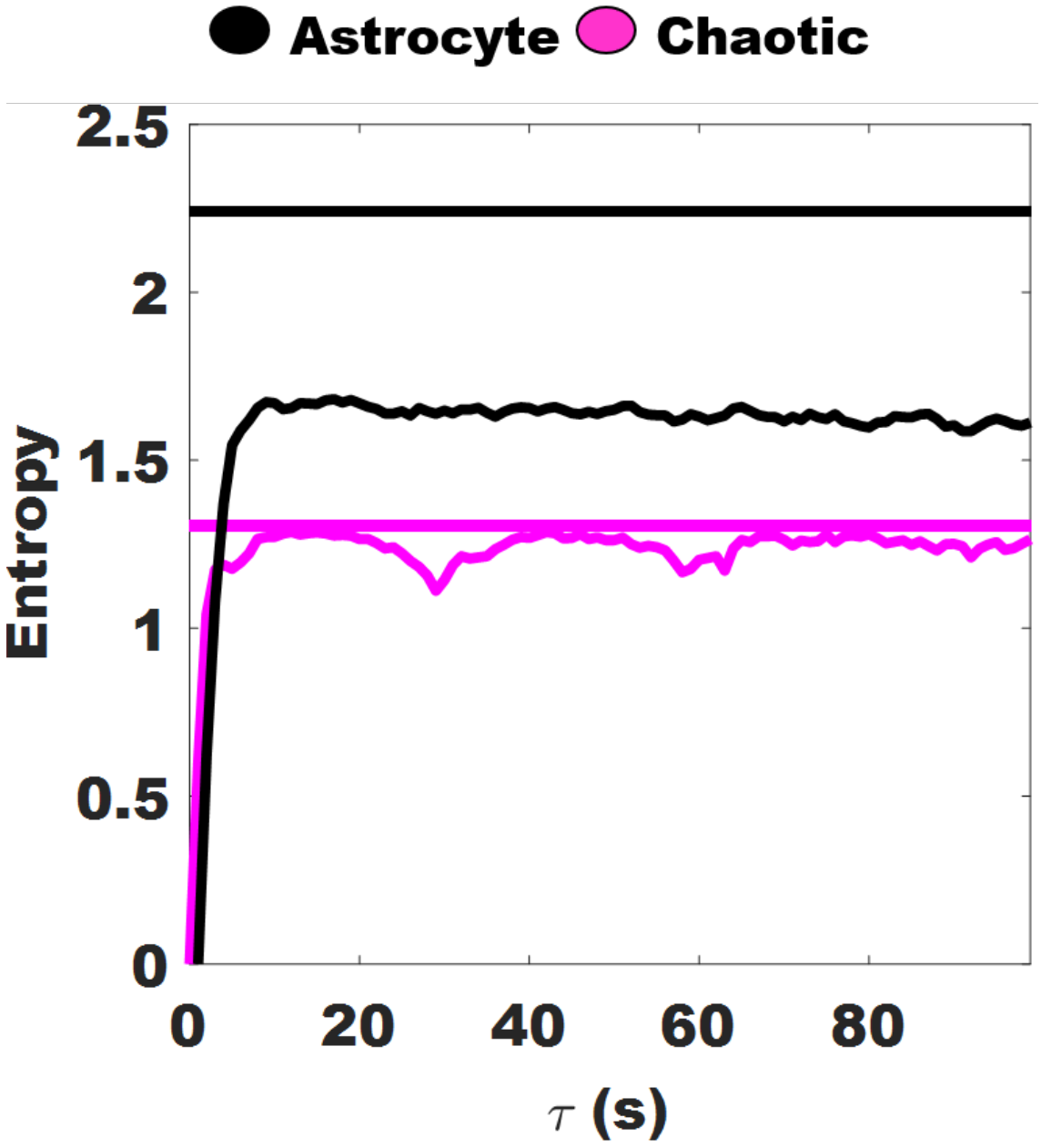

Figure 6.2: Partitioned entropy results from 4 suggest astrocyte signaling is not chaotic. However, the nature of the partitioned entropy curve exhibits behavior more akin to a chaotic time series than a limit cycle. Future studies could investigate this.

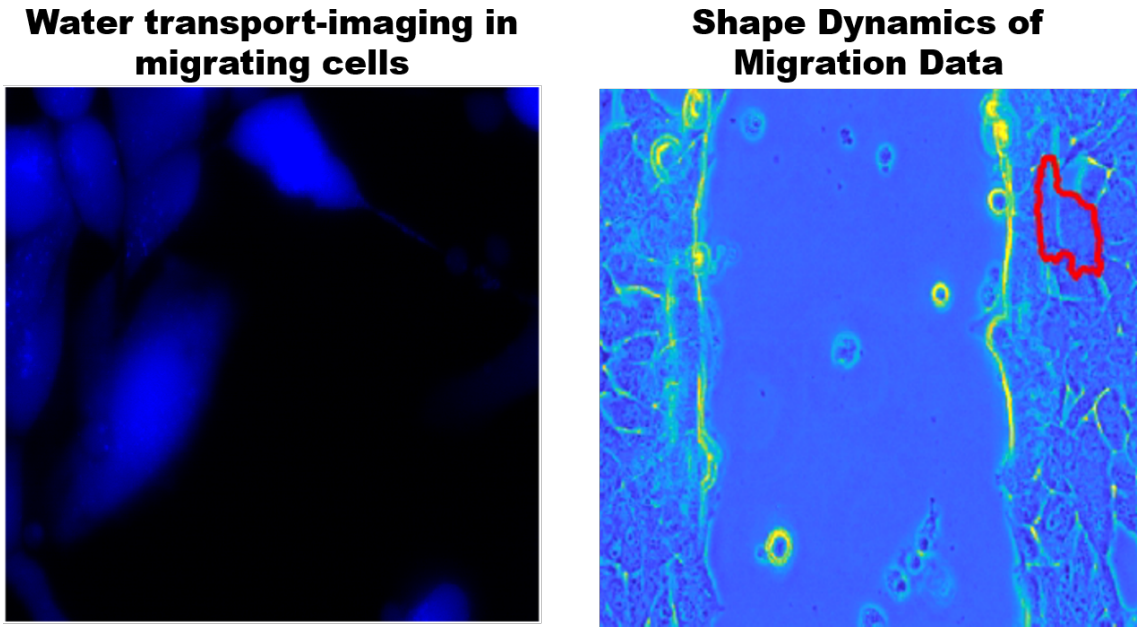

Figure 6.3: Water channels, specifically AQP4, are implicated in CNS health and injury response. Establishing causal links between the injury response (migration) and water fluctuation dynamics (akin to calcium fluorescence data) is the next step to enhance a spatiotemporal understanding of astrocyte-supportive responses. Segmentation for shape dynamics is highlighted in red.

Appendix A: Appendix to Chapter 4

This study does not regard the calcium waves present in astrocyte networks as adaptive mechanisms. Indeed, all astrocyte subtypes in the study spontaneously experience calcium events throughout the network. These complex patterns, rather than represented as analog time series, are shown in a permuted data dimension. This dimension demonstrates the complexity in terms of location, shape, and duration of spontaneous calcium events in astrocyte networks. Information-theoretic tools are well-suited to handle the rich, non-linearity present in this data, illustrated in Fig. A.1 Astrocytes are segmented using FogBank, a morphological watershed segmentation algorithm [207]. A complete FogBank segmentation is shown in Fig. A.2A. The examples used in Fig. 4.2 are replicated here in Fig A.2B, showing the visual transition from FogBank to the figure as displayed in the text. FogBank segmentation provides distances to each other segmented object (astrocyte); we take the center of mass of each object to find distances between FogBank segmented objects.

The use of correlation for astrocytes is modified from the conventional use of Pearson correlation for neurons. Considering the framerates and the millisecond (ms) timescale for electrical neuronal firing, the use of Pearson correlation (referred

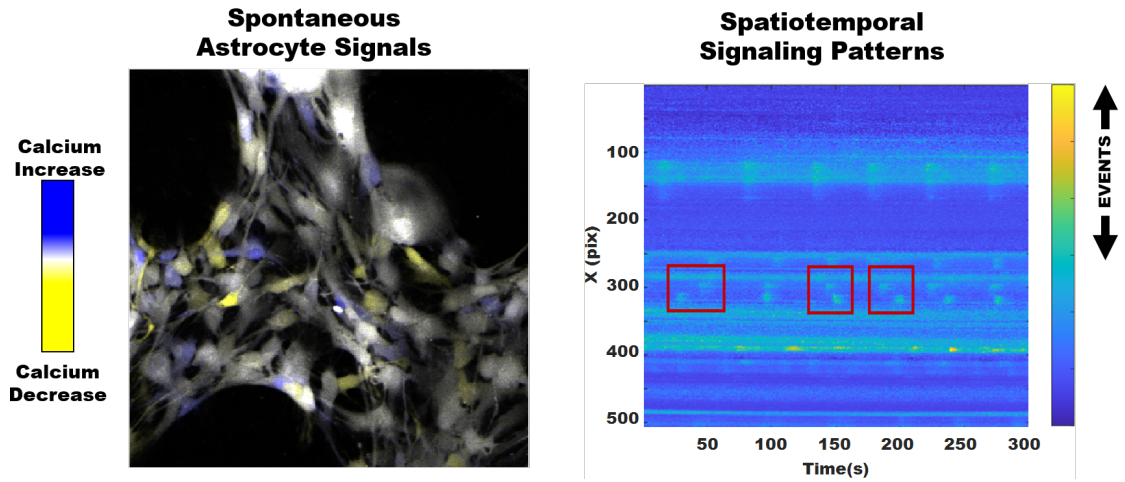

Figure A.1: Spontaneous spatiotemporal calcium patterns. We refigure the snapshots presented in Fig. 4.1 with a transformed view of the spatiotemporal patterns in astrocyte networks. The spatiotemporal patterns are produced from permuting the dimensions of the data to show time on the x-axis. All calcium events are shown. They are localized in elliptical regions.

in this Appendix as simultaneous firing) is appropriate. The simultaneous firing of neurons allows for Pearson correlation to assess connectivity and other related measures accurately. However, in the case of astrocytes with slow firing on the second timescale, Pearson correlation is inappropriate. Notice in the 'temporal window for simultaneous firing,' marked by the bounded rectangle in Fig. A.2C. Visually, we note that the peaks of calcium events are not aligned which leads to poor correlation output in Fig A.2D. However, using Cross Correlation (used in our main text and referred to in this Appendix as a measure of spatial propagation) is appropriate to address the time lags in between calcium events for astrocytes. Shifting the purple (top) and orange (bottom) traces in Fig A.2C, shifted traces shown in Fig A.2E, we see that the calcium events are more in line, in this case indicating that information was transmitted forward to the yellow (middle) trace; backward information was transmitted from the purple trace to the yellow trace (which equally indicates forward

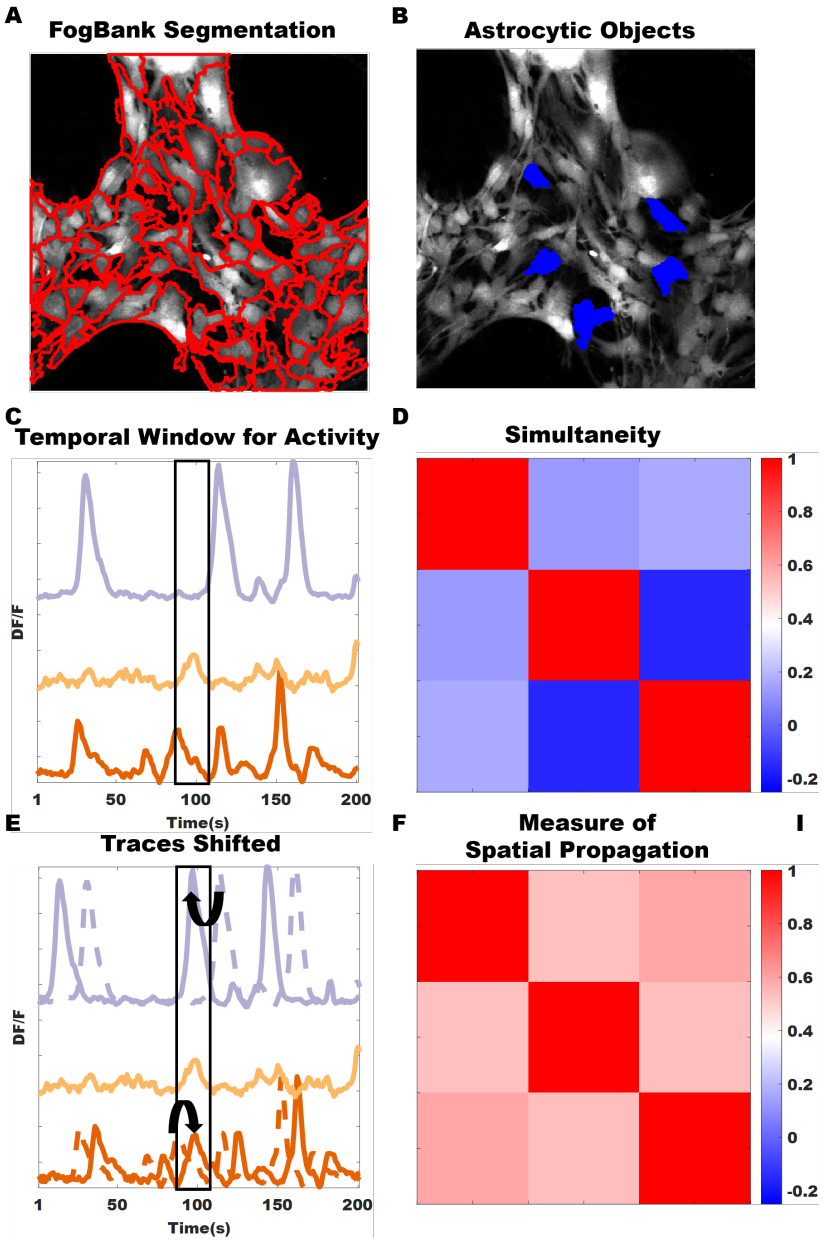

Figure A.2: Construction of objects, and time-delayed correlation versus Pearson. (A) FogBank image shows the boundaries of all segmented cells. For (B) which is reproduced from Fig 2, we show how we went from FogBank to the traces shown in the paper. (C) Demonstrates that for slow traces like astrocytes, Pearson correlation is ineffective in understanding how information is transported. (D) The simultaneity measure of Pearson correlation results in low correlation values. (E) Cross correlation allows traces to be shifted, which makes sense for the slow calcium signals in astrocyte networks. (F) Contrasted to (D), cross correlation values better reflect area overlap in calcium events.

from yellow to purple). Time lags assume positive or negative values, but are taken as positive in the calculation of speed. See improved correlation results, relative to Pearson output, for astrocyte calcium events in Fig A.2F.

In order to verify that the time lags from either cross-correlation or mutual information are properly extracted, we looked at cross correlations for a wide range of time lags. Using cross-correlation as a representative example, we analyze an arbitrary group of stellate calcium traces in Fig. A.3A. Some of the cross-correlation curves between these traces are shown in Fig. A.3B. The curves are smooth, indicating that a well-defined magnitude and time-lag with the largest cross correlation exist. We note that for some curves additional peaks of comparable height are seen. As shown in Figs. A.3C and A.3D, these additional peaks are consistent with the period character of many calcium traces, which yields well-defined peaks in the Fourier spectrum (Fig. A.3D). Corresponding to the peak in Fig.A.3D at 0.05Hz (indicating a 20 second periodicity), we find that the corresponding cross correlation (red curve in Fig. A.3B) has two peaks 20 seconds apart. We systematically choose the largest peak to reflect that most likely time delay and magnitude of cross-correlation.

Partitioned entropy enables a more individualistic interpretation of the calcium events of astrocytes. In order to correctly ensure the measure, here used as a comparative metric to assess difference between astrocyte subtypes, is used appropriately we replicate the results in Shiozawa et al [225]. In Fig. A.4A, for a straight line (green), a sine curve (blue), the Lorenz equation (cyan), and Thomas' cyclically symmetric attractor (pink), we replicate partitioned entropy curves. The maximal entropies for these curves are indicated by the zero slope lines with the same color as

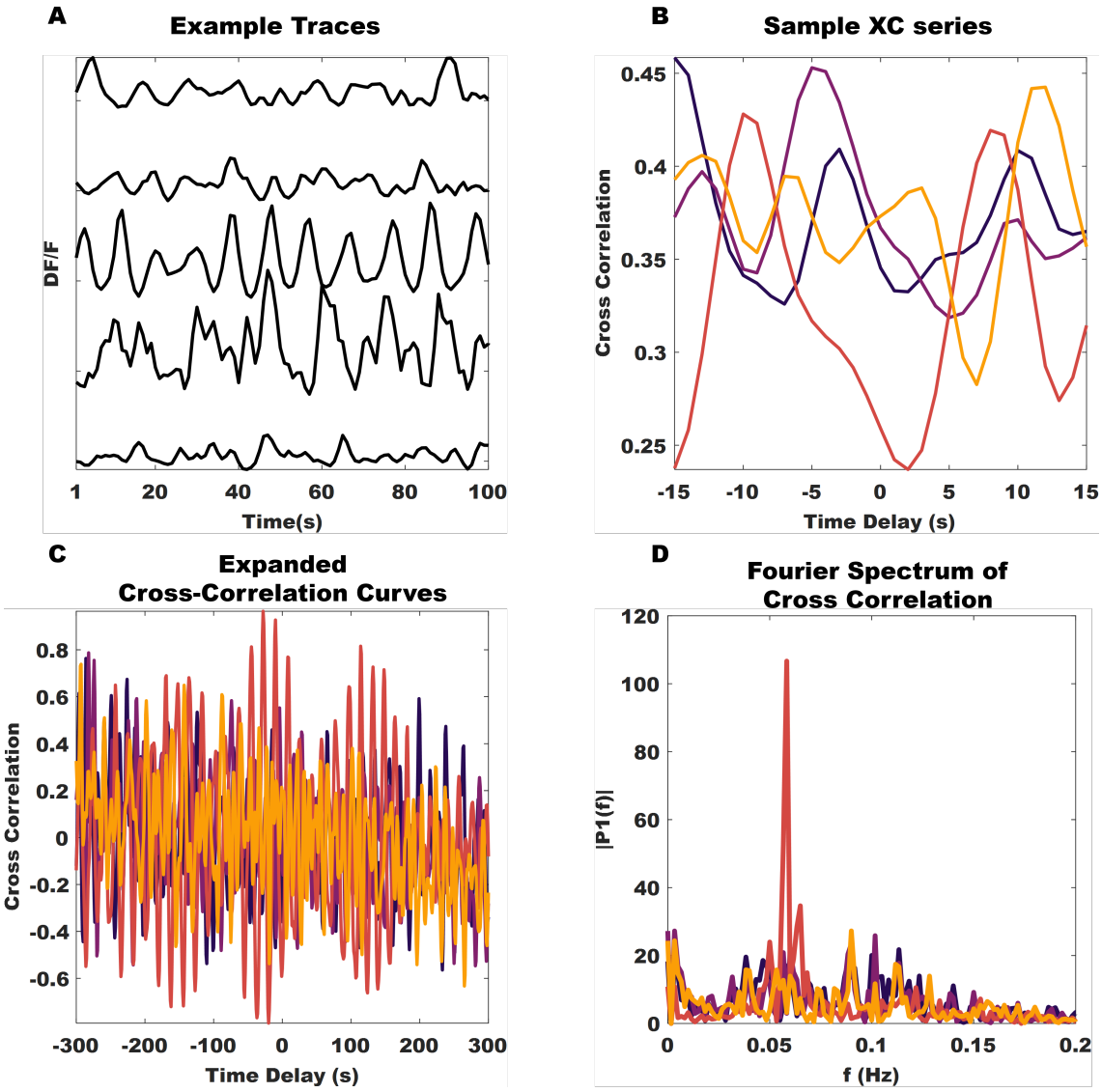

Figure A.3: Analysis of peaks in cross-correlation curves. (A) We reproduced arbitrary stellate time series. (B) For these curves, we report 4 cross-correlation curves associated with time-lags corresponding to the window size used in this study. (C) Expanding this correlation curve to un-physiological time lags, we observe the presence of two modes in this data. (D) Removing the larger mode (subtracting the mean), we find that these peaks associated with maximal correlation are well defined.

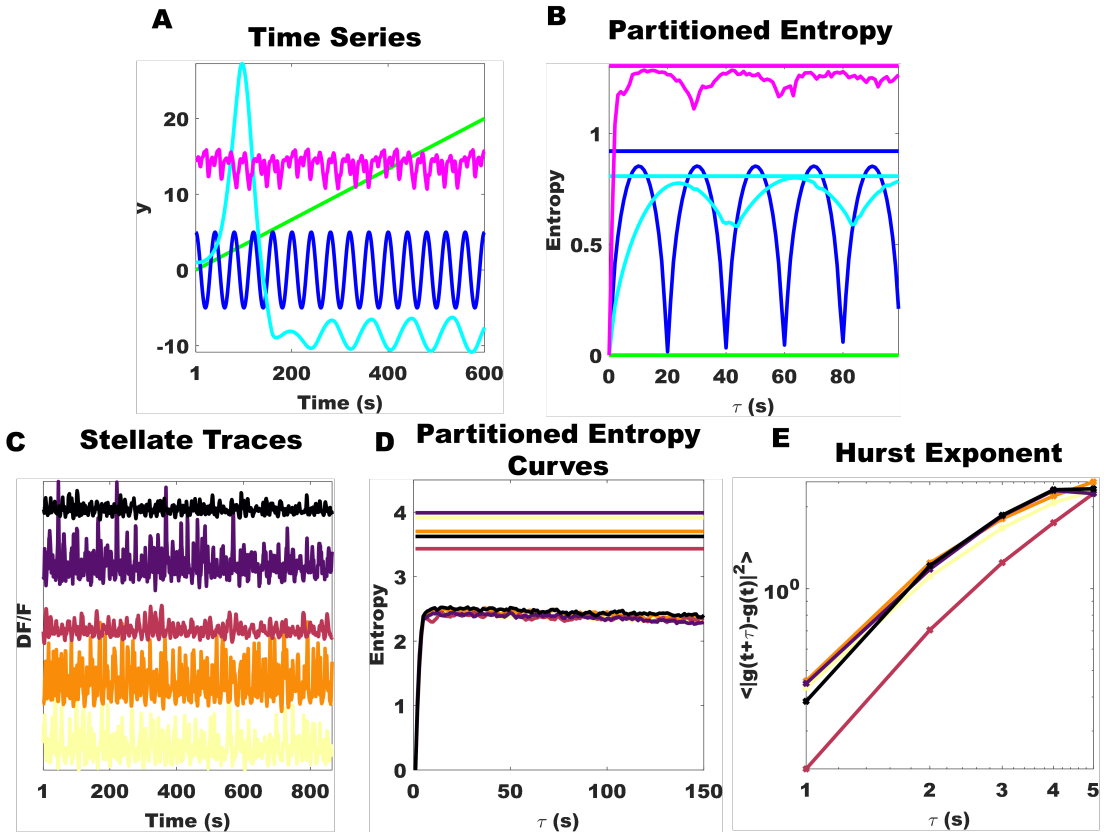

Figure A.4: We reproduced a partitioned entropy figure to demonstrate our code is sound. We plot representative curves for partitioned entropy. Since the partitioned entropy ratio retains the same bounds ([0 1]) are the Hurst exponent, for completeness we show how these are difference metrics. Hurst exponent is finding the slope of the graph shown, loglog plotted, in (E). shown in (D) refers to symbol state time whereas in (E) it reflects acquisition rate of the image sequences.

the partitioned entropy curve in Fig. A.4B. As one can see, there is no partitioned entropy for a line, the partitioned entropy for a sine curve is roughly 0.5 (as indicated by the sinusoidal nature of the partitioned entropy curve), whereas for the Lorenz and Thomas systems, the partitioned entropy curves saturate closer to maximal entropy values, indicating that these time series are chaotic.

For this paper, we reproduce some stellate traces (Fig. A.4C) with respective partitioned entropy curves (Fig. A.4D). We note that these curves visually appear comparable to chaotic partitioned entropy curves; however, these curves hover around $\frac{1}{2}$ the maximal entropy value. Exploring the nature of chaos in astrocyte systems is beyond the scope of this paper, but worthy of further investigation.

Since the partitioned entropy ratio and the Hurst exponent assume comparable values, [0 1], we reproduce the curves for evaluating the Hurst exponent for the stellate traces in Fig. A.4C. As shown in Fig. A.4E, the Hurst exponent is the slope of the log-log plot between the expected squared difference between values in a time series offset by τ and $g(t)$ itself. There is a connection between the Hurst exponent and partitioned entropy, but these metrics are distinct and the values of 0.5 signify different physical meanings.

Due to the nonlinearity of astrocyte signals and the use of symbolization, finding the frequencies of these traces does not logically flow with the structure of the main text. The nature of astrocyte calcium events renders any output frequency a dubious value, i.e. astrocytes need not, and do not, obey the same frequency within certain distinct time windows in a series. However, for completeness, we report these values. The values reported are the peak frequency associated with the periodogram

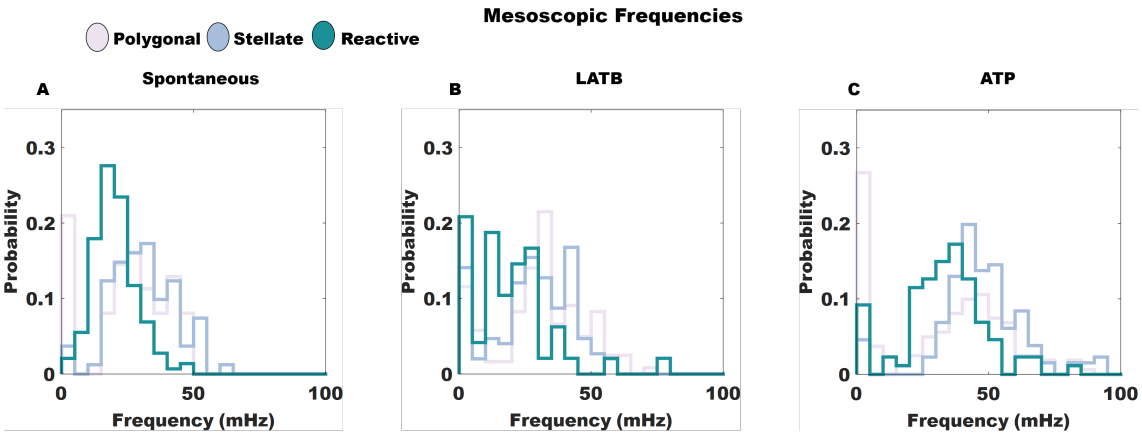

Figure A.5: Fourier frequencies. Peak frequencies for individual traces for polygonal, stellate, and reactive traces in (A) spontaneous conditions, (B) LATB conditions, and (C) ATP conditions are shown for completeness.

of individual traces. Nonetheless, we find that reactive astrocytes have the lowest spontaneous frequency with stellate having the highest (Fig. A.5A). Latrunculin B increases polygonal and stellate distributions while lowering reactive ones (Fig. A.5B). ATP increases the frequencies of all astrocyte subtypes (Fig. A.5C).

Bibliography

[1] Gregory A. Light, Lisa E. Williams, Falk Minow, Joyce Sprock, Anthony Rissling, Richard Sharp, Neal R. Swerdlow, and David L. Braff. Electroencephalography (EEG) and Event-Related Potentials (ERPs) with Human Participants. *Current Protocols in Neuroscience*, 52(1):6.25.1–6.25.24, July 2010. Publisher: John Wiley & Sons, Ltd.

[2] Fikret Emre Kapucu, Andrey Vinogradov, Tanja Hyvärinen, Laura Ylä-Outinen, and Susanna Narkilahti. Comparative microelectrode array data of the functional development of hPSC-derived and rat neuronal networks. *Scientific Data*, 9(1):120, March 2022.

[3] Jan Müller, Marco Ballini, Paolo Livi, Yihui Chen, Milos Radivojevic, Amir Shadmani, Vijay Viswam, Ian L. Jones, Michele Fiscella, Roland Diggelmann, Alexander Stettler, Urs Frey, Douglas J. Bakkum, and Andreas Hierlemann. High-resolution CMOS MEA platform to study neurons at subcellular, cellular, and network levels. *Lab on a Chip*, 15(13):2767–2780, 2015. Publisher: The Royal Society of Chemistry.

[4] Patrick O. Kanold, Israel Nelken, and Daniel B. Polley. Local versus global scales of organization in auditory cortex. *Trends in Neurosciences*, 37(9):502–510, September 2014. Publisher: Elsevier.

[5] Luca Clissa, Antonio Macaluso, Roberto Morelli, Alessandra Occhinegro, Emiliana Piscitiello, Ludovico Taddei, Marco Luppi, Roberto Amici, Matteo Cerri, Timna Hitrec, Lorenzo Rinaldi, and Antonio Zoccoli. Fluorescent Neuronal Cells v2: multi-task, multi-format annotations for deep learning in microscopy. *Scientific Data*, 11(1):184, February 2024.

[6] Linus Manubens-Gil, Zhi Zhou, Hanbo Chen, Arvind Ramanathan, Xiaoxiao Liu, Yufeng Liu, Alessandro Bria, Todd Gillette, Zongcai Ruan, Jian Yang, Miroslav Radojević, Ting Zhao, Li Cheng, Lei Qu, Siqi Liu, Kristofer E. Bouchard, Lin Gu, Weidong Cai, Shuiwang Ji, Badrinath Roysam, Ching-Wei Wang, Hongchuan Yu, Amos Sironi, Daniel Maxim Iascone, Jie Zhou, Erhan

Bas, Eduardo Conde-Sousa, Paulo Aguiar, Xiang Li, Yujie Li, Sumit Nanda, Yuan Wang, Leila Muresan, Pascal Fua, Bing Ye, Hai-yan He, Jochen F. Staiger, Manuel Peter, Daniel N. Cox, Michel Simonneau, Marcel Oberlaender, Gregory Jefferis, Kei Ito, Paloma Gonzalez-Bellido, Jinhyun Kim, Edwin Rubel, Hollis T. Cline, Hongkui Zeng, Aljoscha Nern, Ann-Shyn Chiang, Jianhua Yao, Jane Roskams, Rick Livesey, Janine Stevens, Tianming Liu, Chinh Dang, Yike Guo, Ning Zhong, Georgia Tourassi, Sean Hill, Michael Hawrylycz, Christof Koch, Erik Meijering, Giorgio A. Ascoli, and Hanchuan Peng. BigNeuron: a resource to benchmark and predict performance of algorithms for automated tracing of neurons in light microscopy datasets. *Nature Methods*, 20(6):824–835, June 2023.

[7] Fabian W. Vogel, Sercan Alipek, Jens-Bastian Eppler, Pamela Osuna-Vargas, Jochen Triesch, Diane Bissen, Amparo Acker-Palmer, Simon Rumpel, and Matthias Kaschube. Utilizing 2D-region-based CNNs for automatic dendritic spine detection in 3D live cell imaging. *Scientific Reports*, 13(1):20497, November 2023.

[8] T E J Behrens, H. Johansen-Berg, M W Woolrich, S M Smith, C A M Wheeler-Kingshott, P A Boulby, G J Barker, E L Sillery, K. Sheehan, O. Ciccarelli, A J Thompson, J M Brady, and P M Matthews. Non-invasive mapping of connections between human thalamus and cortex using diffusion imaging. *Nature Neuroscience*, 6(7):750–757, July 2003.

[9] Bryon A. Mueller, Kelvin O. Lim, Laura Hemmy, and Jazmin Camchong. Diffusion MRI and its Role in Neuropsychology. *Neuropsychology Review*, 25(3):250–271, September 2015.

[10] Jeff Duyn and Alan P Koretsky. Magnetic resonance imaging of neural circuits. *Nature Clinical Practice Cardiovascular Medicine*, 5(2):S71–S78, August 2008.

[11] Baxter P. Rogers, Victoria L. Morgan, Allen T. Newton, and John C. Gore. Assessing functional connectivity in the human brain by fMRI. *Magnetic Resonance Imaging*, 25(10):1347–1357, December 2007.

[12] Danielle Smith Bassett and Ed Bullmore. Small-world brain networks. *The Neuroscientist : a review journal bringing neurobiology, neurology and psychiatry*, 12(6):512–523, December 2006. Place: United States.

[13] Kainan S. Wang, David V. Smith, and Mauricio R. Delgado. Using fMRI to study reward processing in humans: past, present, and future. *Journal of Neurophysiology*, 115(3):1664–1678, March 2016. Publisher: American Physiological Society.

[14] Nai-Fang Chi, Hsiao-Lun Ku, David Yen-Ting Chen, Ying-Chi Tseng, Chi-Jen Chen, Ying-Chin Lin, Yi-Chen Hsieh, Lung Chan, Hung-Yi Chiou, Chung Y. Hsu, and Chaur-Jong Hu. Cerebral Motor Functional Connectivity at the

Acute Stage: An Outcome Predictor of Ischemic Stroke. *Scientific Reports*, 8(1):16803, November 2018.

[15] Smadar Ovadia-Caro, Daniel S. Margulies, and Arno Villringer. The Value of Resting-State Functional Magnetic Resonance Imaging in Stroke. *Stroke*, 45(9):2818–2824, September 2014. Publisher: American Heart Association.

[16] Bradley J. Roth. Can MRI Be Used as a Sensor to Record Neural Activity? *Sensors*, 23(3), 2023.

[17] Meryl Malezieux, Alexandra S. Klein, and Nadine Gogolla. Neural Circuits for Emotion. *Annual Review of Neuroscience*, 46(Volume 46, 2023):211–231, 2023. Publisher: Annual Reviews Type: Journal Article.

[18] Parinaz Babaeeghazvini, Laura M. Rueda-Delgado, Jolien Gooijers, Stephan P. Swinnen, and Andreas Daffertshofer. Brain Structural and Functional Connectivity: A Review of Combined Works of Diffusion Magnetic Resonance Imaging and Electro-Encephalography. *Frontiers in Human Neuroscience*, 15, 2021.

[19] Shi Gu, Fabio Pasqualetti, Matthew Cieslak, Qawi K. Telesford, Alfred B. Yu, Ari E. Kahn, John D. Medaglia, Jean M. Vettel, Michael B. Miller, Scott T. Grafton, and Danielle S. Bassett. Controllability of structural brain networks. *Nature Communications*, 6(1):8414, October 2015.

[20] Weidong Cai, Srikanth Ryali, Ramkrishna Pasumarthy, Viswanath Talasila, and Vinod Menon. Dynamic causal brain circuits during working memory and their functional controllability. *Nature Communications*, 12(1):3314, June 2021.

[21] Karolina Finc, Kamil Bonna, Xiaosong He, David M. Lydon-Staley, Simone Kühn, Włodzisław Duch, and Danielle S. Bassett. Dynamic reconfiguration of functional brain networks during working memory training. *Nature Communications*, 11(1):2435, May 2020.

[22] Danielle S Bassett and Olaf Sporns. Network neuroscience. *Nature Neuroscience*, 20(3):353–364, March 2017.

[23] Danielle S. Bassett and Michael S. Gazzaniga. Understanding complexity in the human brain. *Trends in cognitive sciences*, 15(5):200–209, May 2011. Place: England.

[24] Olaf Sporns, Giulio Tononi, and Rolf Kötter. The Human Connectome: A Structural Description of the Human Brain. *PLOS Computational Biology*, 1(4):e42, September 2005. Publisher: Public Library of Science.

[25] John Graham White, Eileen Southgate, J. N. Thomson, and Sydney Brenner. The structure of the nervous system of the nematode Caenorhabditis elegans. *Philosophical Transactions of the Royal Society of London. B, Biological Sciences*, 314(1165):1–340, January 1997. Publisher: Royal Society.

[26] Kerrianne Ryan, Zhiyuan Lu, and Ian A Meinertzhagen. The CNS connectome of a tadpole larva of Ciona intestinalis (L.) highlights sidedness in the brain of a chordate sibling. *eLife*, 5:e16962, December 2016. Publisher: eLife Sciences Publications, Ltd.

[27] Alexei Verkhratsky and Maiken Nedergaard. Physiology of Astroglia. *Physiological Reviews*, 98(1):239–389, January 2018. Publisher: American Physiological Society.

[28] Moritz Helmstaedter, Kevin L. Briggman, Srinivas C. Turaga, Viren Jain, H. Sebastian Seung, and Winfried Denk. Connectomic reconstruction of the inner plexiform layer in the mouse retina. *Nature*, 500(7461):168–174, August 2013.

[29] Winfried Denk and Heinz Horstmann. Serial Block-Face Scanning Electron Microscopy to Reconstruct Three-Dimensional Tissue Nanostructure. *PLOS Biology*, 2(11):e329, October 2004. Publisher: Public Library of Science.

[30] Fei Zhu, Mélissa Cizeron, Zhen Qiu, Ruth Benavides-Piccione, Maksym V. Kopanitsa, Nathan G. Skene, Babis Koniaris, Javier DeFelipe, Erik Fransén, Noboru H. Komiyama, and Seth G.N. Grant. Architecture of the Mouse Brain Synaptome. *Neuron*, 99(4):781–799.e10, August 2018. Publisher: Elsevier.

[31] Seth G N Grant. Synapse diversity and synaptome architecture in human genetic disorders. *Human Molecular Genetics*, 28(R2):R219–R225, November 2019.

[32] Carles Bosch, Albert Martínez, Nuria Masachs, Cátia M. Teixeira, Isabel Fernaud, Fausto Ulloa, Esther Pérez-Martínez, Carlos Lois, Joan X. Comella, Javier DeFelipe, Angel Merchán-Pérez, and Eduardo Soriano. FIB/SEM technology and high-throughput 3D reconstruction of dendritic spines and synapses in GFP-labeled adult-generated neurons. *Frontiers in Neuroanatomy*, 9, 2015.

[33] Alexander Shapson-Coe, Michał Januszewski, Daniel R. Berger, Art Pope, Yuelong Wu, Tim Blakely, Richard L. Schalek, Peter H. Li, Shuohong Wang, Jeremy Maitin-Shepard, Neha Karlupia, Sven Dorkenwald, Evelina Sjostedt, Laramie Leavitt, Dongil Lee, Jakob Troidl, Forrest Collman, Luke Bailey, Angerica Fitzmaurice, Rohin Kar, Benjamin Field, Hank Wu, Julian Wagner-Carena, David Aley, Joanna Lau, Zudi Lin, Donglai Wei, Hanspeter Pfister, Adi Peleg, Viren Jain, and Jeff W. Lichtman. A petavoxel fragment of human cerebral cortex reconstructed at nanoscale resolution. *Science*, 384(6696):eadk4858. Publisher: American Association for the Advancement of Science.

[34] Christopher K. Salmon, Tabish A. Syed, J. Benjamin Kacerovsky, Nensi Alivodej, Alexandra L. Schober, Tyler F.W. Sloan, Michael T. Pratte, Michael P. Rosen, Miranda Green, Adario Chirgwin-Dasgupta, Shaurya Mehta, Affan

Jilani, Yanan Wang, Hojatollah Vali, Craig A. Mandato, Kaleem Siddiqi, and Keith K. Murai. Organizing principles of astrocytic nanoarchitecture in the mouse cerebral cortex. *Current Biology*, 33(5):957–972.e5, March 2023. Publisher: Elsevier.

[35] Stanley Finger. 101Luigi Galvani: Electricity and the Nerves. In Stanley Finger, editor, *Minds Behind the Brain: A history of the pioneers and their discoveries*, page 0. Oxford University Press, March 2005.

[36] Ditte Lovatt, Ursula Sonnewald, Helle S. Waagepetersen, Arne Schousboe, Wei He, Jane H.-C. Lin, Xiaoning Han, Takahiro Takano, Su Wang, Fraser J. Sim, Steven A. Goldman, and Maiken Nedergaard. The Transcriptome and Metabolic Gene Signature of Protoplasmic Astrocytes in the Adult Murine Cortex. *The Journal of Neuroscience*, 27(45):12255, November 2007.

[37] C. E. Shannon. A mathematical theory of communication. *The Bell System Technical Journal*, 27(3):379–423, July 1948.

[38] Abby L. Bull, Leonard Campanello, Matt J. Hourwitz, Qixin Yang, Min Zhao, John T. Fourkas, and Wolfgang Losert. Actin Dynamics as a Multiscale Integrator of Cellular Guidance Cues. *Frontiers in Cell and Developmental Biology*, 10, 2022.

[39] Qixin Yang, Yuchuan Miao, Leonard J Campanello, Matt J Hourwitz, Bedri Abubaker-Sharif, Abby L Bull, Peter N Devreotes, John T Fourkas, and Wolfgang Losert. Cortical waves mediate the cellular response to electric fields. *eLife*, 11:e73198, March 2022. Publisher: eLife Sciences Publications, Ltd.

[40] Anne C. Wolfes, Saheeb Ahmed, Ankit Awasthi, Markus A. Stahlberg, Ashish Rajput, Daniel S. Magruder, Stefan Bonn, and Camin Dean. A novel method for culturing stellate astrocytes reveals spatially distinct Ca2+ signaling and vesicle recycling in astrocytic processes. *Journal of General Physiology*, 149(1):149–170, December 2016.

[41] Anne C. Wolfes, Saheeb Ahmed, Ankit Awasthi, Markus A. Stahlberg, Ashish Rajput, Daniel S. Magruder, Stefan Bonn, and Camin Dean. A novel method for culturing stellate astrocytes reveals spatially distinct Ca2+ signaling and vesicle recycling in astrocytic processes. *The Journal of General Physiology*, 149(1):149–170, January 2017.

[42] Pekka Lappalainen, Tommi Kotila, Antoine Jégou, and Guillaume Romet-Lemonne. Biochemical and mechanical regulation of actin dynamics. *Nature Reviews Molecular Cell Biology*, 23(12):836–852, December 2022.

[43] Leonard Joseph Campanello. *Quantifying the Organization and Dynamics of Excitable Signaling Networks*. Ph.D., University of Maryland, College Park, United States – Maryland, 2020. ISBN: 9798684638374 Publication Title: ProQuest Dissertations and Theses 28086766.

[44] Daniel S.C. Damineli, Maria Teresa Portes, and José A. Feijó. Electrifying rhythms in plant cells. *Current Opinion in Cell Biology*, 77:102113, August 2022.

[45] Hasan Ucar, Satoshi Watanabe, Jun Noguchi, Yuichi Morimoto, Yusuke Iino, Sho Yagishita, Noriko Takahashi, and Haruo Kasai. Mechanical actions of dendritic-spine enlargement on presynaptic exocytosis. *Nature*, 600(7890):686–689, December 2021.

[46] E. M. Izhikevich. Simple model of spiking neurons. *IEEE Transactions on Neural Networks*, 14(6):1569–1572, November 2003.

[47] Carsten Beta, Leah Edelstein-Keshet, Nir Gov, and Arik Yochelis. From actin waves to mechanism and back: How theory aids biological understanding. *eLife*, 12:e87181, July 2023. Publisher: eLife Sciences Publications, Ltd.

[48] Thomas R Insel, Nora D Volkow, Ting-Kai Li, James F Battey, Jr, and Story C Landis. Neuroscience Networks. *PLOS Biology*, 1(1):e17, October 2003. Publisher: Public Library of Science.

[49] Richard F. Betzel and Danielle S. Bassett. Multi-scale brain networks. *Functional Architecture of the Brain*, 160:73–83, October 2017.

[50] A. L. HODGKIN and A. F. HUXLEY. Action Potentials Recorded from Inside a Nerve Fibre. *Nature*, 144(3651):710–711, October 1939.

[51] Michael Häusser. The Hodgkin-Huxley theory of the action potential. *Nature Neuroscience*, 3(11):1165–1165, November 2000.

[52] Chia-Ying Lin, Ping-Han Chen, Hsiu-Hau Lin, and Wen-Min Huang. U(1) dynamics in neuronal activities. *Scientific Reports*, 12(1):17629, October 2022.

[53] Nicholas M. Timme and Christopher Lapish. A Tutorial for Information Theory in Neuroscience. *eneuro*, 5(3):ENEURO.0052–18.2018, May 2018.

[54] Jonathan D. Victor. Approaches to Information-Theoretic Analysis of Neural Activity. *Biological Theory*, 1(3):302–316, September 2006.

[55] Alexander G. Dimitrov, Aurel A. Lazar, and Jonathan D. Victor. Information theory in neuroscience. *Journal of Computational Neuroscience*, 30(1):1–5, February 2011.

[56] Alexander Borst and Frédéric E. Theunissen. Information theory and neural coding. *Nature Neuroscience*, 2(11):947–957, November 1999.

[57] Shuai Shao, Markus Meister, and Julijana Gjorgjieva. Efficient population coding of sensory stimuli. *Physical Review Research*, 5(4):043205, December 2023. Publisher: American Physical Society.

[58] Rodrigo Quian Quiroga and Stefano Panzeri. Extracting information from neuronal populations: information theory and decoding approaches. *Nature Reviews Neuroscience*, 10(3):173–185, March 2009.

[59] Robert P. Gowers and Magnus J. E. Richardson. Upcrossing-rate dynamics for a minimal neuron model receiving spatially distributed synaptic drive. *Physical Review Research*, 5(2):023095, May 2023. Publisher: American Physical Society.

[60] János Végh and Ádám J. Berki. Towards Generalizing the Information Theory for Neural Communication. *Entropy*, 24(8), 2022.

[61] Mikhail Katkov and Misha Tsodyks. Statistics of free memory recall. *Physical Review Research*, 4(3):033090, August 2022. Publisher: American Physical Society.

[62] Yan-Liang Shi, Roxana Zeraati, Anna Levina, and Tatiana A. Engel. Spatial and temporal correlations in neural networks with structured connectivity. *Physical Review Research*, 5(1):013005, January 2023. Publisher: American Physical Society.

[63] Erik D. Fagerholm, Zalina Dezhina, Rosalyn J. Moran, Karl J. Friston, Federico Turkheimer, and Robert Leech. Selection entropy: The information hidden within neuronal patterns. *Physical Review Research*, 5(2):023197, June 2023. Publisher: American Physical Society.

[64] Amin Nejatbakhsh, Francesco Fumarola, Saleh Esteki, Taro Toyoizumi, Roozbeh Kiani, and Luca Mazzucato. Predicting the effect of micro-stimulation on macaque prefrontal activity based on spontaneous circuit dynamics. *Physical Review Research*, 5(4):043211, December 2023. Publisher: American Physical Society.

[65] Siavash Golkar, Jules Berman, David Lipshutz, Robert Mihai Haret, Tim Gollisch, and Dmitri B. Chklovskii. Neuronal temporal filters as normal mode extractors. *Physical Review Research*, 6(1):013111, January 2024. Publisher: American Physical Society.

[66] Rainer Engelken, Fred Wolf, and L. F. Abbott. Lyapunov spectra of chaotic recurrent neural networks. *Physical Review Research*, 5(4):043044, October 2023. Publisher: American Physical Society.

[67] Yue Kris Wu and Julijana Gjorgjieva. Inhibition stabilization and paradoxical effects in recurrent neural networks with short-term plasticity. *Physical Review Research*, 5(3):033023, July 2023. Publisher: American Physical Society.

[68] Tirthabir Biswas and James E. Fitzgerald. Geometric framework to predict structure from function in neural networks. *Physical Review Research*, 4(2):023255, June 2022. Publisher: American Physical Society.

[69] Ifedayo-EmmanuEL Adeyefa-Olasupo. Fundamental law underlying predictive remapping. *Physical Review Research*, 5(1):013214, March 2023. Publisher: American Physical Society.

[70] Francesco Fumarola, Zhengqi He, Łukasz Kuśmierz, and Taro Toyoizumi. Decoding silence in free recall. *Physical Review Research*, 4(3):033089, August 2022. Publisher: American Physical Society.

[71] Yogesh S. Virkar, Woodrow L. Shew, Juan G. Restrepo, and Edward Ott. Feedback control stabilization of critical dynamics via resource transport on multilayer networks: How glia enable learning dynamics in the brain. *Phys. Rev. E*, 94(4):042310, October 2016. Publisher: American Physical Society.

[72] Baljit S Khakh and Michael V Sofroniew. Diversity of astrocyte functions and phenotypes in neural circuits. *Nature Neuroscience*, 18(7):942–952, July 2015.

[73] Nunzio Vicario, Agata Zappalà, Giovanna Calabrese, Rosario Gulino, Carmela Parenti, Massimo Gulisano, and Rosalba Parenti. Connexins in the Central Nervous System: Physiological Traits and Neuroprotective Targets. *Frontiers in Physiology*, 8, 2017.

[74] Eliana Scemes and Christian Giaume. Astrocyte calcium waves: what they are and what they do. *Glia*, 54(7):716–725, November 2006.

[75] Shane A. Liddelow and Ben A. Barres. Reactive Astrocytes: Production, Function, and Therapeutic Potential. *Immunity*, 46(6):957–967, June 2017. Publisher: Elsevier.

[76] Temitope Shoneye, Alessandra Tamashiro Orrego, Rachel Jarvis, Yuqin Men, Ming Sum R. Chiang, and Yongjie Yang. Differential Proliferation and Maturation of Subcortical Astrocytes During Postnatal Development. *Frontiers in Neuroscience*, 14, 2020.

[77] Samira Saadoun, Marios C. Papadopoulos, Hiroyuki Watanabe, Donghong Yan, Geoffrey T. Manley, and A. S. Verkman. Involvement of aquaporin-4 in astroglial cell migration and glial scar formation. *Journal of Cell Science*, 118(24):5691–5698, December 2005.

[78] Mark A. Anderson, Joshua E. Burda, Yilong Ren, Yan Ao, Timothy M. O'Shea, Riki Kawaguchi, Giovanni Coppola, Baljit S. Khakh, Timothy J. Deming, and Michael V. Sofroniew. Astrocyte scar formation aids central nervous system axon regeneration. *Nature*, 532(7598):195–200, April 2016.

[79] Juliane Schiweck, Britta J. Eickholt, and Kai Murk. Important Shapeshifter: Mechanisms Allowing Astrocytes to Respond to the Changing Nervous System During Development, Injury and Disease. *Frontiers in Cellular Neuroscience*, 12, 2018.

[80] Joshua E. Burda, Alexander M. Bernstein, and Michael V. Sofroniew. Astrocyte roles in traumatic brain injury. *Traumatic Brain Injury*, 275:305–315, January 2016.

[81] Joshua E Burda and Michael V Sofroniew. Seducing astrocytes to the dark side. *Cell Research*, 27(6):726–727, June 2017.

[82] Yonghee Kim, Jinhong Park, and Yoon K. Choi. The Role of Astrocytes in the Central Nervous System Focused on BK Channel and Heme Oxygenase Metabolites: A Review. *Antioxidants*, 8(5), 2019.

[83] Ruth Roales-Buján, Patricia Páez, Montserrat Guerra, Sara Rodríguez, Karin Vío, Ailec Ho-Plagaro, María García-Bonilla, Luis-Manuel Rodríguez-Pérez, María-Dolores Domínguez-Pinos, Esteban-Martín Rodríguez, José-Manuel Pérez-Fígares, and Antonio-Jesús Jiménez. Astrocytes acquire morphological and functional characteristics of ependymal cells following disruption of ependyma in hydrocephalus. *Acta Neuropathologica*, 124(4):531–546, October 2012.

[84] Benton S. Purnell, Mariana Alves, and Detlev Boison. Astrocyte-neuron circuits in epilepsy. *Neurobiology of Disease*, 179:106058, April 2023.

[85] Peter Bedner, Alexander Dupper, Kerstin Hüttmann, Julia Müller, Michel K. Herde, Pavel Dublin, Tushar Deshpande, Johannes Schramm, Ute Häussler, Carola A. Haas, Christian Henneberger, Martin Theis, and Christian Steinhäuser. Astrocyte uncoupling as a cause of human temporal lobe epilepsy. *Brain*, 138(5):1208–1222, May 2015.

[86] Bin Zhou, Yun-Xia Zuo, and Ruo-Tian Jiang. Astrocyte morphology: Diversity, plasticity, and role in neurological diseases. *CNS Neuroscience & Therapeutics*, 25(6):665–673, 2019. _eprint: https://onlinelibrary.wiley.com/doi/pdf/10.1111/cns.13123.

[87] Miki Bloch, Nivi Rotenberg, Dan Koren, and Ehud Klein. Risk factors associated with the development of postpartum mood disorders. *Journal of Affective Disorders*, 88(1):9–18, September 2005.

[88] Maria Grazia Mola, Emanuela Saracino, Francesco Formaggio, Arcangela Gabriella Amerotti, Barbara Barile, Tamara Posati, Antonio Cibelli, Antonio Frigeri, Claudia Palazzo, Roberto Zamboni, Marco Caprini, Grazia Paola Nicchia, and Valentina Benfenati. Cell Volume Regulation Mechanisms in Differentiated Astrocytes. *Cellular Physiology and Biochemistry: International Journal of Experimental Cellular Physiology, Biochemistry, and Pharmacology*, 55(S1):196–212, November 2021.

[89] Kate M. O'Neill, Emanuela Saracino, Barbara Barile, Nicholas J. Mennona, Maria Grazia Mola, Spandan Pathak, Tamara Posati, Roberto Zamboni, Grazia P. Nicchia, Valentina Benfenati, and Wolfgang Losert. Decoding Natural

Astrocyte Rhythms: Dynamic Actin Waves Result from Environmental Sensing by Primary Rodent Astrocytes. *Advanced biology*, page e2200269, January 2023. Place: Germany.

[90] Shinghua Ding. Ca2+ Signaling in Astrocytes and its Role in Ischemic Stroke. In Vladimir Parpura, Arne Schousboe, and Alexei Verkhratsky, editors, *Glutamate and ATP at the Interface of Metabolism and Signaling in the Brain*, pages 189–211. Springer International Publishing, Cham, 2014.

[91] Oluwadamilola Lawal, Francesco Paolo Ulloa Severino, and Cagla Eroglu. The role of astrocyte structural plasticity in regulating neural circuit function and behavior. *Glia*, 70(8):1467–1483, August 2022.

[92] Alexey Semyanov, Christian Henneberger, and Amit Agarwal. Making sense of astrocytic calcium signals — from acquisition to interpretation. *Nature Reviews Neuroscience*, 21(10):551–564, October 2020.

[93] Alfonso Araque, Vladimir Parpura, Rita P. Sanzgiri, and Philip G. Haydon. Tripartite synapses: glia, the unacknowledged partner. *Trends in Neurosciences*, 22(5):208–215, May 1999.

[94] Philip G. Haydon. Glia: listening and talking to the synapse. *Nature Reviews Neuroscience*, 2(3):185–193, March 2001.

[95] Carlos Eyzaguirre and Stephen W. Kuffler. FURTHER STUDY OF SOMA, DENDRITE, AND AXON EXCITATION IN SINGLE NEURONS. *Journal of General Physiology*, 39(1):121–153, September 1955.

[96] Raúl Lagos-Cabré, Francesca Burgos-Bravo, Ana María Avalos, and Lisette Leyton. Connexins in Astrocyte Migration. *Frontiers in Pharmacology*, 10, 2020.

[97] Gertrudis Perea, Mriganka Sur, and Alfonso Araque. Neuron-glia networks: integral gear of brain function. *Frontiers in Cellular Neuroscience*, 8, 2014.

[98] Christian Giaume, Annette Koulakoff, Lisa Roux, David Holcman, and Nathalie Rouach. Astroglial networks: a step further in neuroglial and gliovascular interactions. *Nature Reviews Neuroscience*, 11(2):87–99, February 2010.

[99] Iaroslav Savtchouk and Andrea Volterra. Gliotransmission: Beyond Black-and-White. *Journal of Neuroscience*, 38(1):14–25, 2018. Publisher: Society for Neuroscience _eprint: https://www.jneurosci.org/content/38/1/14.full.pdf.

[100] Annamaria Lia, Vanessa Jorge Henriques, Micaela Zonta, Angela Chiavegato, Giorgio Carmignoto, Marta Gómez-Gonzalo, and Gabriele Losi. Calcium Signals in Astrocyte Microdomains, a Decade of Great Advances. *Frontiers in Cellular Neuroscience*, 15, 2021.

[101] Sara Mederos, Candela González-Arias, and Gertrudis Perea. Astrocyte–Neuron Networks: A Multilane Highway of Signaling for Homeostatic Brain Function. *Frontiers in Synaptic Neuroscience*, 10, 2018.

[102] Fernando Aguado, Juan F. Espinosa-Parrilla, María A. Carmona, and Eduardo Soriano. Neuronal Activity Regulates Correlated Network Properties of Spontaneous Calcium Transients in Astrocytes In Situ. *The Journal of Neuroscience*, 22(21):9430–9444, November 2002.

[103] Claudia Compagnucci, Fiorella Piemonte, Antonella Sferra, Emanuela Piermarini, and Enrico Bertini. The cytoskeletal arrangements necessary to neurogenesis. *Oncotarget; Vol 7, No 15*, 2016.

[104] PAUL A. JANMEY. The Cytoskeleton and Cell Signaling: Component Localization and Mechanical Coupling. *Physiological Reviews*, 78(3):763–781, January 1998. Publisher: American Physiological Society.

[105] Dong-Hwee Kim and Denis Wirtz. Cytoskeletal tension induces the polarized architecture of the nucleus. *Biomaterials*, 48:161–172, April 2015.

[106] Kevin C. Flynn, Chi W. Pak, Alisa E. Shaw, Frank Bradke, and James R. Bamburg. Growth cone-like waves transport actin and promote axonogenesis and neurite branching. *Developmental Neurobiology*, 69(12):761–779, October 2009. Publisher: John Wiley & Sons, Ltd.

[107] Juliana E. Gentile, Melissa G. Carrizales, and Anthony J. Koleske. Control of Synapse Structure and Function by Actin and Its Regulators. *Cells*, 11(4), 2022.

[108] Anja Konietzny, Julia Bär, and Marina Mikhaylova. Dendritic Actin Cytoskeleton: Structure, Functions, and Regulations. *Frontiers in Cellular Neuroscience*, 11, 2017.

[109] Sreetama Basu and Raphael Lamprecht. The Role of Actin Cytoskeleton in Dendritic Spines in the Maintenance of Long-Term Memory. *Frontiers in Molecular Neuroscience*, 11, 2018.

[110] Rachel M. Lee, Leonard Campanello, Matt J. Hourwitz, Phillip Alvarez, Ava Omidvar, John T. Fourkas, and Wolfgang Losert. Quantifying topography-guided actin dynamics across scales using optical flow. *Molecular Biology of the Cell*, 31(16):1753–1764, July 2020. Publisher: American Society for Cell Biology (mboc).

[111] Shiladitya Banerjee, Margaret L. Gardel, and Ulrich S. Schwarz. The Actin Cytoskeleton as an Active Adaptive Material. *Annual Review of Condensed Matter Physics*, 11(Volume 11, 2020):421–439, 2020. Publisher: Annual Reviews Type: Journal Article.

[112] Yuchuan Miao, Sayak Bhattacharya, Tatsat Banerjee, Bedri Abubaker-Sharif, Yu Long, Takanari Inoue, Pablo A Iglesias, and Peter N Devreotes. Wave patterns organize cellular protrusions and control cortical dynamics. *Molecular Systems Biology*, 15(3):e8585, March 2019. Publisher: John Wiley & Sons, Ltd.

[113] Naoyuki Inagaki and Hiroko Katsuno. Actin Waves: Origin of Cell Polarization and Migration? *Trends in Cell Biology*, 27(7):515–526, July 2017. Publisher: Elsevier.

[114] Sylvester J. Gates, Phillip Alvarez, Kan Cao, Kate O'Neill, and Wolfgang Losert. Coupled Biomechanical and Ionic Excitability in Developing Neural Cell Networks. *bioRxiv*, page 2023.02.15.528510, January 2023.

[115] Takunori Minegishi, Ria Fajarwati Kastian, and Naoyuki Inagaki. Mechanical regulation of synapse formation and plasticity. *Special issue: Driving forces behind the wiring of neuronal circuits*, 140:82–89, May 2023.

[116] Krishna Chaitanya Kasuba, Alessio Paolo Buccino, Julian Bartram, Benjamin M. Gaub, Felix J. Fauser, Silvia Ronchi, Sreedhar Saseendran Kumar, Sydney Geissler, Michele M. Nava, Andreas Hierlemann, and Daniel J. Müller. Mechanical stimulation and electrophysiological monitoring at subcellular resolution reveals differential mechanosensation of neurons within networks. *Nature Nanotechnology*, February 2024.

[117] Katherine T. Baldwin, Keith K. Murai, and Baljit S. Khakh. Astrocyte morphology. *Trends in cell biology*, pages S0962–8924(23)00204–0, October 2023. Place: England.

[118] Alfonso Araque, Giorgio Carmignoto, Philip G. Haydon, Stéphane H.R. Oliet, Richard Robitaille, and Andrea Volterra. Gliotransmitters Travel in Time and Space. *Neuron*, 81(4):728–739, February 2014.

[119] Laurent Blanchoin, Rajaa Boujemaa-Paterski, Cécile Sykes, and Julie Plastino. Actin Dynamics, Architecture, and Mechanics in Cell Motility. *Physiological Reviews*, 94(1):235–263, January 2014. Publisher: American Physiological Society.

[120] Nicolai T. Urban, Katrin I. Willig, Stefan W. Hell, and U. Valentin Nägerl. STED Nanoscopy of Actin Dynamics in Synapses Deep Inside Living Brain Slices. *Biophysical Journal*, 101(5):1277–1284, September 2011. Publisher: Elsevier.

[121] Marileen Dogterom and Gijsje H. Koenderink. Actin–microtubule crosstalk in cell biology. *Nature Reviews Molecular Cell Biology*, 20(1):38–54, January 2019.

[122] Ivan Rey-Suarez, Nate Rogers, Sarah Kerr, Hari Shroff, and Arpita Upadhyaya. Actomyosin dynamics modulate microtubule deformation and growth during T-cell activation. *Molecular Biology of the Cell*, 32(18):1641–1653, August 2021. Publisher: American Society for Cell Biology (mboc).

[123] Manuela De Bellis, Francesco Pisani, Maria Grazia Mola, Stefania Rosito, Laura Simone, Cinzia Buccoliero, Maria Trojano, Grazia Paola Nicchia, Maria Svelto, and Antonio Frigeri. Translational readthrough generates new astrocyte AQP4 isoforms that modulate supramolecular clustering, glial endfeet localization, and water transport. *Glia*, 65(5):790–803, May 2017. Place: United States.

[124] Manuela de Bellis, Antonio Cibelli, Maria Grazia Mola, Francesco Pisani, Barbara Barile, Maria Mastrodonato, Shervin Banitalebi, Mahmood Amiry-Moghaddam, Pasqua Abbrescia, Antonio Frigeri, Maria Svelto, and Grazia Paola Nicchia. Orthogonal arrays of particle assembly are essential for normal aquaporin-4 expression level in the brain. *Glia*, 69(2):473–488, February 2021. Place: United States.

[125] Valentina Benfenati, Marco Caprini, Mario Nobile, Carmela Rapisarda, and Stefano Ferroni. Guanosine promotes the up-regulation of inward rectifier potassium current mediated by Kir4.1 in cultured rat cortical astrocytes. *Journal of Neurochemistry*, 98(2):430–445, July 2006. Publisher: John Wiley & Sons, Ltd.

[126] J. E. Huettner and R. W. Baughman. Primary culture of identified neurons from the visual cortex of postnatal rats. *The Journal of neuroscience : the official journal of the Society for Neuroscience*, 6(10):3044–3060, October 1986. Place: United States.

[127] David Wasilewski, Nelson David Villalba-Moreno, Inke Stange, Markus Glatzel, Diego Sepulveda-Falla, and Susanne Krasemann. Reactive Astrocytes Contribute to Alzheimer's Disease-Related Neurotoxicity and Synaptotoxicity in a Neuron-Astrocyte Co-culture Assay. *Frontiers in Cellular Neuroscience*, 15, 2022.

[128] E. P. Simoncelli. Design of multi-dimensional derivative filters. In *Proceedings of 1st International Conference on Image Processing*, volume 1, pages 790–794 vol.1, November 1994. Journal Abbreviation: Proceedings of 1st International Conference on Image Processing.

[129] Manuel Guizar-Sicairos, Samuel T. Thurman, and James R. Fienup. Efficient subpixel image registration algorithms. *Optics Letters*, 33(2):156–158, January 2008. Publisher: Optica Publishing Group.

[130] Johannes Hirrlinger, Swen Hülsmann, and Frank Kirchhoff. Astroglial processes show spontaneous motility at active synaptic terminals in situ. *European Journal of Neuroscience*, 20(8):2235–2239, October 2004. Publisher: John Wiley & Sons, Ltd.

[131] Gertrudis Perea, Marta Navarrete, and Alfonso Araque. Tripartite synapses: astrocytes process and control synaptic information. *Trends in neurosciences*, 32(8):421–431, August 2009. Place: England.

[132] George M. Smith, Urs Rutishauser, Jerry Silver, and Robert H. Miller. Maturation of astrocytes in vitro alters the extent and molecular basis of neurite outgrowth. *Developmental Biology*, 138(2):377–390, April 1990.

[133] Yanping Shao and Ken D. McCarthy. Plasticity of astrocytes. *Glia*, 11(2):147–155, June 1994. Publisher: John Wiley & Sons, Ltd.

[134] Nathan Curry, Grégory Ghézali, Gabriele S. Kaminski Schierle, Nathalie Rouach, and Clemens F. Kaminski. Correlative STED and Atomic Force Microscopy on Live Astrocytes Reveals Plasticity of Cytoskeletal Structure and Membrane Physical Properties during Polarized Migration. *Frontiers in Cellular Neuroscience*, 11, 2017.

[135] H. Maldonado, C. Calderon, F. Burgos-Bravo, O. Kobler, W. Zuschratter, O. Ramirez, S. Härtel, P. Schneider, A.F.G. Quest, R. Herrera-Molina, and L. Leyton. Astrocyte-to-neuron communication through integrin-engaged Thy-1/CBP/Csk/Src complex triggers neurite retraction via the RhoA/ROCK pathway. *Biochimica et Biophysica Acta (BBA) - Molecular Cell Research*, 1864(2):243–254, February 2017.

[136] Tamara Posati, Assunta Pistone, Emanuela Saracino, Francesco Formaggio, Maria Grazia Mola, Elisabetta Troni, Anna Sagnella, Morena Nocchetti, Marianna Barbalinardo, Francesco Valle, Simone Bonetti, Marco Caprini, Grazia Paola Nicchia, Roberto Zamboni, Michele Muccini, and Valentina Benfenati. A Nanoscale Interface Promoting Molecular and Functional Differentiation of Neural Cells. *Scientific Reports*, 6(1):31226, August 2016.

[137] Valentina Benfenati, Grazia Paola Nicchia, Maria Svelto, Carmela Rapisarda, Antonio Frigeri, and Stefano Ferroni. Functional down-regulation of volume-regulated anion channels in AQP4 knockdown cultured rat cortical astrocytes. *Journal of Neurochemistry*, 100(1):87–104, January 2007. Publisher: John Wiley & Sons, Ltd.

[138] Stefano Ferroni, Cristina Marchini, Mario Nobile, and Carmela Rapisarda. Characterization of an inwardly rectifying chloride conductance expressed by cultured rat cortical astrocytes. *Glia*, 21(2):217–227, October 1997. Publisher: John Wiley & Sons, Ltd.

[139] Grazia Paola Nicchia, Antonio Frigeri, Grazia Maria Liuzzi, Maria Pia Santacroce, Beatrice Nico, Giuseppe Procino, Fabio Quondamatteo, Reiner Herken, Luisa Roncali, and Maria Svelto. Aquaporin-4-containing astrocytes sustain a temperature- and mercury-insensitive swelling in vitro. *Glia*, 31(1):29–38, July 2000. Publisher: John Wiley & Sons, Ltd.

[140] Nicholas J. Mennona, Anna Sedelnikova, Ibtissam Echchgadda, and Wolfgang Losert. Filament displacement image analytics tool for use in investigating dynamics of dense microtubule networks. *Physical Review E*, 108(3):034411, September 2023. Publisher: American Physical Society.

[141] Andreas Nebenführ and Ram Dixit. Kinesins and Myosins: Molecular Motors that Coordinate Cellular Functions in Plants. *Annual Review of Plant Biology*, 69(1):329–361, April 2018. Publisher: Annual Reviews.

[142] M. G. L. Van den Heuvel, M. P. de Graaff, and C. Dekker. Microtubule curvatures under perpendicular electric forces reveal a low persistence length. *Proceedings of the National Academy of Sciences*, 105(23):7941, June 2008.

[143] Jan Pokorný, Jiří Pokorný, and Jan Vrba. Generation of Electromagnetic Field by Microtubules. *International journal of molecular sciences*, 22(15):8215, July 2021. Publisher: MDPI.

[144] Francesco Pampaloni, Gianluca Lattanzi, Alexandr Jonáš, Thomas Surrey, Erwin Frey, and Ernst-Ludwig Florin. Thermal fluctuations of grafted microtubules provide evidence of a length-dependent persistence length. *Proceedings of the National Academy of Sciences*, 103(27):10248, July 2006.

[145] M. G. L. van den Heuvel, S. Bolhuis, and C. Dekker. Persistence Length Measurements from Stochastic Single-Microtubule Trajectories. *Nano Letters*, 7(10):3138–3144, October 2007. Publisher: American Chemical Society.

[146] A. Kis, S. Kasas, B. Babić, A. J. Kulik, W. Benoît, G. A. D. Briggs, C. Schönenberger, S. Catsicas, and L. Forró. Nanomechanics of Microtubules. *Physical Review Letters*, 89(24):248101, November 2002. Publisher: American Physical Society.

[147] A. Kis, S. Kasas, A. J. Kulik, S. Catsicas, and L. Forró. Temperature-Dependent Elasticity of Microtubules. *Langmuir*, 24(12):6176–6181, June 2008. Publisher: American Chemical Society.

[148] Mahito Kikumoto, Masashi Kurachi, Valer Tosa, and Hideo Tashiro. Flexural Rigidity of Individual Microtubules Measured by a Buckling Force with Optical Traps. *Biophysical Journal*, 90(5):1687–1696, March 2006.

[149] Kaustubh Wagh, Momoko Ishikawa, David A. Garcia, Diana A. Stavreva, Arpita Upadhyaya, and Gordon L. Hager. Mechanical Regulation of Transcription: Recent Advances. *Trends in Cell Biology*, 31(6):457–472, June 2021.

[150] Nasrin Syeda Rubaiya, Ganser Christian, Nishikawa Seiji, Kabir Arif Md. Rashedul, Sada Kazuki, Yamashita Takefumi, Ikeguchi Mitsunori, Uchihashi Takayuki, Hess Henry, and Kakugo Akira. Deformation of microtubules regulates translocation dynamics of kinesin. *Science Advances*, 7(42):eabf2211. Publisher: American Association for the Advancement of Science.

[151] Pattipong Wisanpitayakorn, Keith J. Mickolajczyk, William O. Hancock, Luis Vidali, and Erkan Tüzel. Measurement of the persistence length of cytoskeletal filaments using curvature distributions. *Biophysical Journal*, 121(10):1813–1822, May 2022.

[152] Mary Ann Jordan and Leslie Wilson. Microtubules as a target for anticancer drugs. *Nature Reviews Cancer*, 4(4):253–265, April 2004.

[153] Amelia L. Parker, Maria Kavallaris, and Joshua A. McCarroll. Microtubules and Their Role in Cellular Stress in Cancer. *Frontiers in Oncology*, 4, 2014.

[154] April L. Blajeski, Vy A. Phan, Timothy J. Kottke, and Scott H. Kaufmann. G1 and G2 cell-cycle arrest following microtubule depolymerization in human breast cancer cells. *The Journal of Clinical Investigation*, 110(1):91–99, July 2002. Publisher: The American Society for Clinical Investigation.

[155] Paolo Marracino, Daniel Havelka, Jiří Průša, Micaela Liberti, Jack Tuszynski, Ahmed T. Ayoub, Francesca Apollonio, and Michal Cifra. Tubulin response to intense nanosecond-scale electric field in molecular dynamics simulation. *Scientific Reports*, 9(1):10477, July 2019.

[156] Alexandre Matov, Kathryn Applegate, Praveen Kumar, Claudio Thoma, Wilhelm Krek, Gaudenz Danuser, and Torsten Wittmann. Analysis of microtubule dynamic instability using a plus-end growth marker. *Nature Methods*, 7(9):761–768, September 2010. Number: 9 Publisher: Nature Publishing Group.

[157] Alexander James Zwetsloot, Gokhan Tut, and Anne Straube. Measuring microtubule dynamics. *Essays in Biochemistry*, 62(6):725–735, October 2018.

[158] R. Dhar, R. Gupta, and K. L. Baishnab. An analysis of CANNY and LAPLACIAN of GAUSSIAN image filters in regard to evaluating retinal image. In *2014 International Conference on Green Computing Communication and Electrical Engineering (ICGCCEE)*, pages 1–6, March 2014. Journal Abbreviation: 2014 International Conference on Green Computing Communication and Electrical Engineering (ICGCCEE).

[159] J. L. Barron, D. J. Fleet, and S. S. Beauchemin. Performance of optical flow techniques. *International Journal of Computer Vision*, 12(1):43–77, February 1994.

[160] Evelyn Garlick, Steven G. Thomas, and Dylan M. Owen. Super-Resolution Imaging Approaches for Quantifying F-Actin in Immune Cells. *Frontiers in Cell and Developmental Biology*, 9, 2021.

[161] Clifford P. Brangwynne, F. C. MacKintosh, and David A. Weitz. Force fluctuations and polymerization dynamics of intracellular microtubules. *Proceedings of the National Academy of Sciences*, 104(41):16128, October 2007.

[162] C.P. Broedersz and F.C. MacKintosh. Modeling semiflexible polymer networks. *Reviews of Modern Physics*, 86(3):995–1036, July 2014. Publisher: American Physical Society.

[163] Nicholas J. Mennona, Barbara Barile, Hoony Kang, Valentina Benfenati, Grazia P. Nicchia, Kate M. O'Neill, and Wolfgang Losert. Collective Information and Communication in Morphologically Distinct Astrocytes. *bioRxiv*, page 2023.11.01.565176, January 2023.

[164] Alba Bellot-Saez, Orsolya Kékesi, John W. Morley, and Yossi Buskila. Astrocytic modulation of neuronal excitability through K+ spatial buffering. *Neuroscience & Biobehavioral Reviews*, 77:87–97, June 2017.

[165] Shaimaa Mahmoud, Marjan Gharagozloo, Camille Simard, and Denis Gris. Astrocytes Maintain Glutamate Homeostasis in the CNS by Controlling the Balance between Glutamate Uptake and Release. *Cells*, 8(2):184, February 2019.

[166] Mireille Bélanger, Igor Allaman, and Pierre J. Magistretti. Brain Energy Metabolism: Focus on Astrocyte-Neuron Metabolic Cooperation. *Cell Metabolism*, 14(6):724–738, December 2011. Publisher: Elsevier.

[167] Christof Koch and Idan Segev. The role of single neurons in information processing. *Nature Neuroscience*, 3(11):1171–1177, November 2000.

[168] Liqun Luo, Eugenio Rodriguez, Karim Jerbi, Jean-Philippe Lachaux, Jacques Martinerie, Maurizio Corbetta, Gordon L. Shulman, Daniele Piomelli, Gina G. Turrigiano, Sacha B. Nelson, Marian Joëls, E. Ronald de Kloet, Florian Holsboer, David M. Amodio, Chris D. Frith, Michelle L. Block, Luigi Zecca, Jau-Shyong Hong, Robert Dantzer, Keith W. Kelley, and A. D. (Bud) Craig. Ten years of Nature Reviews Neuroscience: insights from the highly cited. *Nature Reviews Neuroscience*, 11(10):718–726, October 2010.

[169] Anders Krogh. What are artificial neural networks? *Nature Biotechnology*, 26(2):195–197, February 2008.

[170] Yizhi Wang, Nicole V. DelRosso, Trisha V. Vaidyanathan, Michelle K. Cahill, Michael E. Reitman, Silvia Pittolo, Xuelong Mi, Guoqiang Yu, and Kira E. Poskanzer. Accurate quantification of astrocyte and neurotransmitter fluorescence dynamics for single-cell and population-level physiology. *Nature Neuroscience*, 22(11):1936–1944, November 2019. Number: 11 Publisher: Nature Publishing Group.

[171] Amit Agarwal, Pei-Hsun Wu, Ethan G. Hughes, Masahiro Fukaya, Max A. Tischfield, Abraham J. Langseth, Denis Wirtz, and Dwight E. Bergles. Transient Opening of the Mitochondrial Permeability Transition Pore Induces Microdomain Calcium Transients in Astrocyte Processes. *Neuron*, 93(3):587–605.e7, February 2017. Publisher: Elsevier.

[172] Egor Dzyubenko, Wojciech Prazuch, Matthias Pillath-Eilers, Joanna Polanska, and Dirk M. Hermann. Analysing Intercellular Communication in Astrocytic Networks Using "Astral". *Frontiers in Cellular Neuroscience*, 15, 2021.

[173] Luis Abrego, Susanna Gordleeva, Oleg Kanakov, Mikhail Krivonosov, and Alexey Zaikin. Estimating integrated information in bidirectional neuron-astrocyte communication. *Physical Review E*, 103(2):022410, February 2021. Publisher: American Physical Society.

[174] Andrea Volterra and Jacopo Meldolesi. Astrocytes, from brain glue to communication elements: the revolution continues. *Nature Reviews Neuroscience*, 6(8):626–640, August 2005. Number: 8 Publisher: Nature Publishing Group.

[175] Michelle K. Cahill, Max Collard, Vincent Tse, Michael E. Reitman, Roberto Etchenique, Christoph Kirst, and Kira E. Poskanzer. Network-level encoding of local neurotransmitters in cortical astrocytes. *Nature*, 629(8010):146–153, May 2024.

[176] Ksenia V. Kastanenka, Rubén Moreno-Bote, Maurizio De Pittà, Gertrudis Perea, Abel Eraso-Pichot, Roser Masgrau, Kira E. Poskanzer, and Elena Galea. A roadmap to integrate astrocytes into Systems Neuroscience. *Glia*, 68(1):5–26, January 2020. Place: United States.

[177] Narges Bazargani and David Attwell. Astrocyte calcium signaling: the third wave. *Nature Neuroscience*, 19(2):182–189, February 2016.

[178] Jenny I. Szu and Devin K. Binder. The Role of Astrocytic Aquaporin-4 in Synaptic Plasticity and Learning and Memory. *Frontiers in Integrative Neuroscience*, 10, 2016.

[179] Alessandro Bortolami and Federico Sesti. Ion channels in neurodevelopment: lessons from the Integrin-KCNB1 channel complex. *Neural Regeneration Research*, 18(11), 2023.

[180] Erlend A. Nagelhus and Ole P. Ottersen. Physiological Roles of Aquaporin-4 in Brain. *Physiological Reviews*, 93(4):1543–1562, October 2013. Publisher: American Physiological Society.

[181] Yukihiro Ohno, Naofumi Kunisawa, and Saki Shimizu. Emerging Roles of Astrocyte Kir4.1 Channels in the Pathogenesis and Treatment of Brain Diseases. *International Journal of Molecular Sciences*, 22(19), 2021.

[182] Valentina Benfenati, Marco Caprini, Melania Dovizio, Maria N. Mylonakou, Stefano Ferroni, Ole P. Ottersen, and Mahmood Amiry-Moghaddam. An aquaporin-4/transient receptor potential vanilloid 4 (AQP4/TRPV4) complex is essential for cell-volume control in astrocytes. *Proceedings of the National Academy of Sciences*, 108(6):2563–2568, February 2011. Publisher: Proceedings of the National Academy of Sciences.

[183] Yan-Ying Fan and Jing Huo. A1/A2 astrocytes in central nervous system injuries and diseases: Angels or devils? *Neurochemistry International*, 148:105080, September 2021.

[184] Lucile Ben Haim, Kelly Ceyzériat, Maria Angeles Carrillo-de Sauvage, Fabien Aubry, Gwennaëlle Auregan, Martine Guillermier, Marta Ruiz, Fanny Petit, Diane Houitte, Emilie Faivre, Matthias Vandesquille, Romina Aron-Badin, Marc Dhenain, Nicole Déglon, Philippe Hantraye, Emmanuel Brouillet, Gilles Bonvento, and Carole Escartin. The JAK/STAT3 Pathway Is a Common Inducer of Astrocyte Reactivity in Alzheimer's and Huntington's Diseases. *The Journal of Neuroscience*, 35(6):2817, February 2015.

[185] B. Homkajorn, N.R. Sims, and H. Muyderman. Connexin 43 regulates astrocytic migration and proliferation in response to injury. *Neuroscience Letters*, 486(3):197–201, December 2010.

[186] Richard Burnard Rodnight and Carmem Gottfried. Morphological plasticity of rodent astroglia. *Journal of Neurochemistry*, 124(3):263–275, 2013. _eprint: https://onlinelibrary.wiley.com/doi/pdf/10.1111/jnc.12087.

[187] Lidija Gradisnik and Tomaz Velnar. Astrocytes in the central nervous system and their functions in health and disease: A review. *World Journal of Clinical Cases*, 11(15):3385–3394, May 2023.

[188] Carole Escartin, Elena Galea, András Lakatos, James P. O'Callaghan, Gabor C. Petzold, Alberto Serrano-Pozo, Christian Steinhäuser, Andrea Volterra, Giorgio Carmignoto, Amit Agarwal, Nicola J. Allen, Alfonso Araque, Luis Barbeito, Ari Barzilai, Dwight E. Bergles, Gilles Bonvento, Arthur M. Butt, Wei-Ting Chen, Martine Cohen-Salmon, Colm Cunningham, Benjamin Deneen, Bart De Strooper, Blanca Díaz-Castro, Cinthia Farina, Marc Freeman, Vittorio Gallo, James E. Goldman, Steven A. Goldman, Magdalena Götz, Antonia Gutiérrez, Philip G. Haydon, Dieter H. Heiland, Elly M. Hol, Matthew G. Holt, Masamitsu Iino, Ksenia V. Kastanenka, Helmut Kettenmann, Baljit S. Khakh, Schuichi Koizumi, C. Justin Lee, Shane A. Liddelow, Brian A. MacVicar, Pierre Magistretti, Albee Messing, Anusha Mishra, Anna V. Molofsky, Keith K. Murai, Christopher M. Norris, Seiji Okada, Stéphane H. R. Oliet, João F. Oliveira, Aude Panatier, Vladimir Parpura, Marcela Pekna, Milos Pekny, Luc Pellerin, Gertrudis Perea, Beatriz G. Pérez-Nievas, Frank W. Pfrieger, Kira E. Poskanzer, Francisco J. Quintana, Richard M. Ransohoff, Miriam Riquelme-Perez, Stefanie Robel, Christine R. Rose, Jeffrey D. Rothstein, Nathalie Rouach, David H. Rowitch, Alexey Semyanov, Swetlana Sirko, Harald Sontheimer, Raymond A. Swanson, Javier Vitorica, Ina-Beate Wanner, Levi B. Wood, Jiaqian Wu, Binhai Zheng, Eduardo R. Zimmer, Robert Zorec, Michael V. Sofroniew, and Alexei Verkhratsky. Reactive astrocyte nomenclature, definitions, and future directions. *Nature Neuroscience*, 24(3):312–325, March 2021.

[189] Albert Giralt, Renata Coura, and Jean-Antoine Girault. Pyk2 is essential for astrocytes mobility following brain lesion. *Glia*, 64(4):620–634, April 2016. Publisher: John Wiley & Sons, Ltd.

[190] Masaru Mitsushima, Honami Takahashi, Tomoyuki Shishido, Kazumitsu Ueda, and Noriyuki Kioka. Abl kinase interacts with and phosphorylates vinexin. *FEBS Letters*, 580(17):4288–4295, July 2006. Publisher: John Wiley & Sons, Ltd.

[191] Mónica Tomás, Francisco Lázaro-Diéguez, Juan M. Durán, Pilar Marín, Jaime Renau-Piqueras, and Gustavo Egea. Protective effects of lysophosphatidic acid (LPA) on chronic ethanol-induced injuries to the cytoskeleton and on glucose uptake in rat astrocytes. *Journal of Neurochemistry*, 87(1):220–229, October 2003. Publisher: John Wiley & Sons, Ltd.

[192] David N. Bowser and Baljit S. Khakh. ATP Excites Interneurons and Astrocytes to Increase Synaptic Inhibition in Neuronal Networks. *The Journal of Neuroscience*, 24(39):8606, September 2004.

[193] Peter B. Guthrie, Joshua Knappenberger, Menahem Segal, Michael V. L. Bennett, Andrew C. Charles, and S. B. Kater. ATP Released from Astrocytes Mediates Glial Calcium Waves. *The Journal of Neuroscience*, 19(2):520, January 1999.

[194] Herbert Zimmermann. Signalling via ATP in the nervous system. *Trends in Neurosciences*, 17(10):420–426, January 1994.

[195] Geoffrey Burnstock. Cotransmission. *Current Opinion in Pharmacology*, 4(1):47–52, February 2004.

[196] Christian Giaume and Laurent Venance. Intercellular calcium signaling and gap junctional communication in astrocytes. *Glia*, 24(1):50–64, 1998. _eprint: https://onlinelibrary.wiley.com/doi/pdf/10.1002/%28SICI%291098-1136%28199809%2924%3A1%3C50%3A%3AAID-GLIA6%3E3.0.CO%3B2-4.

[197] Panpan Yu, Hang Wang, Yasuhiro Katagiri, and Herbert M. Geller. An In Vitro Model of Reactive Astrogliosis and Its Effect on Neuronal Growth. *Methods in molecular biology (Clifton, N.J.)*, 814:327–340, 2012.

[198] Zainab Sabry Othman Ahmed, Shaymaa Hussein, Rehab A. Ghandour, Asmaa A. Azouz, and Mohamed A. El-Sakhawy. Evaluation of the effect of methotrexate on the hippocampus, cerebellum, liver, and kidneys of adult male albino rat: Histopathological, immunohistochemical and biochemical studies. *Acta Histochemica*, 123(2):151682, February 2021.

[199] Vincenzo Bramanti, Daniele Tomassoni, Marcello Avitabile, Francesco Amenta, and Roberto Avola. Biomarkers of glial cell proliferation and differentiation in culture. *FBS*, 2(2):558–570, 2010.

[200] Antonio Cibelli, Maria Grazia Mola, Emanuela Saracino, Barbara Barile, Pasqua Abbrescia, Guido Mogni, David C. Spray, Eliana Scemes, Andrea Rossi, Diletta Spennato, Maria Svelto, Antonio Frigeri, Valentina Benfenati, and Grazia Paola Nicchia. Aquaporin-4 and transient receptor potential vanilloid 4 balance in early postnatal neurodevelopment. *Glia*, 72(5):938–959, May 2024. Publisher: John Wiley & Sons, Ltd.

[201] J.V. Berger, A.O. Dumont, M.C. Focant, M. Vergouts, A. Sternotte, A.-G. Calas, S. Goursaud, and E. Hermans. Opposite regulation of metabotropic glutamate receptor 3 and metabotropic glutamate receptor 5 by inflammatory stimuli in cultured microglia and astrocytes. *Neuroscience*, 205:29–38, March 2012.

[202] Cai Song, Ye Zhang, and Yilong Dong. Acute and subacute IL-1 administrations differentially modulate neuroimmune and neurotrophic systems: possible implications for neuroprotection and neurodegeneration. *Journal of Neuroinflammation*, 10(1):826, May 2013.

[203] Sébastien Tilleux, Julie Berger, and Emmanuel Hermans. Induction of astrogliosis by activated microglia is associated with a down-regulation of metabotropic glutamate receptor 5. *Journal of Neuroimmunology*, 189(1):23–30, September 2007.

[204] Sébastien Tilleux and Emmanuel Hermans. Neuroinflammation and regulation of glial glutamate uptake in neurological disorders. *Journal of Neuroscience Research*, 85(10):2059–2070, August 2007. Publisher: John Wiley & Sons, Ltd.

[205] Susan M. Sullivan, Aven Lee, S. Tracey Björkman, Stephanie M. Miller, Robert K.P. Sullivan, Philip Poronnik, Paul B. Colditz, and David V. Pow. Cytoskeletal Anchoring of GLAST Determines Susceptibility to Brain Damage: AN IDENTIFIED ROLE FOR GFAP *. *Journal of Biological Chemistry*, 282(40):29414–29423, October 2007. Publisher: Elsevier.

[206] Kimberly A. Toops, Tracy L. Hagemann, Albee Messing, and Robert W. Nickells. The effect of glial fibrillary acidic protein expression on neurite outgrowth from retinal explants in a permissive environment. *BMC Research Notes*, 5(1):693, December 2012.

[207] Joe Chalfoun, Michael Majurski, Alden Dima, Christina Stuelten, Adele Peskin, and Mary Brady. FogBank: a single cell segmentation across multiple cell lines and image modalities. *BMC Bioinformatics*, 15(1):431, December 2014.

[208] Andrea Giovannucci, Johannes Friedrich, Pat Gunn, Jérémie Kalfon, Brandon L Brown, Sue Ann Koay, Jiannis Taxidis, Farzaneh Najafi, Jeffrey L Gauthier, Pengcheng Zhou, Baljit S Khakh, David W Tank, Dmitri B Chklovskii, and Eftychios A Pnevmatikakis. CaImAn an open source tool for scalable calcium imaging data analysis. *eLife*, 8:e38173, January 2019. Publisher: eLife Sciences Publications, Ltd.

[209] Zac Bowen, Daniel E. Winkowski, Saurav Seshadri, Dietmar Plenz, and Patrick O. Kanold. Neuronal Avalanches in Input and Associative Layers of Auditory Cortex. *Frontiers in Systems Neuroscience*, 13, 2019.

[210] Ingve Simonsen, Alex Hansen, and Olav Magnar Nes. Determination of the Hurst exponent by use of wavelet transforms. *Physical Review E*, 58(3):2779–2787, September 1998. Publisher: American Physical Society.

[211] Generalized Hurst exponent, August 2023.

[212] Bruno B. Averbeck, Peter E. Latham, and Alexandre Pouget. Neural correlations, population coding and computation. *Nature Reviews Neuroscience*, 7(5):358–366, May 2006. Number: 5 Publisher: Nature Publishing Group.

[213] S Panzeri, S R Schultz, A Treves, and E T Rolls. Correlations and the encoding of information in the nervous system. *Proceedings of the Royal Society B: Biological Sciences*, 266(1423):1001–1012, May 1999.

[214] Marlene R. Cohen and Adam Kohn. Measuring and interpreting neuronal correlations. *Nature Neuroscience*, 14(7):811–819, July 2011. Number: 7 Publisher: Nature Publishing Group.

[215] Adam Kohn, Ruben Coen-Cagli, Ingmar Kanitscheider, and Alexandre Pouget. Correlations and Neuronal Population Information. *Annual Review of Neuroscience*, 39(1):237–256, 2016. _eprint: https://doi.org/10.1146/annurev-neuro-070815-013851.

[216] C. S. Daw, C. E. A. Finney, and E. R. Tracy. A review of symbolic analysis of experimental data. *Review of Scientific Instruments*, 74(2):915–930, January 2003.

[217] Yinhe Cao, Wen-wen Tung, J. B. Gao, V. A. Protopopescu, and L. M. Hively. Detecting dynamical changes in time series using the permutation entropy. *Physical Review E*, 70(4):046217, October 2004. Publisher: American Physical Society.

[218] Max Lungarella, Alex Pitti, and Yasuo Kuniyoshi. Information transfer at multiple scales. *Physical Review E*, 76(5):056117, November 2007. Publisher: American Physical Society.

[219] Thomas Schreiber. Measuring Information Transfer. *Physical Review Letters*, 85(2):461–464, July 2000. Publisher: American Physical Society.

[220] Klaus Lehnertz. Ordinal methods for a characterization of evolving functional brain networks. *Chaos: An Interdisciplinary Journal of Nonlinear Science*, 33(2):022101, February 2023.

[221] MATTHÄUS STANIEK and KLAUS LEHNERTZ. PARAMETER SELECTION FOR PERMUTATION ENTROPY MEASUREMENTS. *International Journal of Bifurcation and Chaos*, 17(10):3729–3733, October 2007. Publisher: World Scientific Publishing Co.

[222] Matthäus Staniek and Klaus Lehnertz. Symbolic Transfer Entropy. *Physical Review Letters*, 100(15):158101, April 2008. Publisher: American Physical Society.

[223] Matthäus Staniek and Klaus Lehnertz. Symbolic transfer entropy: inferring directionality in biosignals. 54(6):323–328, 2009.

[224] Christoph Bandt and Bernd Pompe. Permutation Entropy: A Natural Complexity Measure for Time Series. *Physical Review Letters*, 88(17):174102, April 2002. Publisher: American Physical Society.

[225] Kota Shiozawa, Taisuke Uemura, and Isao T. Tokuda. Detecting the dynamical instability of complex time series via partitioned entropy. *Physical Review E*, 107(1):014207, January 2023. Publisher: American Physical Society.

[226] Songting Li, Yanyang Xiao, Douglas Zhou, and David Cai. Causal inference in nonlinear systems: Granger causality versus time-delayed mutual information. *Physical Review E*, 97(5):052216, May 2018. Publisher: American Physical Society.

[227] John A. Vastano and Harry L. Swinney. Information transport in spatiotemporal systems. *Physical Review Letters*, 60(18):1773–1776, May 1988. Publisher: American Physical Society.

[228] Andrew C. Charles, Jean E. Merrill, Ellen R. Dirksen, and Michael J. Sandersont. Intercellular signaling in glial cells: Calcium waves and oscillations in response to mechanical stimulation and glutamate. *Neuron*, 6(6):983–992, June 1991.

[229] S R Glaum, J A Holzwarth, and R J Miller. Glutamate receptors activate Ca2+ mobilization and Ca2+ influx into astrocytes. *Proceedings of the National Academy of Sciences*, 87(9):3454–3458, May 1990. Publisher: Proceedings of the National Academy of Sciences.

[230] Si Li, E. Scott Graham, and Charles P. Unsworth. Extracellular ATP release predominantly mediates Ca2+ communication locally in highly organised, stellate-Like patterned networks of adult human astrocytes. *PLOS ONE*, 18(10):e0289350, October 2023. Publisher: Public Library of Science.

[231] Hajime Takano, Jai-Yoon Sul, Mary L. Mazzanti, Robert T. Doyle, Philip G. Haydon, and Marc D. Porter. Micropatterned Substrates: Approach to Probing Intercellular Communication Pathways. *Analytical Chemistry*, 74(18):4640–4646, September 2002. Publisher: American Chemical Society.

[232] Judea Pearl. *Causality*. Cambridge University Press, Cambridge, 2 edition, 2009.

[233] Xiangying Meng, Krystyna Solarana, Zac Bowen, Ji Liu, Daniel A Nagode, Aminah Sheikh, Daniel E Winkowski, Joseph P Y Kao, and Patrick O Kanold. Transient Subgranular Hyperconnectivity to L2/3 and Enhanced Pairwise Correlations During the Critical Period in the Mouse Auditory Cortex. *Cerebral Cortex*, 30(3):1914–1930, March 2020.

[234] Jeffrey L. Elman. Finding Structure in Time. *Cognitive Science*, 14(2):179–211, March 1990. Publisher: John Wiley & Sons, Ltd.

[235] Mantas Lukoševičius and Herbert Jaeger. Reservoir computing approaches to recurrent neural network training. *Computer Science Review*, 3(3):127–149, August 2009.

[236] David G. Clark and L.F. Abbott. Theory of Coupled Neuronal-Synaptic Dynamics. *Physical Review X*, 14(2):021001, April 2024. Publisher: American Physical Society.

[237] Lou Beaulieu-Laroche, Enrique H. S. Toloza, Marie-Sophie van der Goes, Mathieu Lafourcade, Derrick Barnagian, Ziv M. Williams, Emad N. Eskandar, Matthew P. Frosch, Sydney S. Cash, and Mark T. Harnett. Enhanced Dendritic Compartmentalization in Human Cortical Neurons. *Cell*, 175(3):643–651.e14, October 2018. Place: United States.

[238] Jakob Voigts and Mark T. Harnett. Somatic and Dendritic Encoding of Spatial Variables in Retrosplenial Cortex Differs during 2D Navigation. *Neuron*, 105(2):237–245.e4, January 2020. Place: United States.

[239] Alberto Perez-Alvarez, Florian Huhn, Céline D. Dürst, Andreas Franzelin, Paul J. Lamothe-Molina, and Thomas G. Oertner. Freeze-Frame Imaging of Dendritic Calcium Signals With TubuTag. *Frontiers in Molecular Neuroscience*, 14, 2021.

[240] Farhan Ali and Alex C. Kwan. Interpreting in vivo calcium signals from neuronal cell bodies, axons, and dendrites: a review. *Neurophotonics*, 7(1):011402, July 2019.

[241] Mehmet Fişek and Michael Häusser. Are Human Dendrites Different? *Trends in cognitive sciences*, 24(6):411–412, June 2020. Place: England.

[242] Jordan Guerguiev, Timothy P. Lillicrap, and Blake A. Richards. Towards deep learning with segregated dendrites. *eLife*, 6:e22901, December 2017. Place: England.

[243] Michael London and Michael Häusser. Dendritic computation. *Annual review of neuroscience*, 28:503–532, 2005. Place: United States.

[244] Michael Häusser and Bartlett Mel. Dendrites: bug or feature? *Current opinion in neurobiology*, 13(3):372–383, June 2003. Place: England.

[245] Won-Suk Chung, Nicola J. Allen, and Cagla Eroglu. Astrocytes Control Synapse Formation, Function, and Elimination. *Cold Spring Harbor perspectives in biology*, 7(9):a020370, February 2015. Place: United States.

[246] Wannan Tang, Karolina Szokol, Vidar Jensen, Rune Enger, Chintan A. Trivedi, Øivind Hvalby, P. Johannes Helm, Loren L. Looger, Rolf Sprengel, and Erlend A. Nagelhus. Stimulation-Evoked Ca2+ Signals in Astrocytic Processes at Hippocampal CA3–CA1 Synapses of Adult Mice Are Modulated by Glutamate and ATP. *Journal of Neuroscience*, 35(7):3016–3021, 2015. Publisher: Society for Neuroscience _eprint: https://www.jneurosci.org/content/35/7/3016.full.pdf.

[247] Audrey Denizot, Misa Arizono, U. Valentin Nägerl, Hédi Soula, and Hugues Berry. Simulation of calcium signaling in fine astrocytic processes: Effect of spatial properties on spontaneous activity. *PLOS Computational Biology*, 15(8):e1006795, August 2019. Publisher: Public Library of Science.

[248] Wendy Flores-Fuentes, Oleg Sergiyenko, Julio C. Rodríguez-Quiñonez, and Jesús E. Miranda-Vega. Application of Information Theory to Computer Vision and Image Processing. *Entropy*, 26(2), 2024.

[249] Wendy Garcia-González, Wendy Flores-Fuentes, Oleg Sergiyenko, Julio C. Rodríguez-Quiñonez, Jesús E. Miranda-Vega, and Daniel Hernández-Balbuena. Shannon Entropy Used for Feature Extractions of Optical Patterns in the Context of Structural Health Monitoring. *Entropy*, 25(8), 2023.

[250] Huei-Yung Lin and Chin-Yu Hsu. Structured Cluster Detection from Local Feature Learning for Text Region Extraction. *Entropy*, 25(4), 2023.

[251] Flavie Lavoie-Cardinal, Anthony Bilodeau, Mado Lemieux, Marc-André Gardner, Theresa Wiesner, Gabrielle Laramée, Christian Gagné, and Paul De Koninck. Neuronal activity remodels the F-actin based submembrane lattice in dendrites but not axons of hippocampal neurons. *Scientific Reports*, 10(1):11960, July 2020.

[252] G.R. Erickson, D.L. Northrup, and F. Guilak. Hypo-osmotic stress induces calcium-dependent actin reorganization in articular chondrocytes. *Osteoarthritis and Cartilage*, 11(3):187–197, March 2003.

[253] Máté Maus, David Medgyesi, Endre Kiss, Andrea E Schneider, Ágnes Enyedi, Nóra Szilágyi, János Matkó, and Gabriella Sármay. B cell receptor-induced Ca2+ mobilization mediates F-actin rearrangements and is indispensable for adhesion and spreading of B lymphocytes. *Journal of Leukocyte Biology*, 93(4):537–547, April 2013.

[254] V. Garib, K. Lang, B. Niggemann, K. S. Zänker, L. Brandt, and T. Dittmar. Propofol-induced calcium signalling and actin reorganization within breast carcinoma cells. *European Journal of Anaesthesiology | EJA*, 22(8), 2005.

[255] Thomas G. Oertner and Andrew Matus. Calcium regulation of actin dynamics in dendritic spines. *Calcium in the function of the nervous system: New implications*, 37(5):477–482, May 2005.

[256] Ina Brünig, Stefanie Kaech, Heike Brinkhaus, Thomas G. Oertner, and Andrew Matus. Influx of extracellular calcium regulates actin-dependent morphological plasticity in dendritic spines. *The Cytoskeleton and Synaptic Function*, 47(5):669–676, October 2004.

[257] Guanyu Lin, Madison Rennie, Ayobami Adeeko, and Suzanne Scarlata. The role of calcium in neuronal membrane tension and synaptic plasticity. *Biochemical Society Transactions*, 52(2):937–945, March 2024.

[258] Maria Luisa Cotrina, Jane H.-C. Lin, and Maiken Nedergaard. Cytoskeletal Assembly and ATP Release Regulate Astrocytic Calcium Signaling. *The Journal of Neuroscience*, 18(21):8794, November 1998.

[259] S.R. Lopes, T.L. Prado, G. Corso, G.Z. dos S. Lima, and J. Kurths. Parameter-free quantification of stochastic and chaotic signals. *Chaos, Solitons & Fractals*, 133:109616, April 2020.

[260] C Quintero-Quiroz, S Pigolotti, M C Torrent, and C Masoller. Numerical and experimental study of the effects of noise on the permutation entropy. *New Journal of Physics*, 17(9):093002, September 2015. Publisher: IOP Publishing.

[261] Martín Gómez Ravetti, Laura C. Carpi, Bruna Amin Gonçalves, Alejandro C. Frery, and Osvaldo A. Rosso. Distinguishing Noise from Chaos: Objective versus Subjective Criteria Using Horizontal Visibility Graph. *PLOS ONE*, 9(9):e108004, September 2014. Publisher: Public Library of Science.

[262] O. A. Rosso, H. A. Larrondo, M. T. Martin, A. Plastino, and M. A. Fuentes. Distinguishing Noise from Chaos. *Physical Review Letters*, 99(15):154102, October 2007. Publisher: American Physical Society.

[263] L. Zunino, M. C. Soriano, and O. A. Rosso. Distinguishing chaotic and stochastic dynamics from time series by using a multiscale symbolic approach. *Physical Review E*, 86(4):046210, October 2012. Publisher: American Physical Society.

[264] B. R. R. Boaretto, R. C. Budzinski, K. L. Rossi, T. L. Prado, S. R. Lopes, and C. Masoller. Discriminating chaotic and stochastic time series using permutation entropy and artificial neural networks. *Scientific Reports*, 11(1):15789, August 2021.

[265] C. W. Kulp and L. Zunino. Discriminating chaotic and stochastic dynamics through the permutation spectrum test. *Chaos: An Interdisciplinary Journal of Nonlinear Science*, 24(3):033116, July 2014.

[266] Tohru Ikeguchi and Kazuyuki Aihara. Difference correlation can distinguish deterministic chaos from 1/${\mathrm{f}}ˆ{\mathrm{\ensuremath{\alpha}}}$-type colored noise. *Physical Review E*, 55(3):2530–2538, March 1997. Publisher: American Physical Society.

[267] Lucas Lacasa and Raul Toral. Description of stochastic and chaotic series using visibility graphs. *Physical Review E*, 82(3):036120, September 2010. Publisher: American Physical Society.

[268] Daniel Toker, Friedrich T. Sommer, and Mark D'Esposito. A simple method for detecting chaos in nature. *Communications Biology*, 3(1):11, January 2020.

[269] S. Saadoun, M C Papadopoulos, D C Davies, B A Bell, and S. Krishna. Increased aquaporin 1 water channel expression inhuman brain tumours. *British Journal of Cancer*, 87(6):621–623, September 2002.

[270] Jérôme Badaut, François Lasbennes, Pierre J. Magistretti, and Luca Regli. Aquaporins in Brain: Distribution, Physiology, and Pathophysiology. *Journal of Cerebral Blood Flow & Metabolism*, 22(4):367–378, April 2002. Publisher: SAGE Publications Ltd STM.

[271] Marios C. Papadopoulos and Alan S. Verkman. Aquaporin-4 and brain edema. *Pediatric Nephrology*, 22(6):778–784, June 2007.

[272] Meghan K. Driscoll, Colin McCann, Rael Kopace, Tess Homan, John T. Fourkas, Carole Parent, and Wolfgang Losert. Cell Shape Dynamics: From Waves to Migration. *PLOS Computational Biology*, 8(3):e1002392, March 2012. Publisher: Public Library of Science.